The Epoch of Reionization

Saleem Zaroubi
University of Groningen

The History

Credit: Science magazi

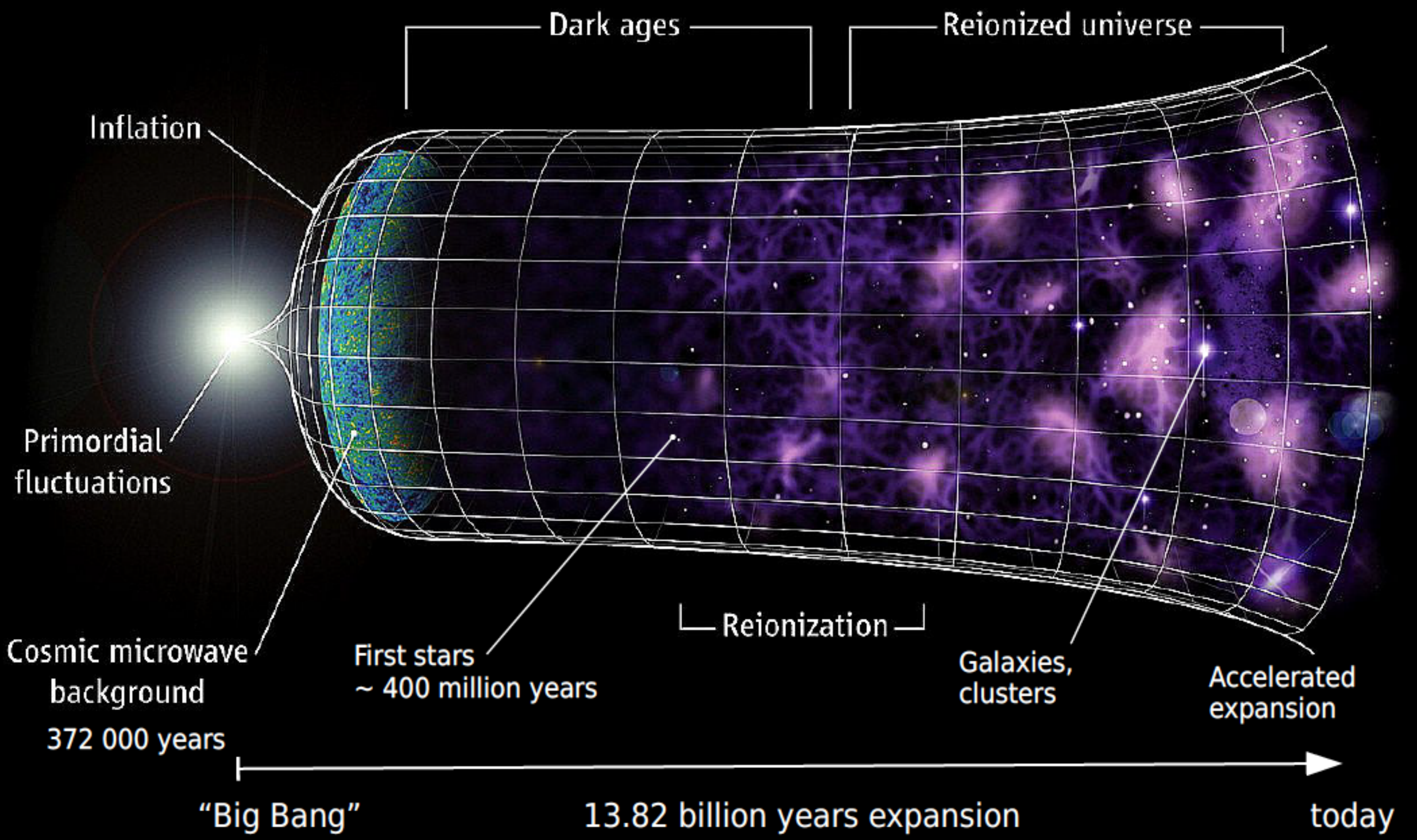

Sources of Reionization

- Galaxies
  - POP III vs POP II
- QSOs and faint AGNs
- X-ray bianries
- Dark Matter annihilation
- Other exotic scenarios

The first Stars

- The first generation of stars is formed with a primordial gas which has only Hydrogen and Helium.
- The cooling issue
- The fragmentation issue: free fall time scale vs. cooling time scale
- What do they do to the rest of IGM and to further star formation

"Let there be Light": The first stars and Galaxies

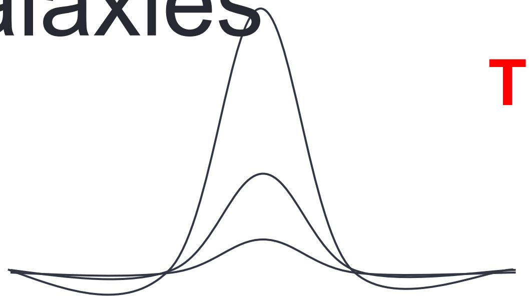

0.000001
overdensity

The rich gets richer and the poor gets poorer

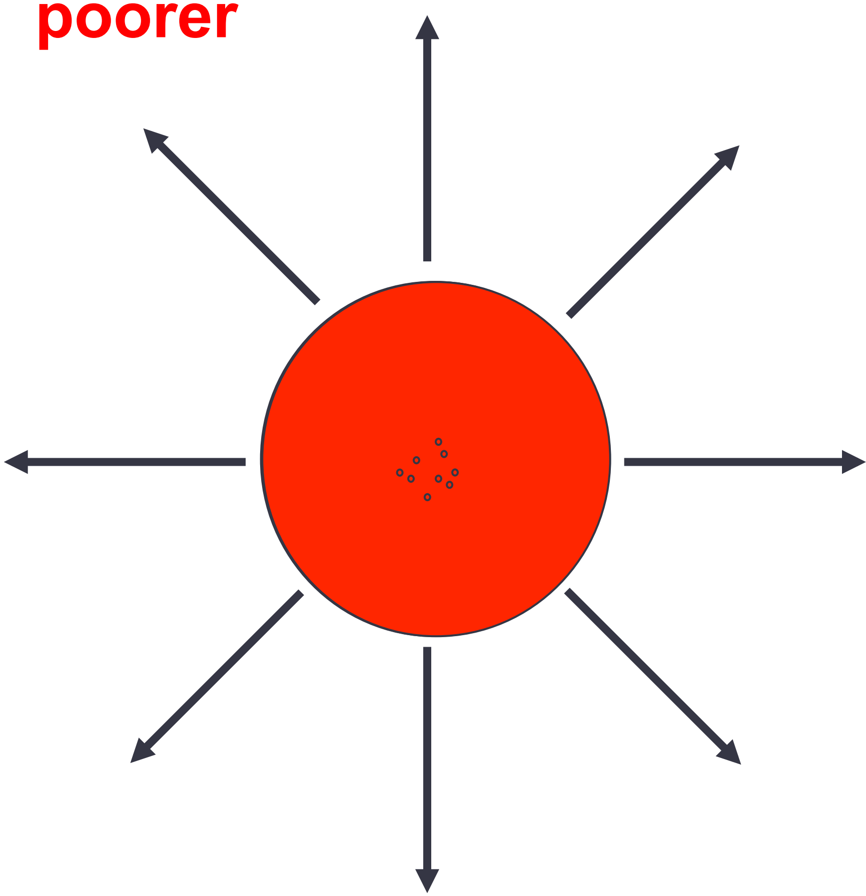

Formation of Stars

First stars are very big and short lived

Mass fraction in halos

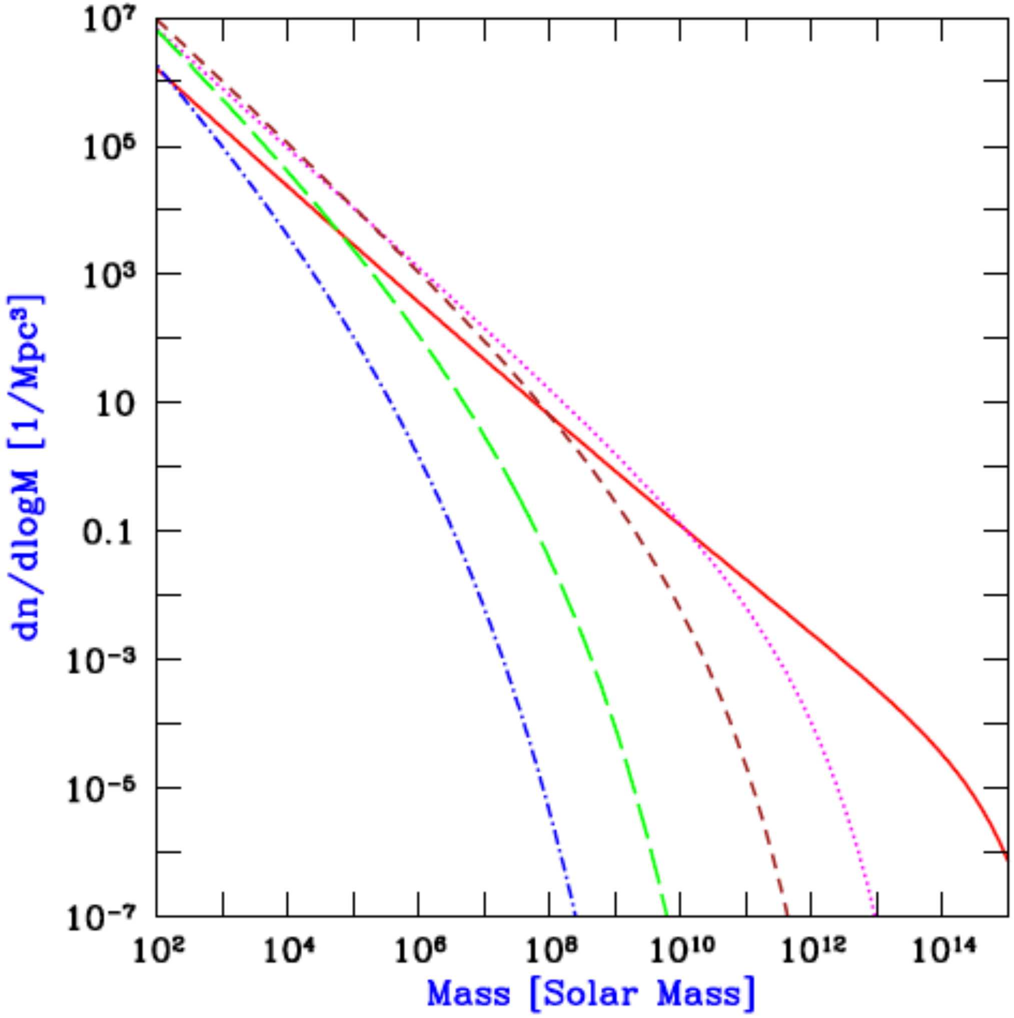

Barkana & Loeb 2001

Properties of collapsing halos

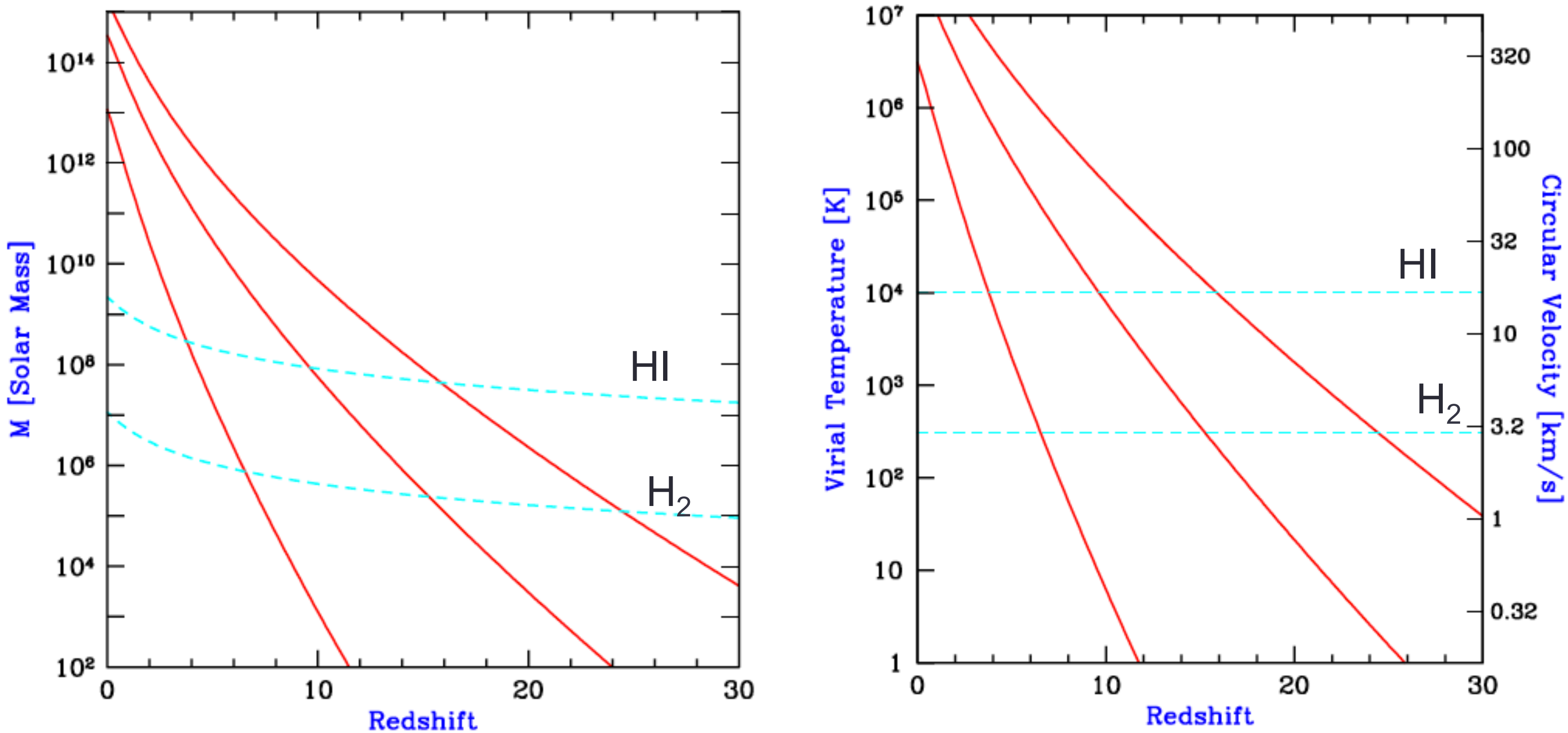

Barkana & Loeb 2001

Cooling rate of Primordial gas

Radiative Cooling for HI alone starts at T=10^4K which corresponds to Lyman-alpha transition

H2 has vibrational and rotational modes that allow cooling at lower temperatures

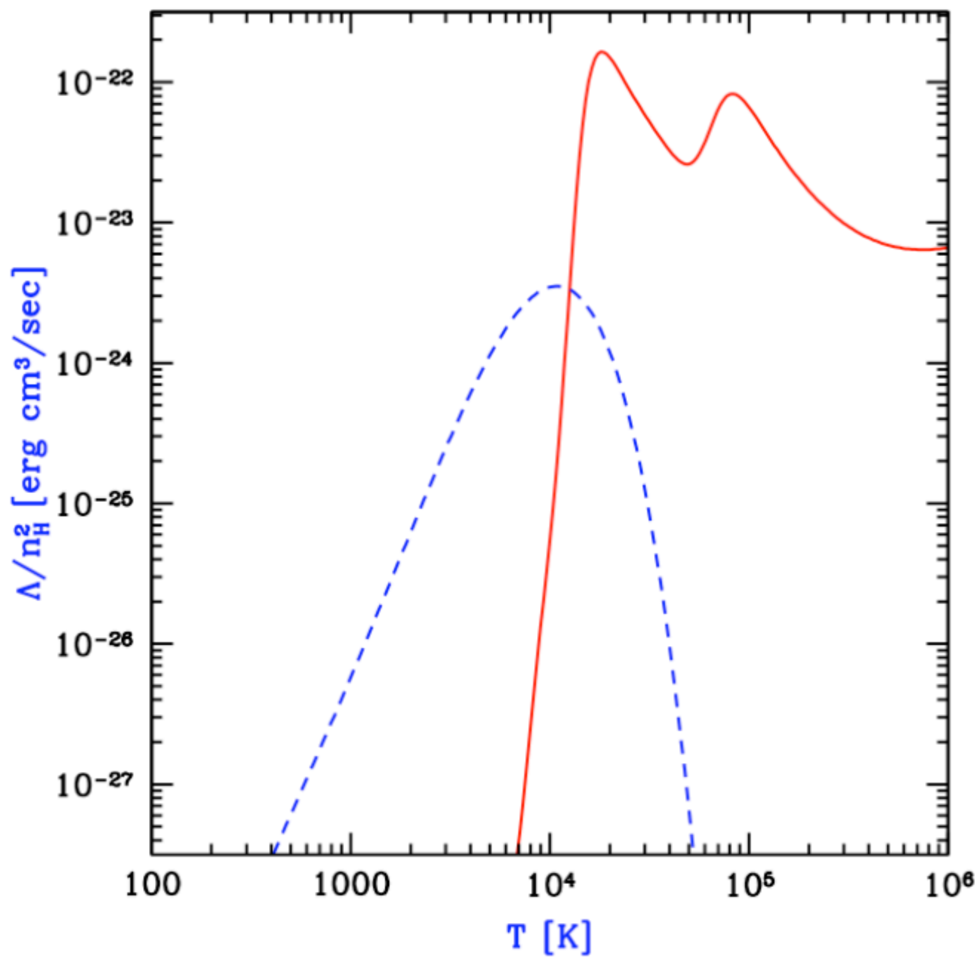

Fragmentation and formation of first stars

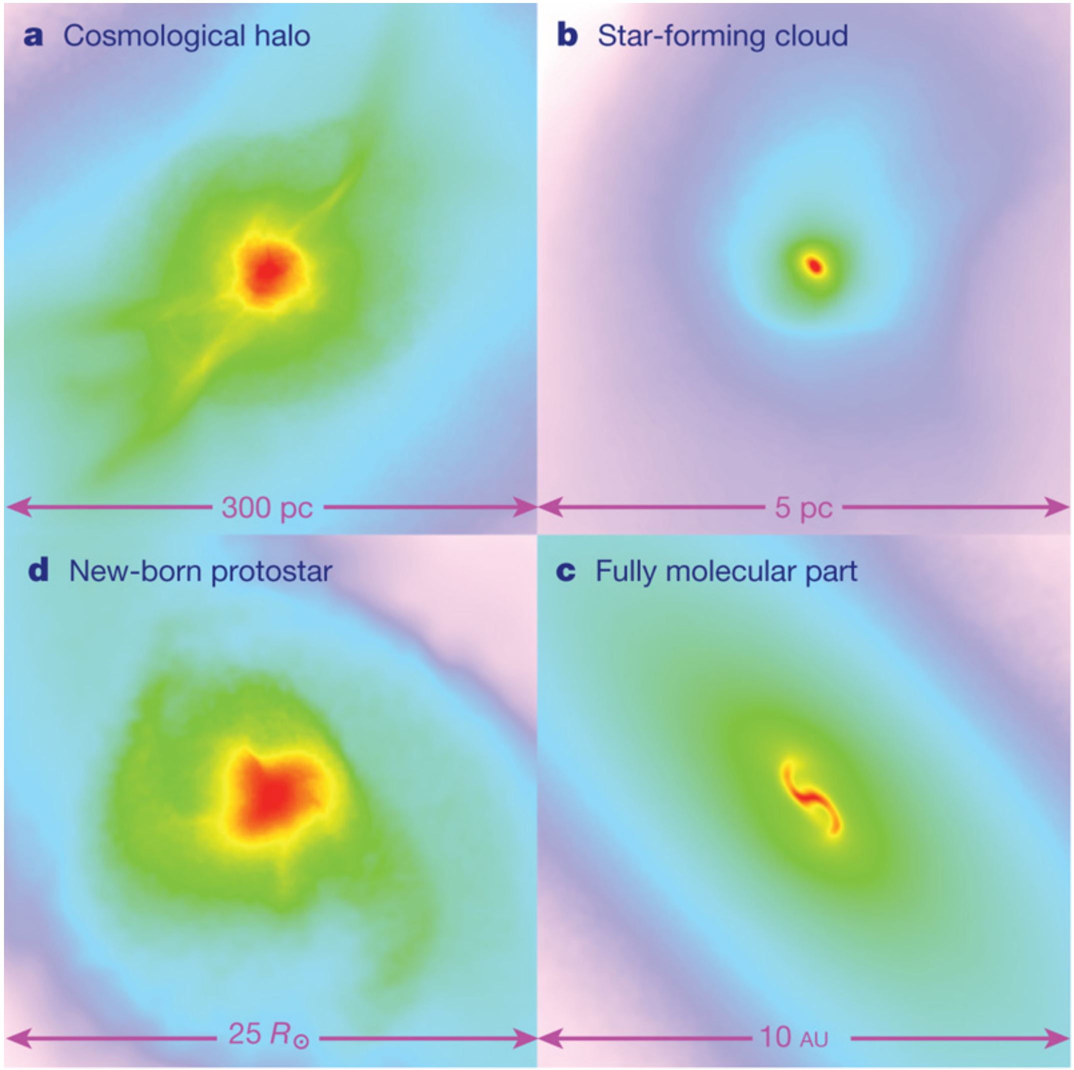

Projected gas distribution around a primordial protostar.

Bromm *et al.* 2009

Further fragmentation

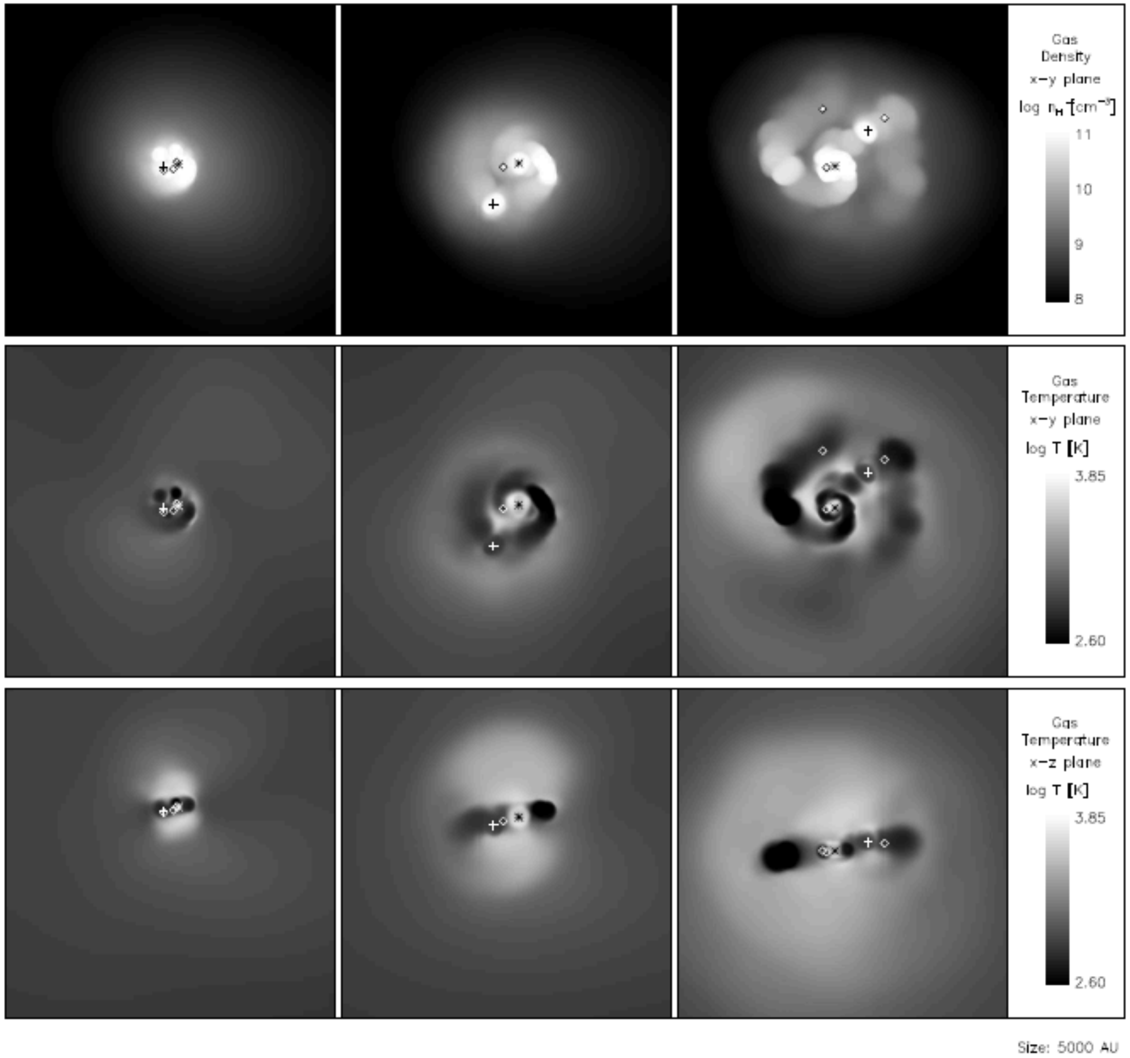

Stacy et al 2009

The rise of POP II stars oversimplified story

- Population III stars are expected to have masses of 10-100 solar masses. They live short life and contaminate the IGM after they SN explode.
- This feedback contamination gives rise to PopII stars (due to metals) which is thought to also create the bulk of ionizing radiation.
- Production of Lyman-Werner photons (11.2 to 13.6 eV) that prevent small haloes from creating more stars (distorys H_2).
- This finally creates stable galaxies at $T_{virial} = 10^4$K

Reionization: God's view

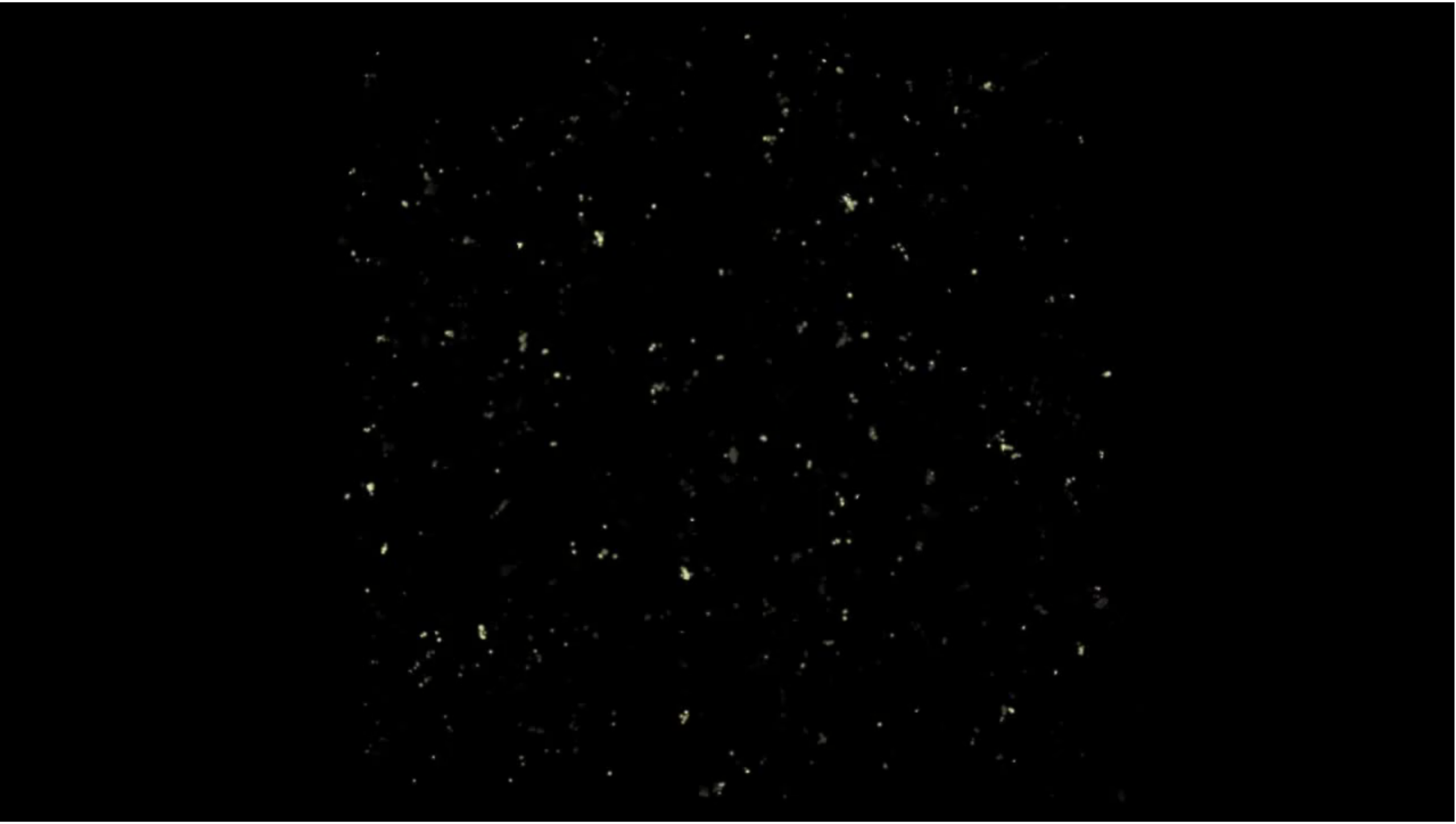

Credit: Marcelo Alvarez

Observational Probes of Reionization

- CMB (integral constraint)
- Redshifted 21 cm emission (absorption)
- 21 cm forest at high z
- Gamma ray bursts: How many we should have to constrain reionization?
- Luminosity function of first objects, e.g., Galaxies: Recent results from the new WFC3 aboard HST.
- Background detections: IR, soft x-ray.
- Lyman-α absorption system: ionization, metallicity, thermal history, UV background, proximity effect.
- Lyman alpha emitters
- Metals at high redshift.
- Using the local volume to study reionization.

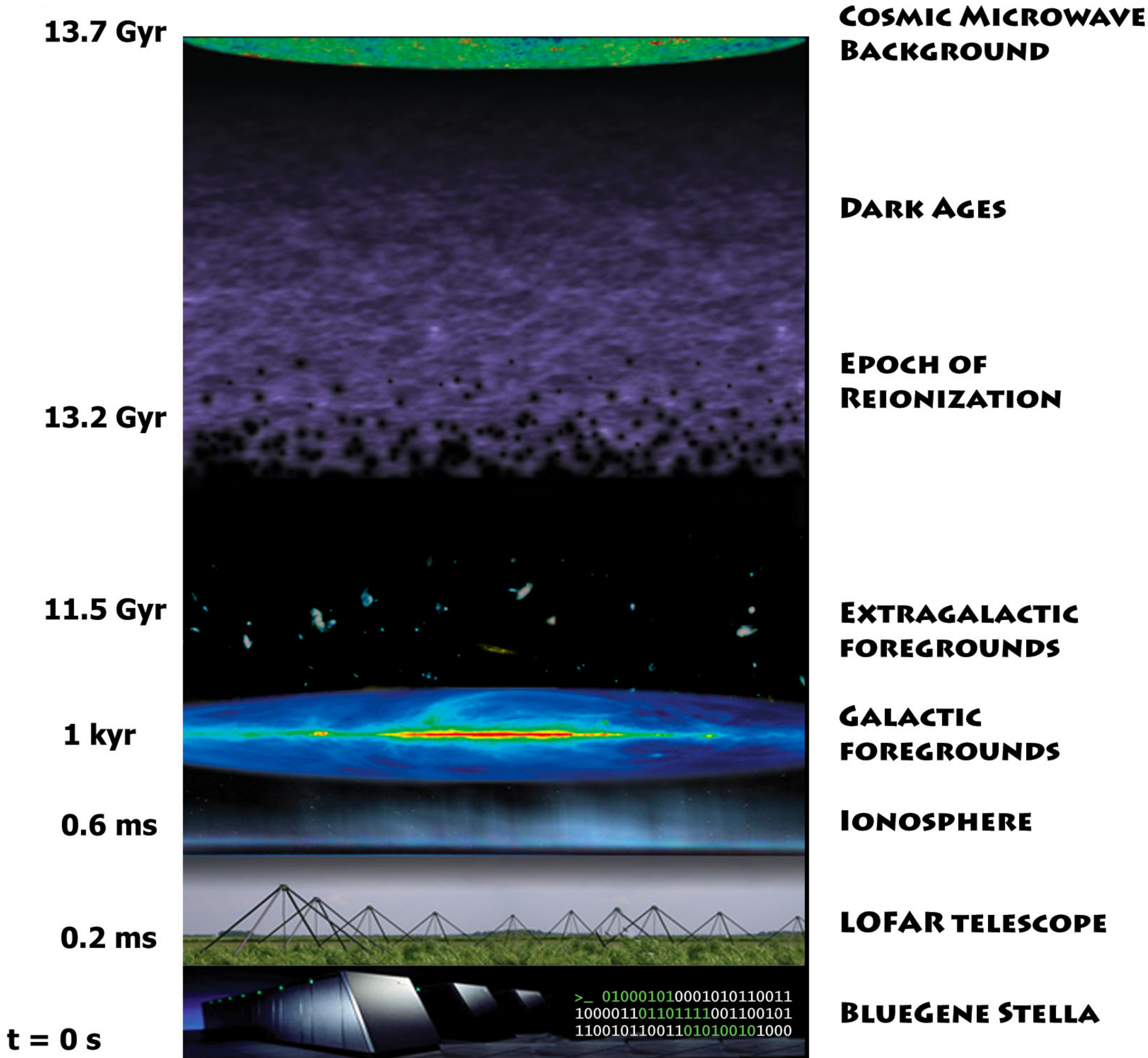

13.7 Gyr
Cosmic Microwave Background
Dark Ages
Epoch of Reionization
13.2 Gyr
11.5 Gyr
Extragalactic foregrounds
1 kyr
Galactic foregrounds
0.6 ms
Ionosphere
0.2 ms
LOFAR telescope
>_ 010001010001010110011
100001101101111001100101
1100101100110101001011000
t = 0 s
BlueGene Stella

CMB and Reionization

- Influence of reionization on CMB Temperature fluctuations
- Influence of reionization on CMB polarization.

References:

1. Scott, White & Silk 1994 (review).
2. Hu & White 1997
3. Aghanim,Subhabrata & Silk 2008 (review)
4. WMAP & Planck papers.

CMB photons Thomson scatter off free electrons

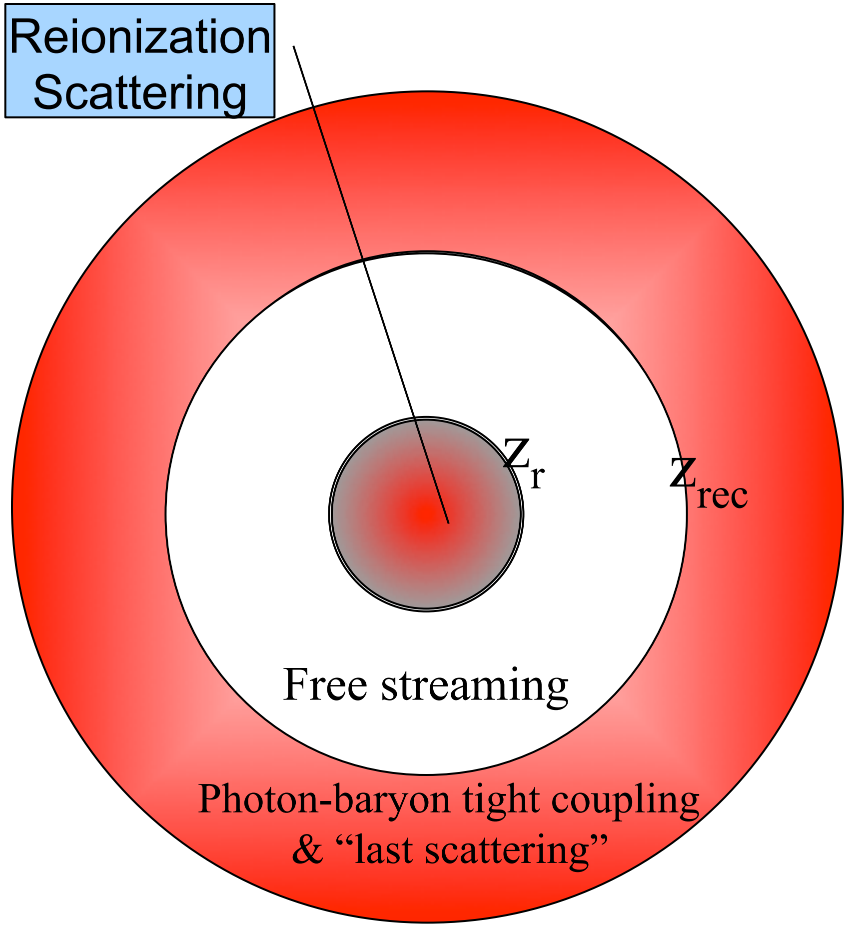

The dominant contribution to temperature anisotropies generated during reionization are Doppler shifts of the scatterers

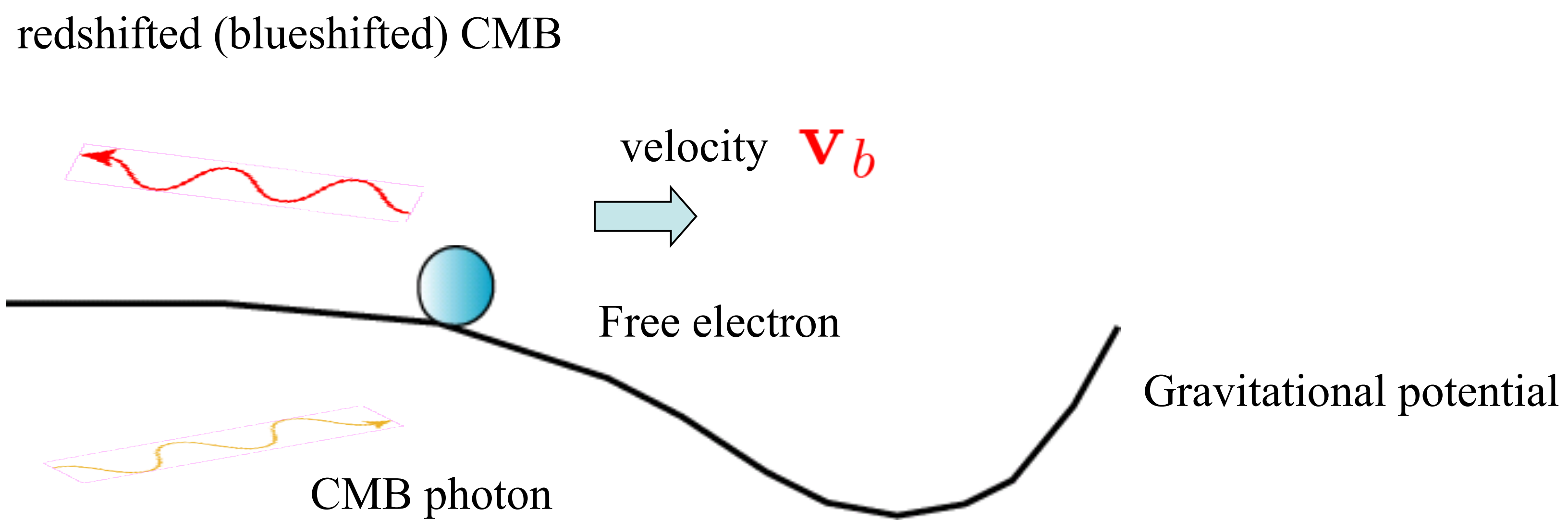

$$T_D(\hat{\mathbf{n}}) = -T_{\rm cmb} \int_0^{\eta_0} d\eta\, g(\eta)\, \hat{\mathbf{n}} \cdot \mathbf{v}_b(\hat{\mathbf{n}}, \eta)$$

$$g(\eta) = \dot{\tau} e^{-\tau}, \;\; \tau = x_e n_b \sigma_T$$

The CMB and Reionization: Temperature

- Imprint on CMB anisotropies governed by the visibility – or probability that a photon scatters out of the line of sight:

$$g = \dot{\tau} e^{-\tau}$$

- τ is the optical depth given by

$$\dot{\tau} = x_e n_H \sigma_T$$

with $x_e n_H$ the number density of free electrons

Reionization & CMB Temperature

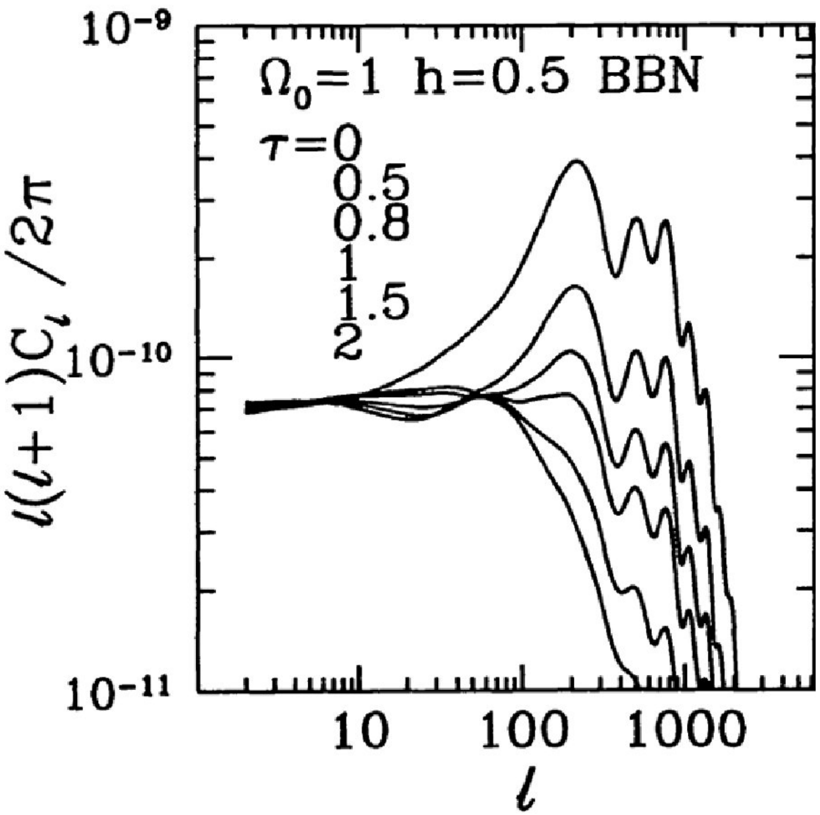

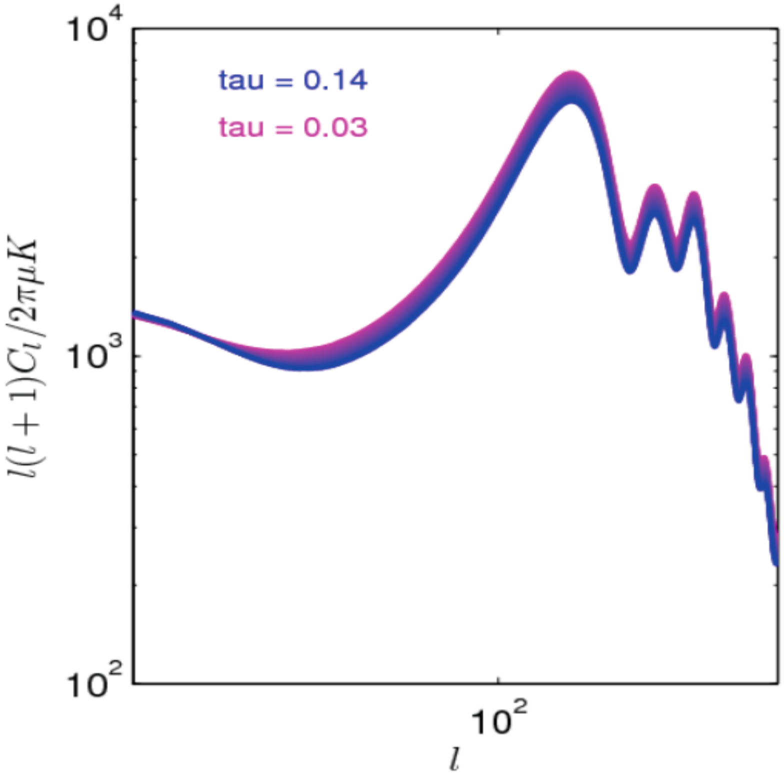

The influence of reionization on the CMB temperature angular power spectrum. (from Sugiyama 1995)

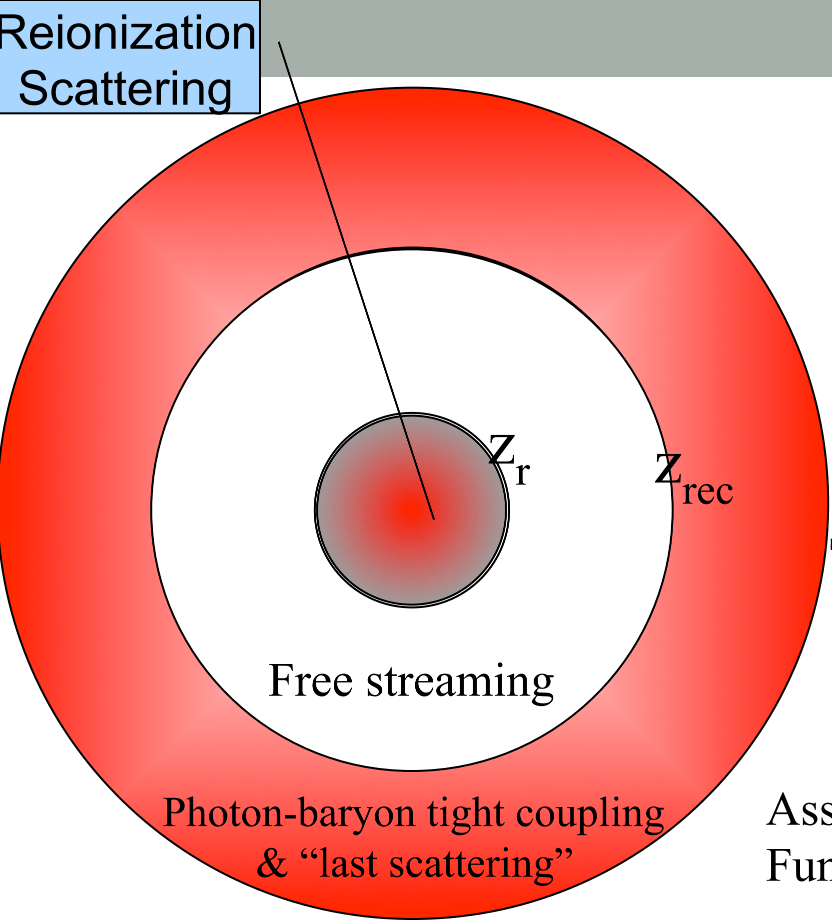

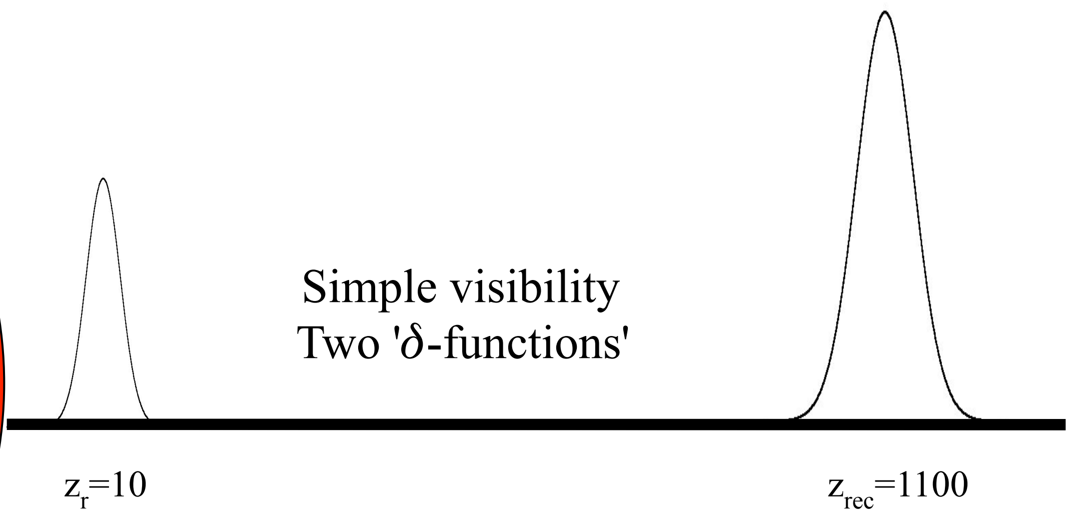

Assuming that the visibility is given by two delta Functions, the CMB is given by the following expression:

$$\Delta_l = e^{-\tau(z_r)} F_l(z_{rec}) + \left[1 - e^{-\tau(z_r)}\right] F_l(z_r) + ISW + \ldots$$

For the astrophysical reionization scenarios (low optical depth) second term negligible

CMB and Reionization: Polarization

Polarization: Stokes parameters

Q → -Q, U → -U under 90 degree rotation
Q → U, U → -Q under 45 degree rotation

$$P = \sqrt{Q^2 + U^2} \quad \text{and} \quad \alpha = \frac{1}{2}\arctan(U/Q).$$

amplitude angle

Thomson scattering

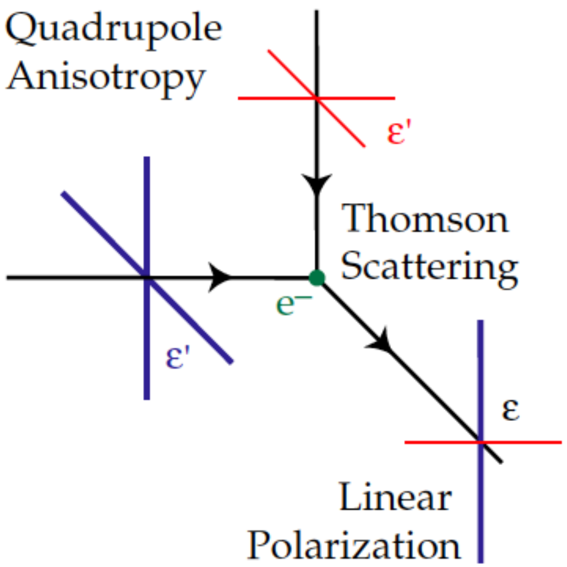

Q and U are generated by Thomson scattering of unpolarized light. Notice no V (circular polarization) is generated.

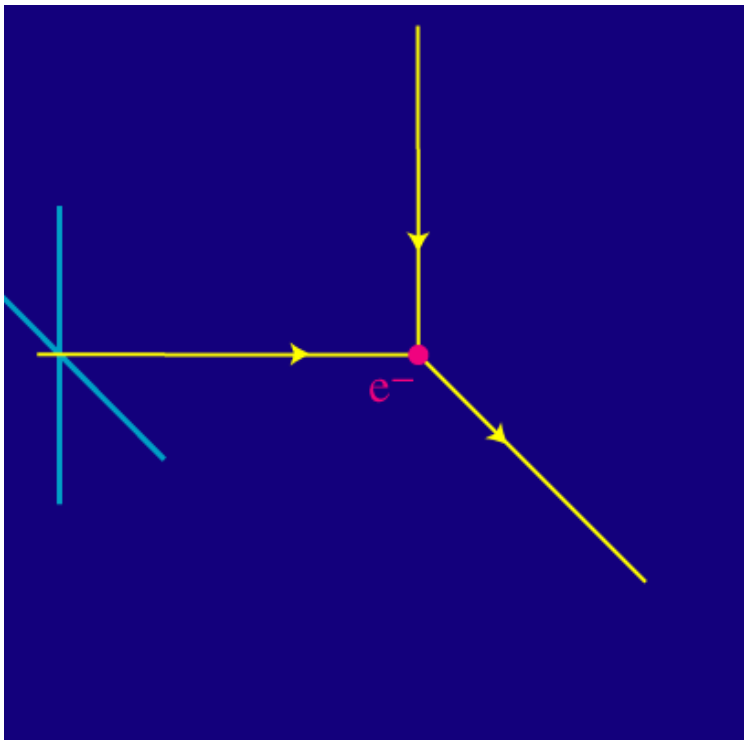

$$\frac{d\sigma_T}{d\Omega} = \frac{e^4}{m_e^2 c^4} |\vec{\epsilon} \cdot \vec{\epsilon}'|^2$$

E and B polarization modes

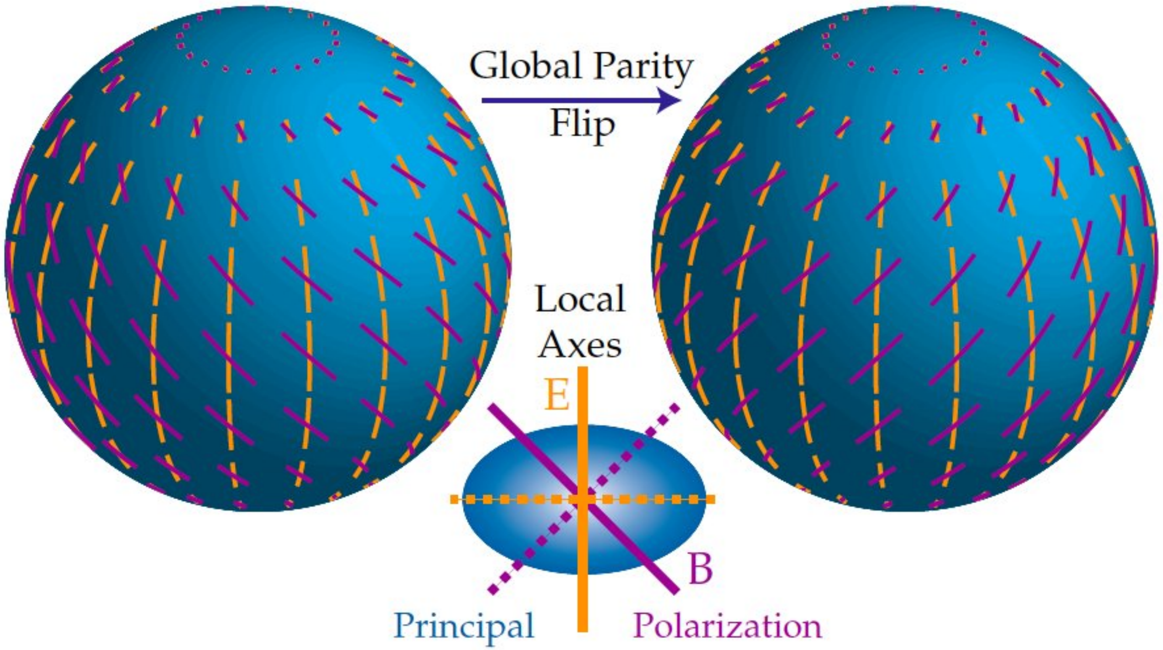

E-mode has $(-1)^{l}$ parity whereas B-mode $(-1)^{l+1}$

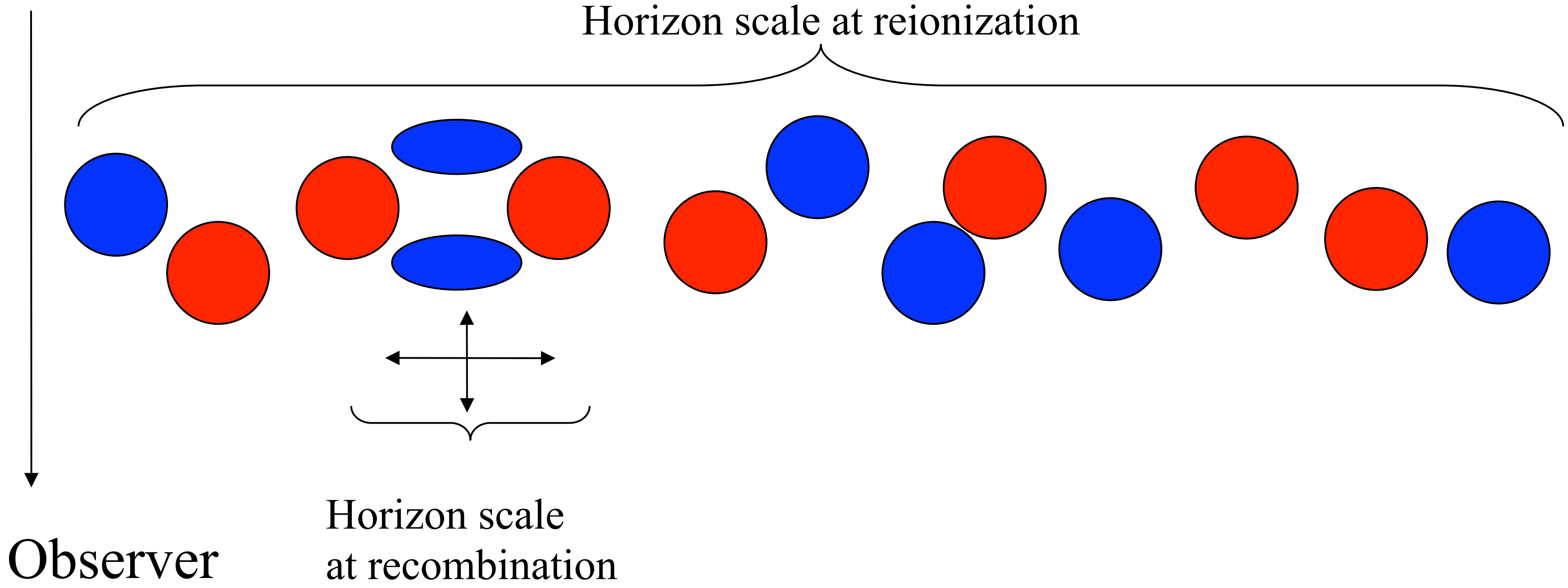

Given the geometry of linear polarization the amplitude of the signal at any scale depends on the local quadrupole that scatters the photons. However, at scales larger than horizon scales (either at recombination or during reionization) there is no coherence and the signal decays.

The influence of τ on EE and TE

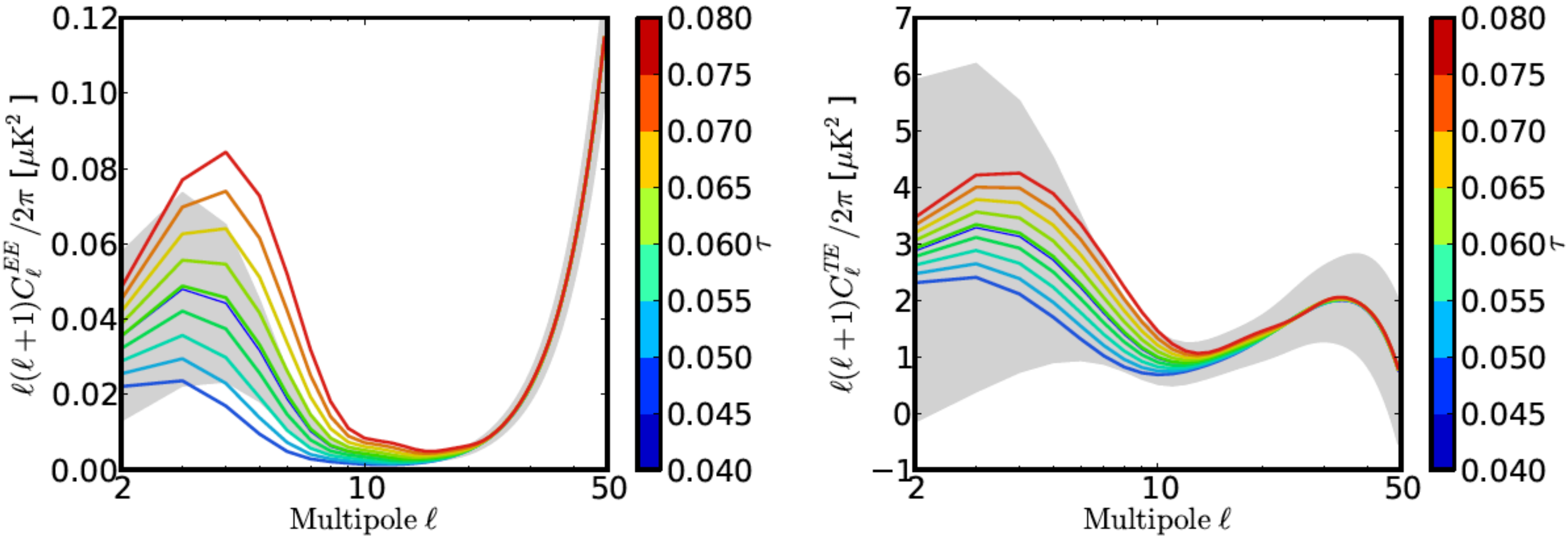

Planck XLVII paper

It is and Integral constrain

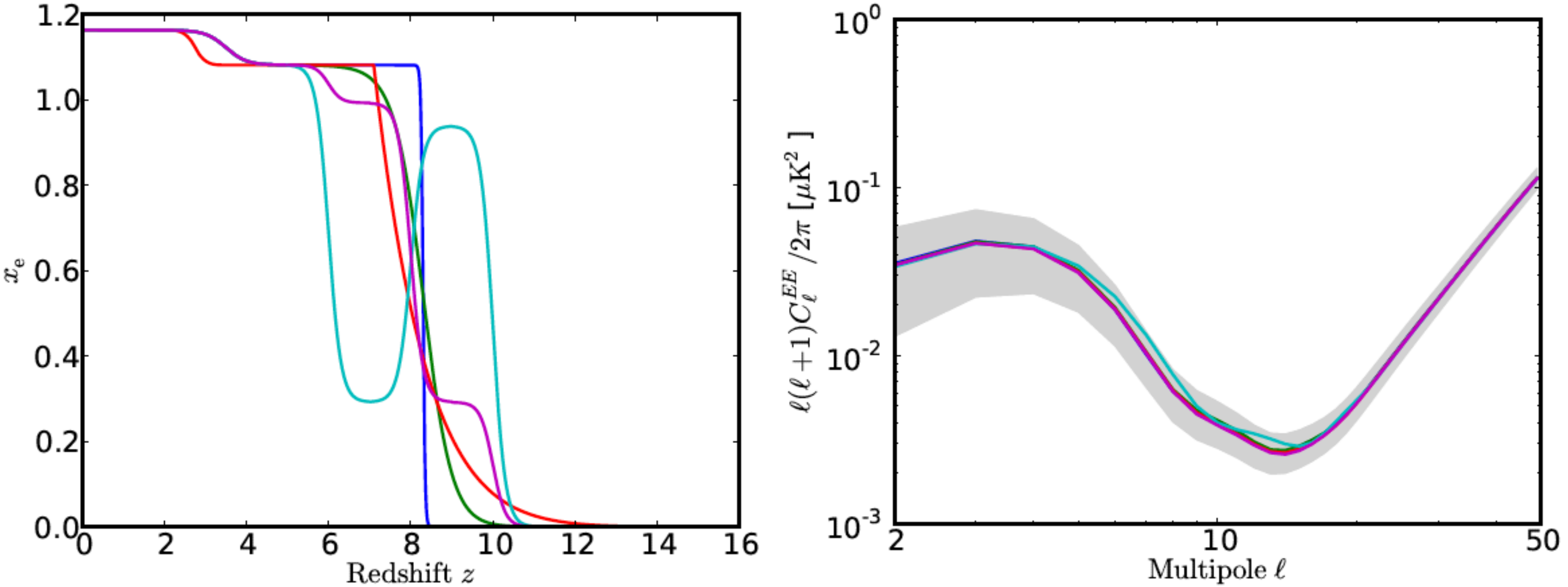

Planck XLVII paper

The WMAP cosntraint

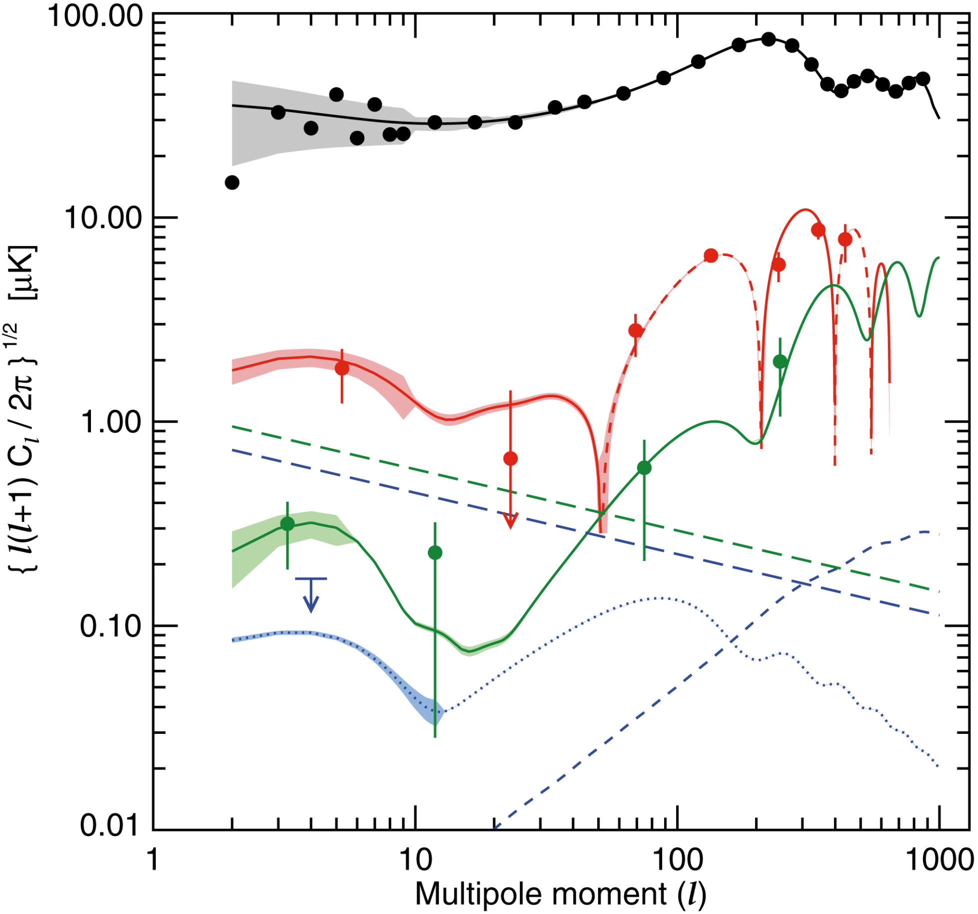

τ~ 0.088

- The WMAP polarization measurement tells us only about the optical depth not about exact ionization redshift. For that one needs a reionization history model. However, reasonable reionization models suggest that ionization has happened at about z~10.

The Planck constraint

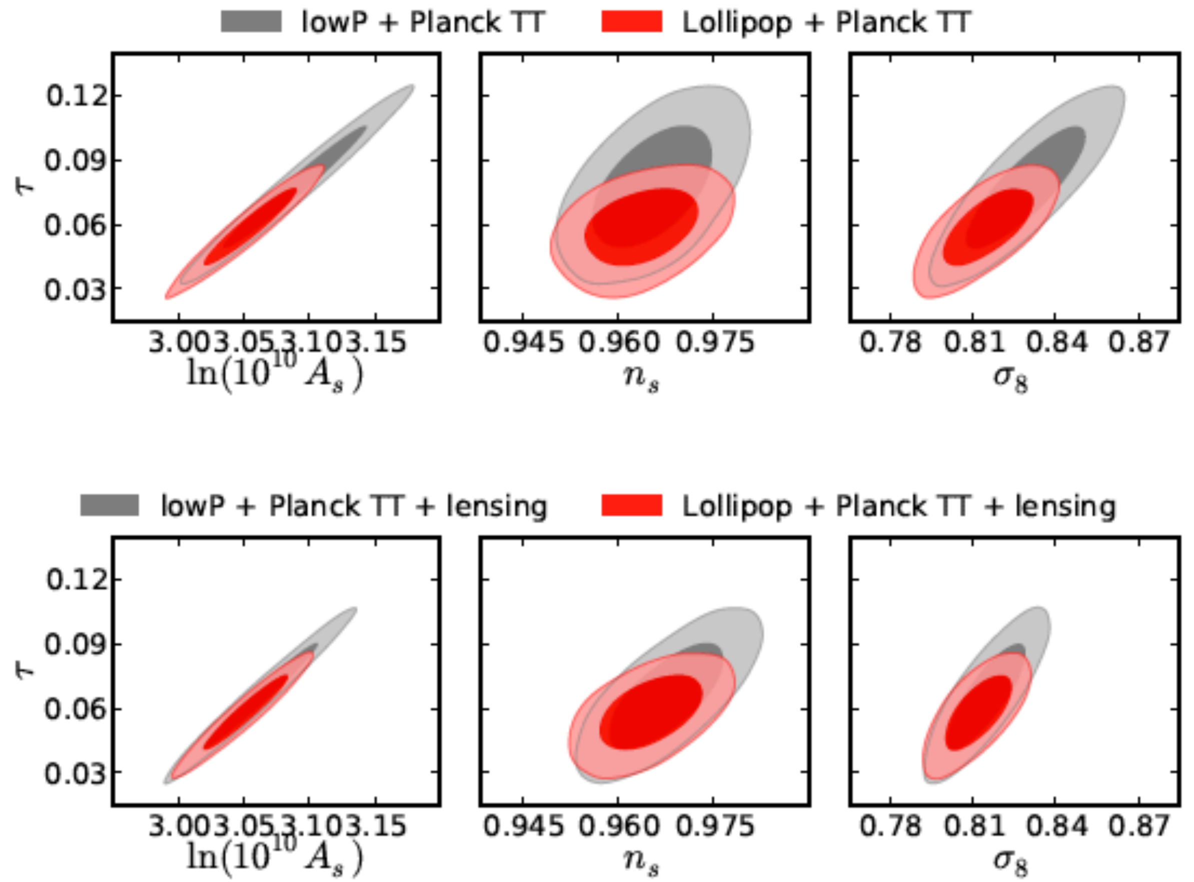

$$\tau = 0.053^{+0.014}_{-0.016}, \quad \texttt{lollipop}^{5};$$

$$\tau = 0.058^{+0.012}_{-0.012}, \quad \texttt{lollipop}\text{+PlanckTT};$$

$$\tau = 0.058^{+0.011}_{-0.012}, \quad \texttt{lollipop}\text{+PlanckTT+lensing};$$

$$\tau = 0.054^{+0.012}_{-0.013}, \quad \texttt{lollipop}\text{+PlanckTT+VHL}.$$

Reionization Redshift from Planck

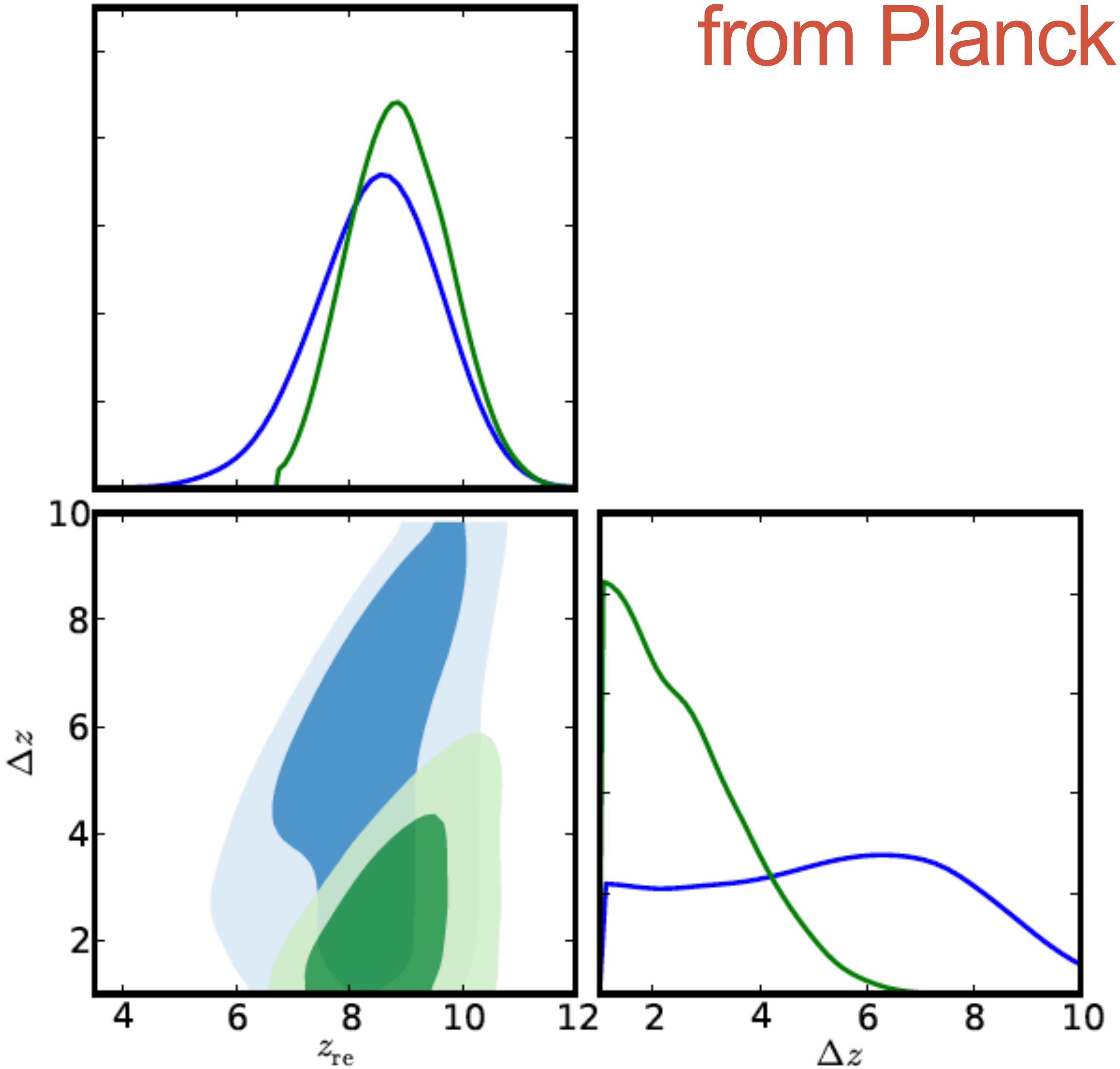

The Lyman-α optical depth from Quasar spectra

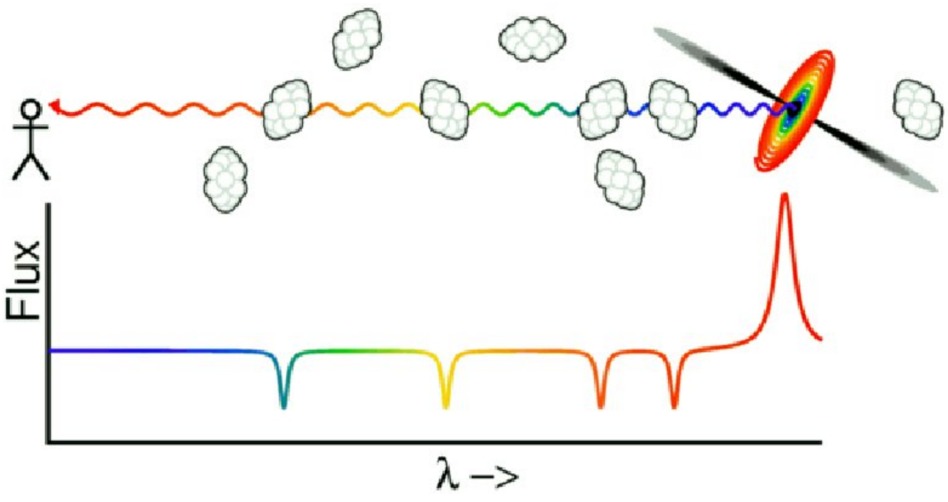

Absorption features due to Lyman-α in the IGM.

$$\tau_\alpha(\nu_0) = \int_{x_A}^{x_B} n_{HI}\sigma_\alpha dx/(1+z)$$

τ_α is the optical depth.x is the comoving radial distance. σ_α is the cross section & n_{HI} is the neutral hydrogen number density

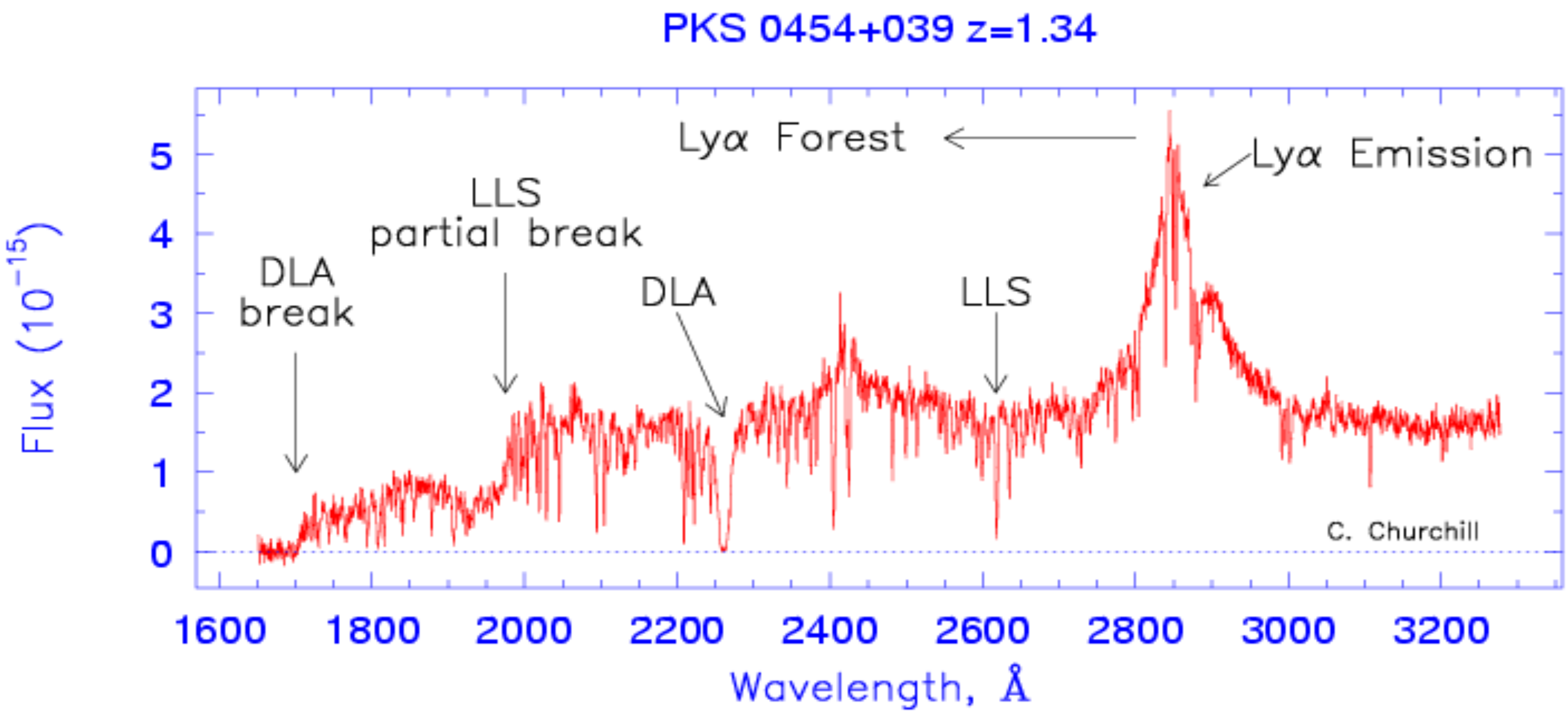

Three main classifications

Lyman-α forest $10^{12} \leq N(\mathrm{HI}) \leq 10^{16}$ cm^{-2}

Ly limit systems $10^{18} \leq N(\mathrm{HI}) \leq 10^{20}$ cm^{-2}

Damped Lyα $N(\mathrm{HI}) \geq 10^{20}$ cm^{-2}

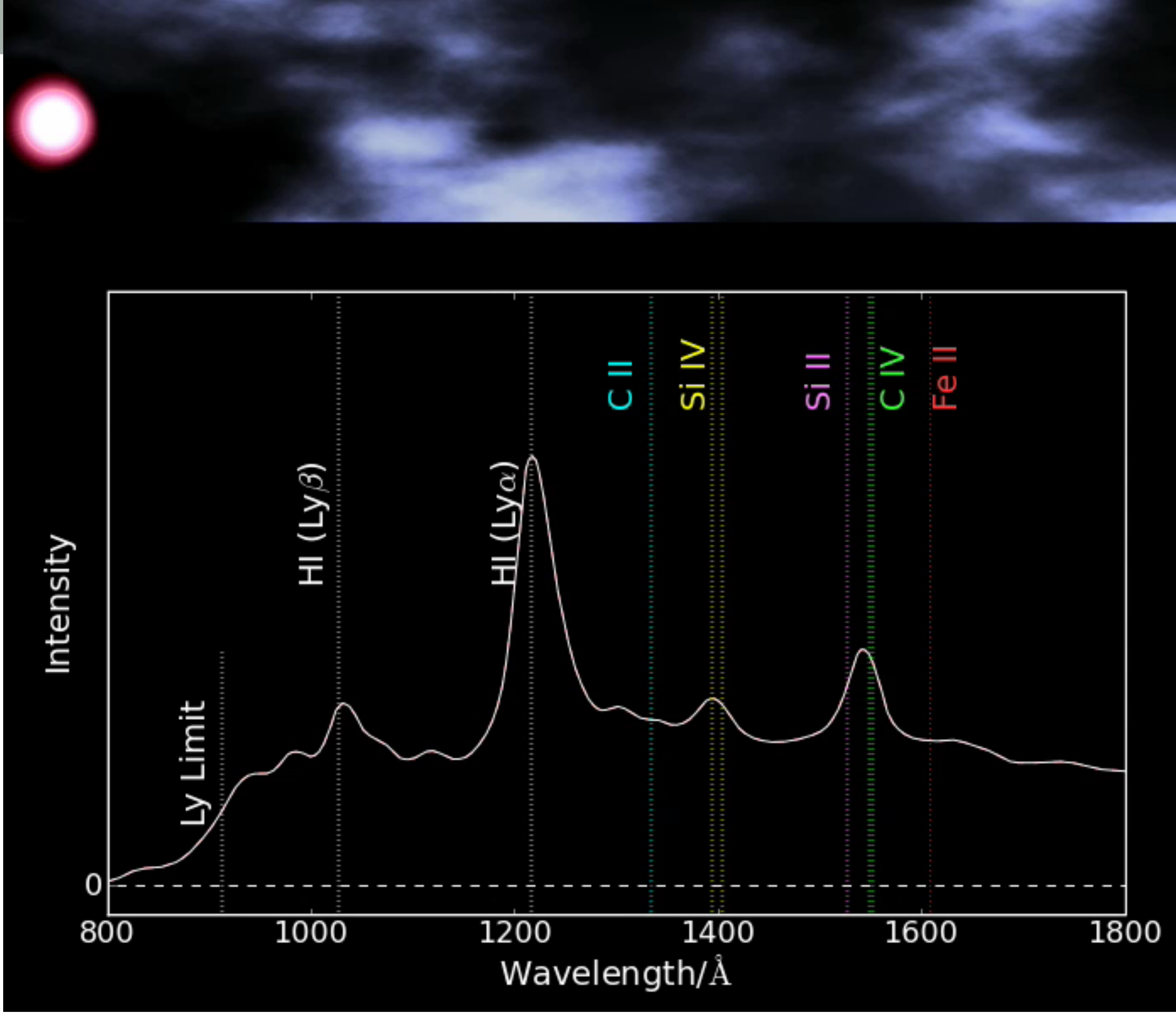
Intensity
Ly Limit
HI (Lyβ)
HI (Lyα)
C II
Si IV
Si II
C IV
Fe II
0
800
1000
1200
1400
1600
1800
Wavelength/Å

The Lyman-α optical depth from Quasar spectra

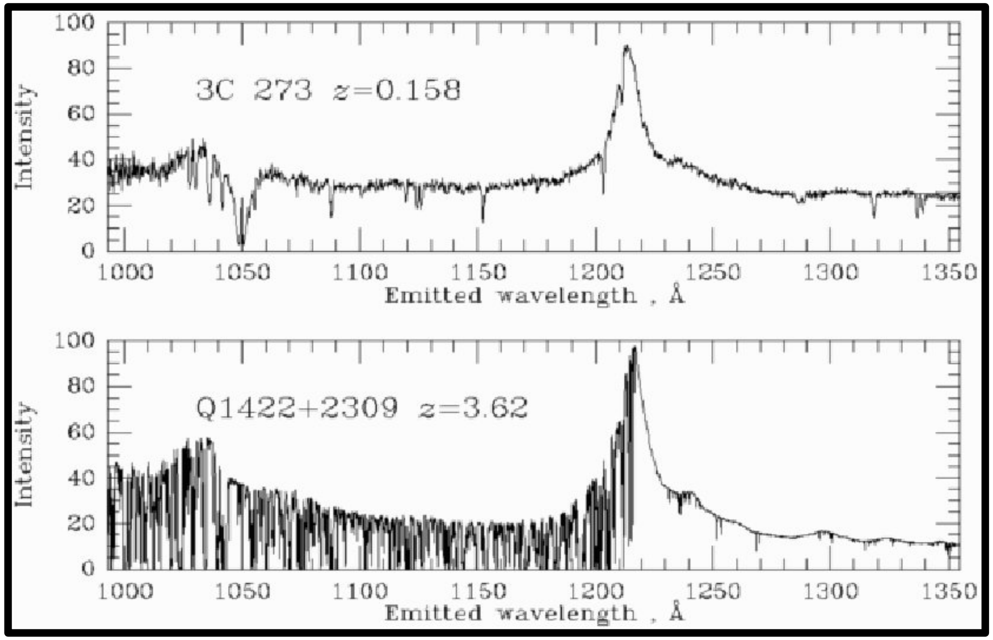

The cross section peaks at the observed frequency:

$$\nu = \nu_0(1+z)\left(1+\frac{v_{pec}}{c}\right)$$

Then substitution in the optical depth (written in terms Redshift) yields:

$$\tau_\alpha = \int n_{HI}\sigma_\alpha(\nu)\frac{cH_o^{-1}dz}{(1+z)\sqrt{\Omega_m(1+z)^3+\Omega_\Lambda}}$$

Which gives the simple result:

$$\frac{n_{HI}}{n_H} = x_{HI} \approx 10^{-4}\Omega_m^{1/2}(1+z)^{\frac{3}{2}}\tau_\alpha$$

The Lyman-α optical depth from Quasar spectra

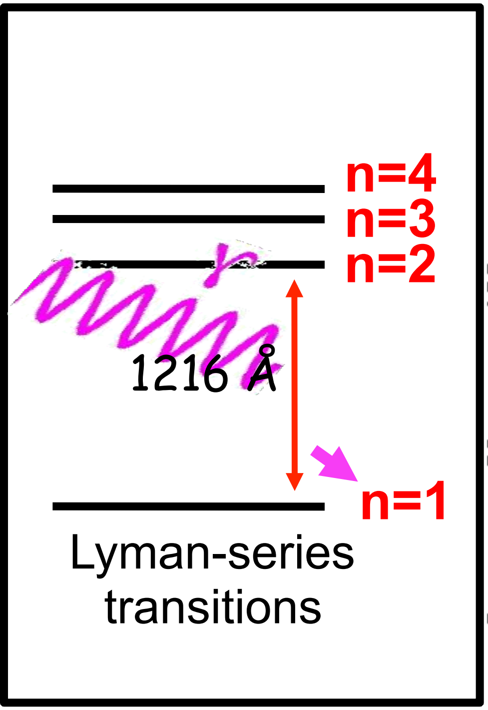

- The Lyman-α Forest Along Distant
- Quasar Spectra ($t_{Universe}$~1 Billion yr)

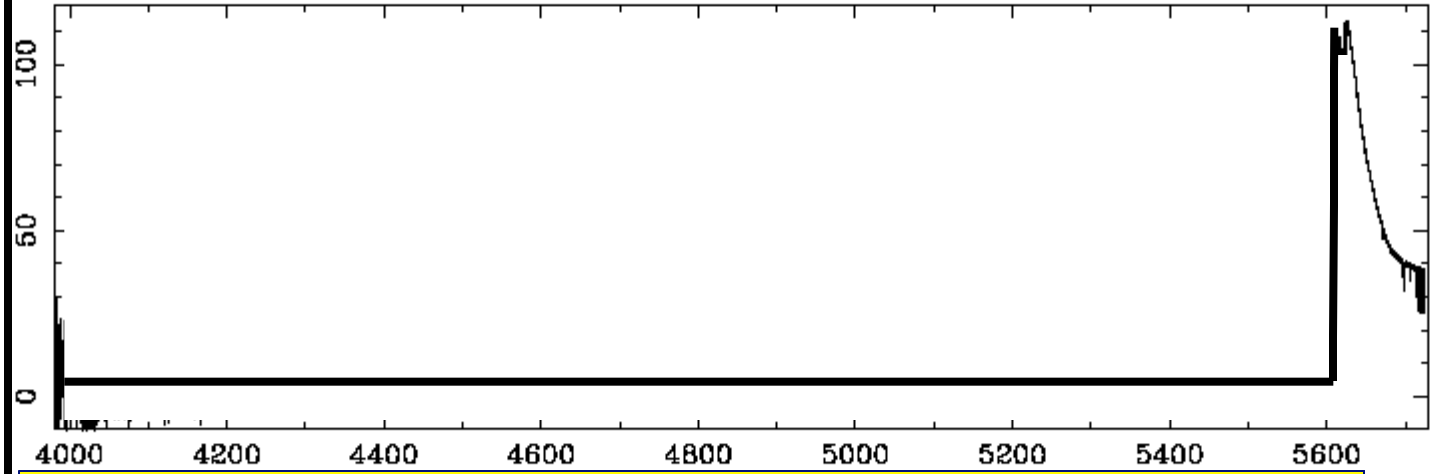

At z ~ 4 the IGM is 10^{-4} neutral

The Lyman-α forest optical depth at z about 6

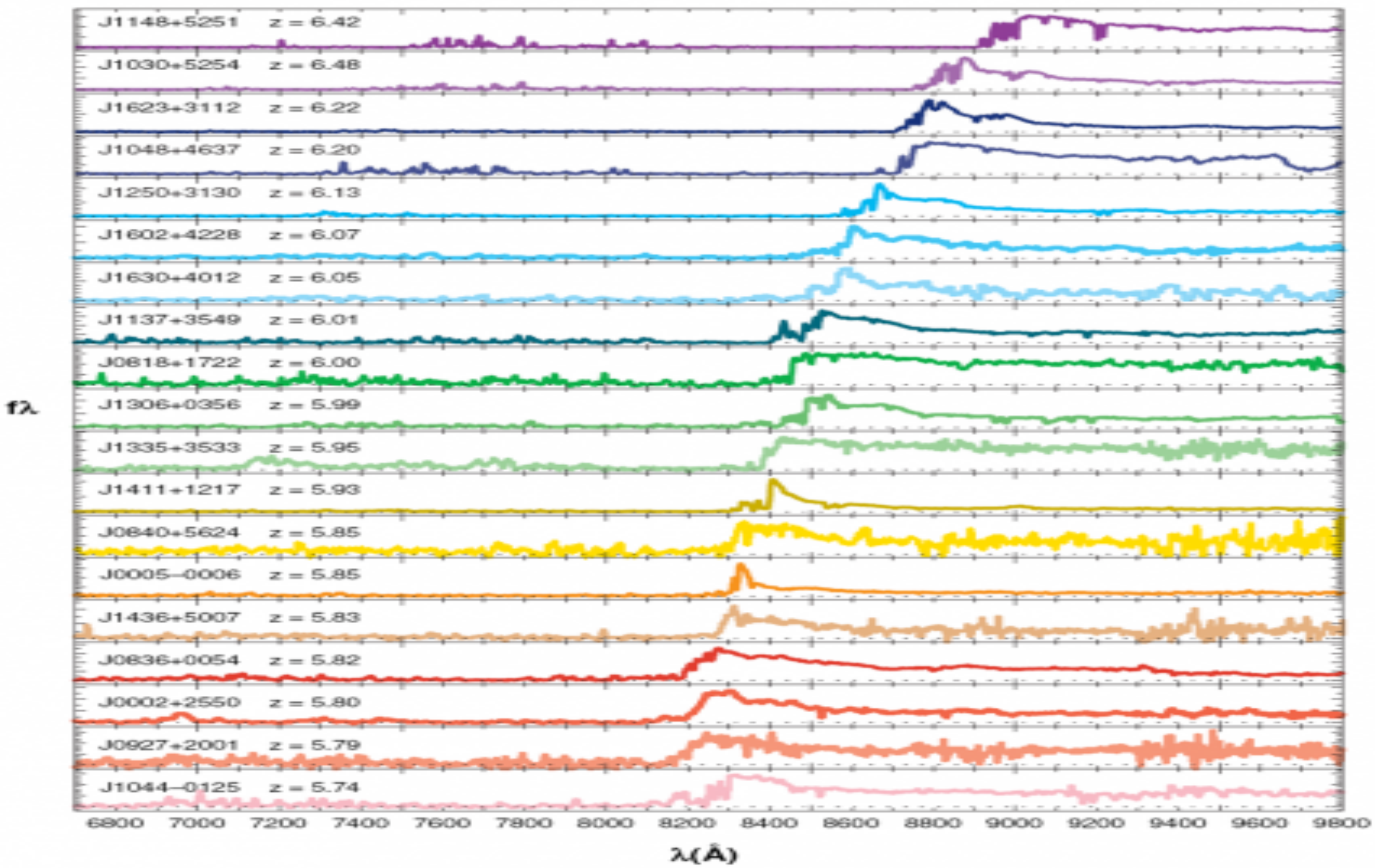

Fan et al. 2003, 2006

The end of the reionization process

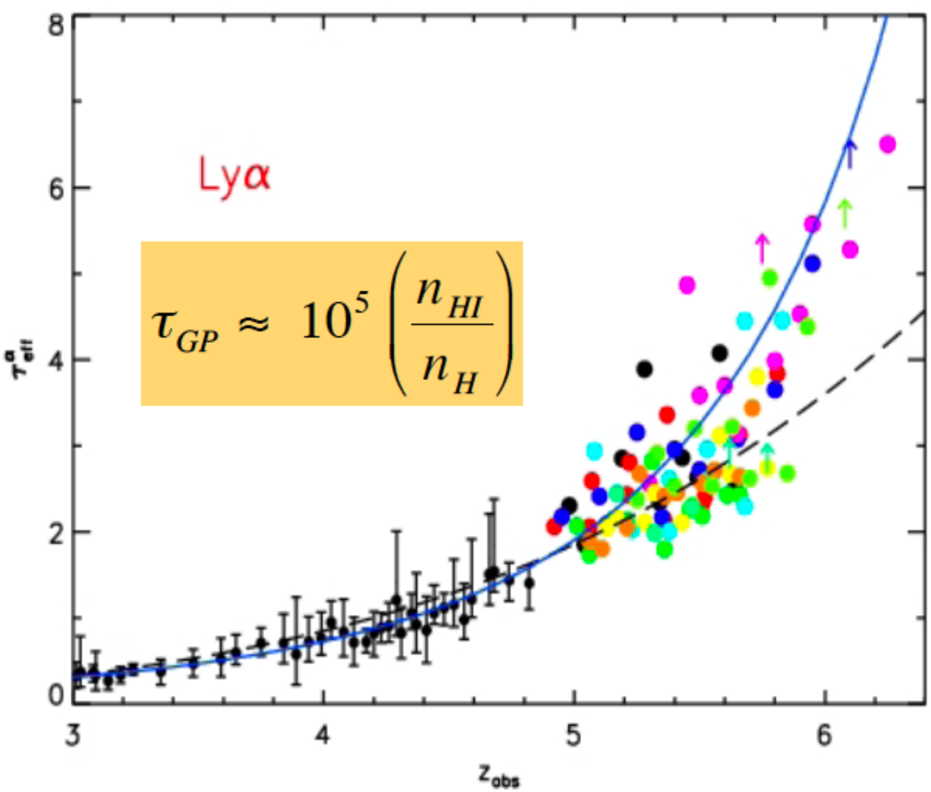

- The Lyman-alpha forest: At z<6 he Universe is completely ionized
- The Universe has completed its ionization by redshift 6: SSDS quasars (however, some, e.g., Mesinger 2009, still claim it is still about 10% neutral)

Even Higher redshift Quasars (z = 7.085)

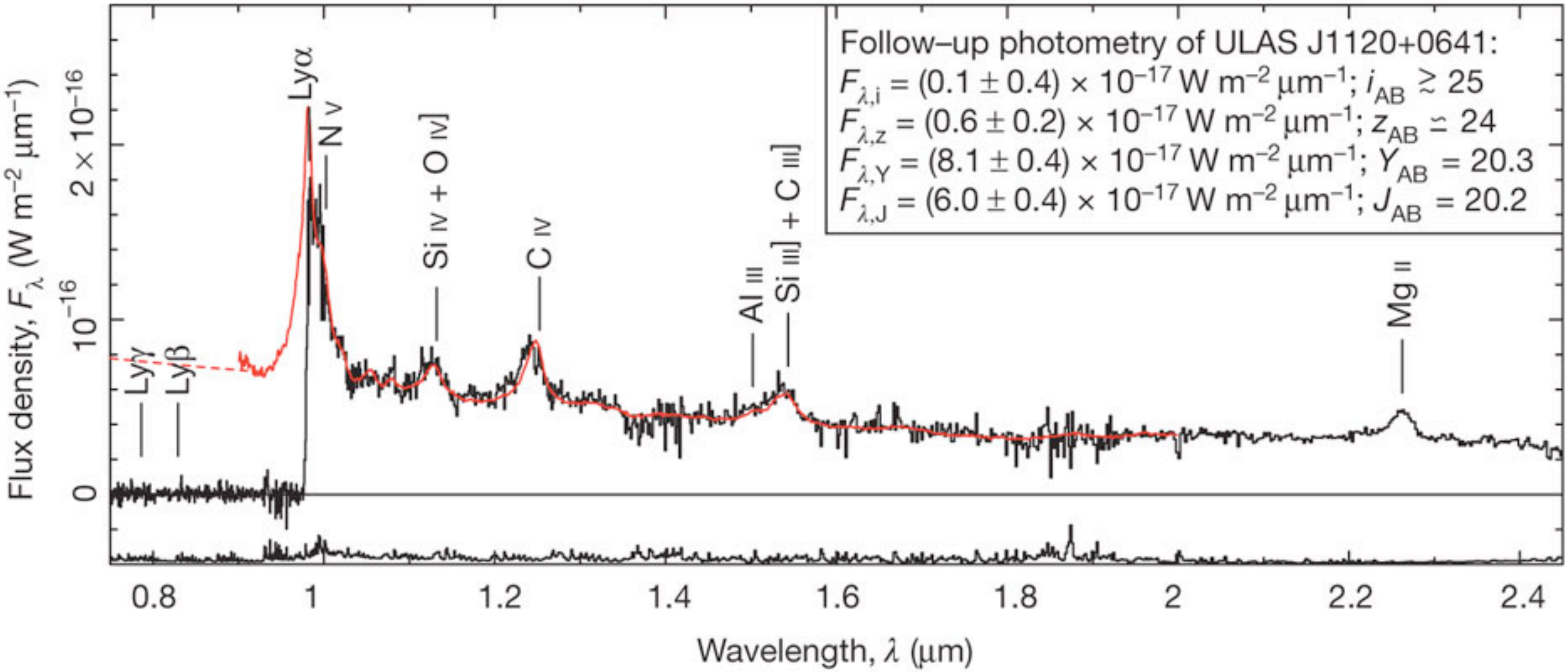

Mortlock et al. 2011

Comparison with other high z QSOs: is this an indication of reionization?

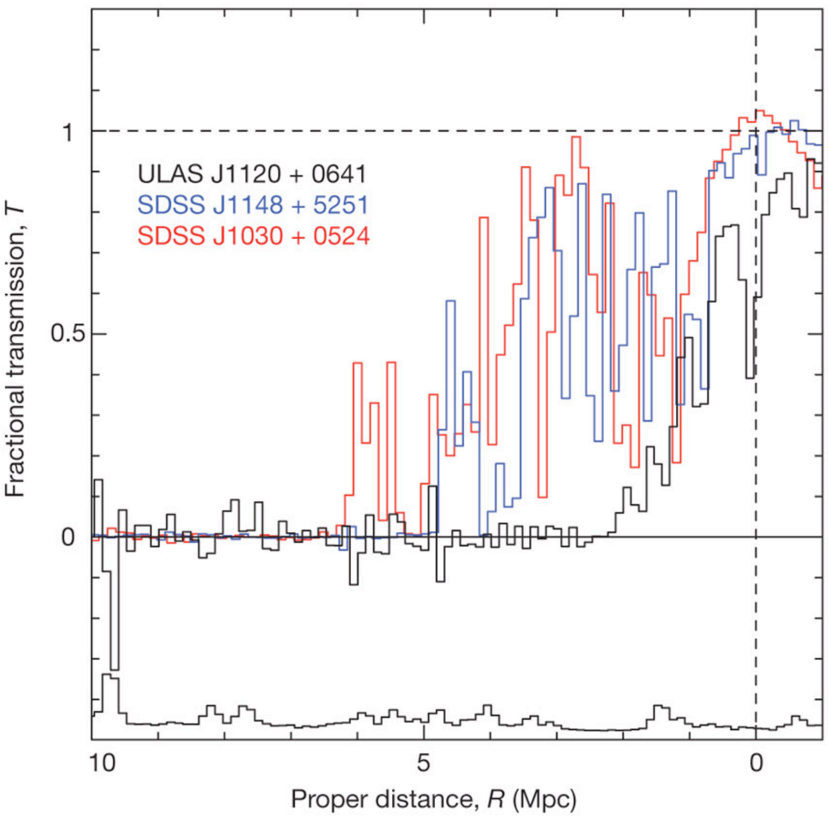

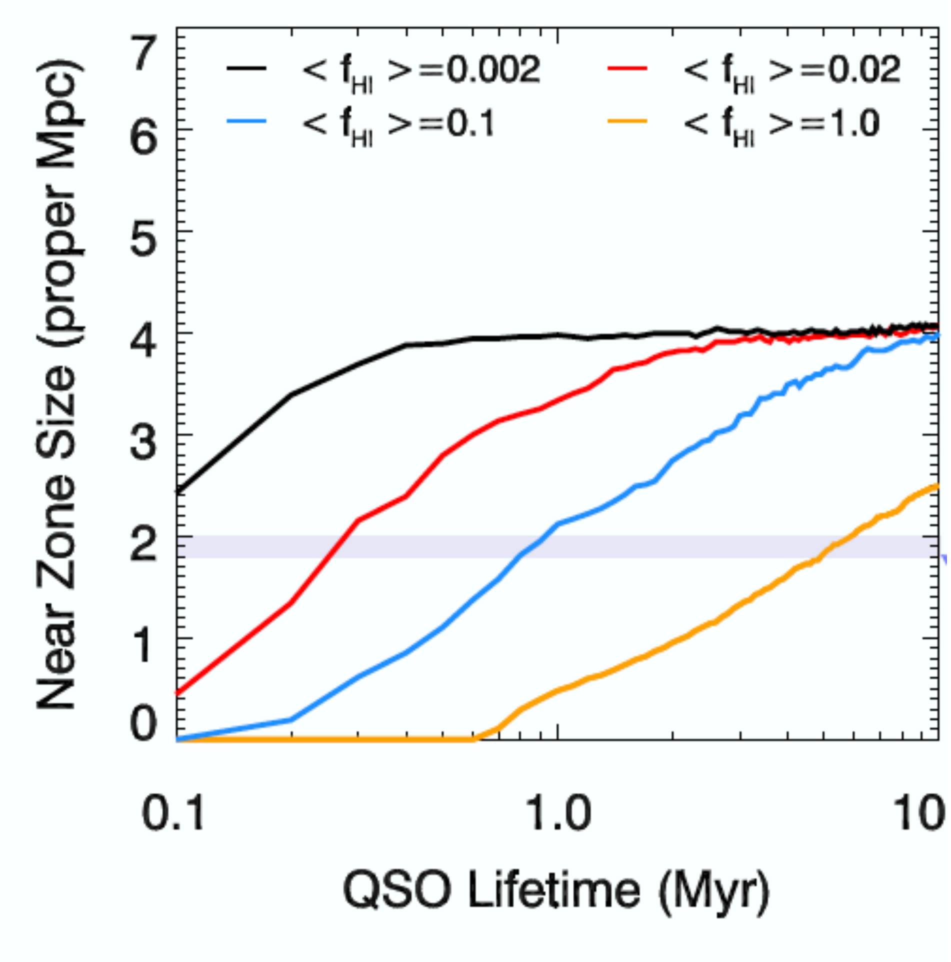

Lyman alpha emitters

- High redshift galaxies with high fraction of flux in Lyman alpha
- They are relatively dust free
- Selected through narrow band filters (Subaru has been very useful for these studies)
- They probe reionization because their abundance is expected to decrease with higher fraction of neutral hydrogen due to scattering. Their clustering is also used to measure the neutral fraction.
- They apparently live in relatively low mass haloes (10^{10}-10^{11} M_{sun})

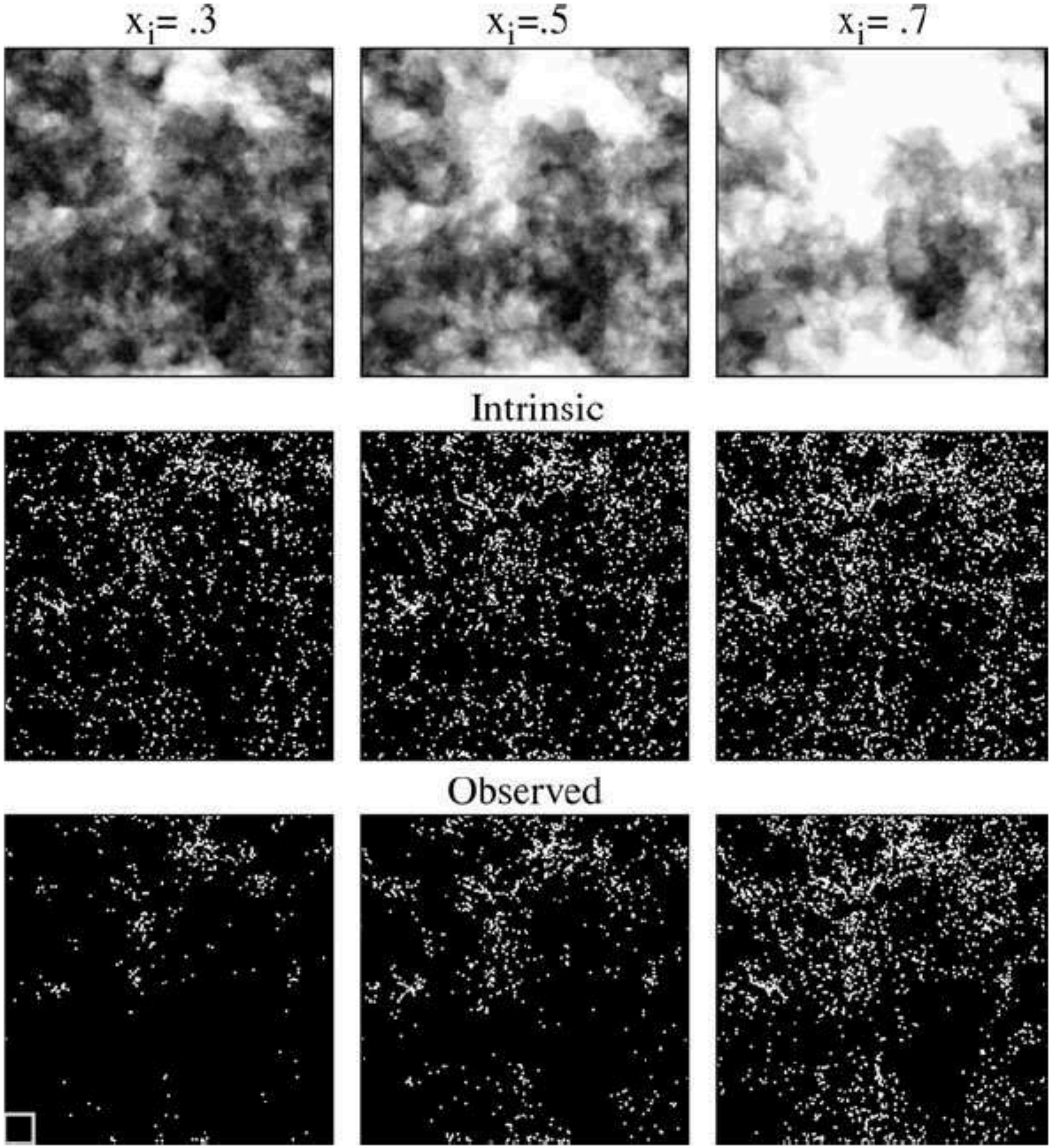

- Luminosity Func.
- Clustering
- Line Profile

McQuinn + 2007

Example

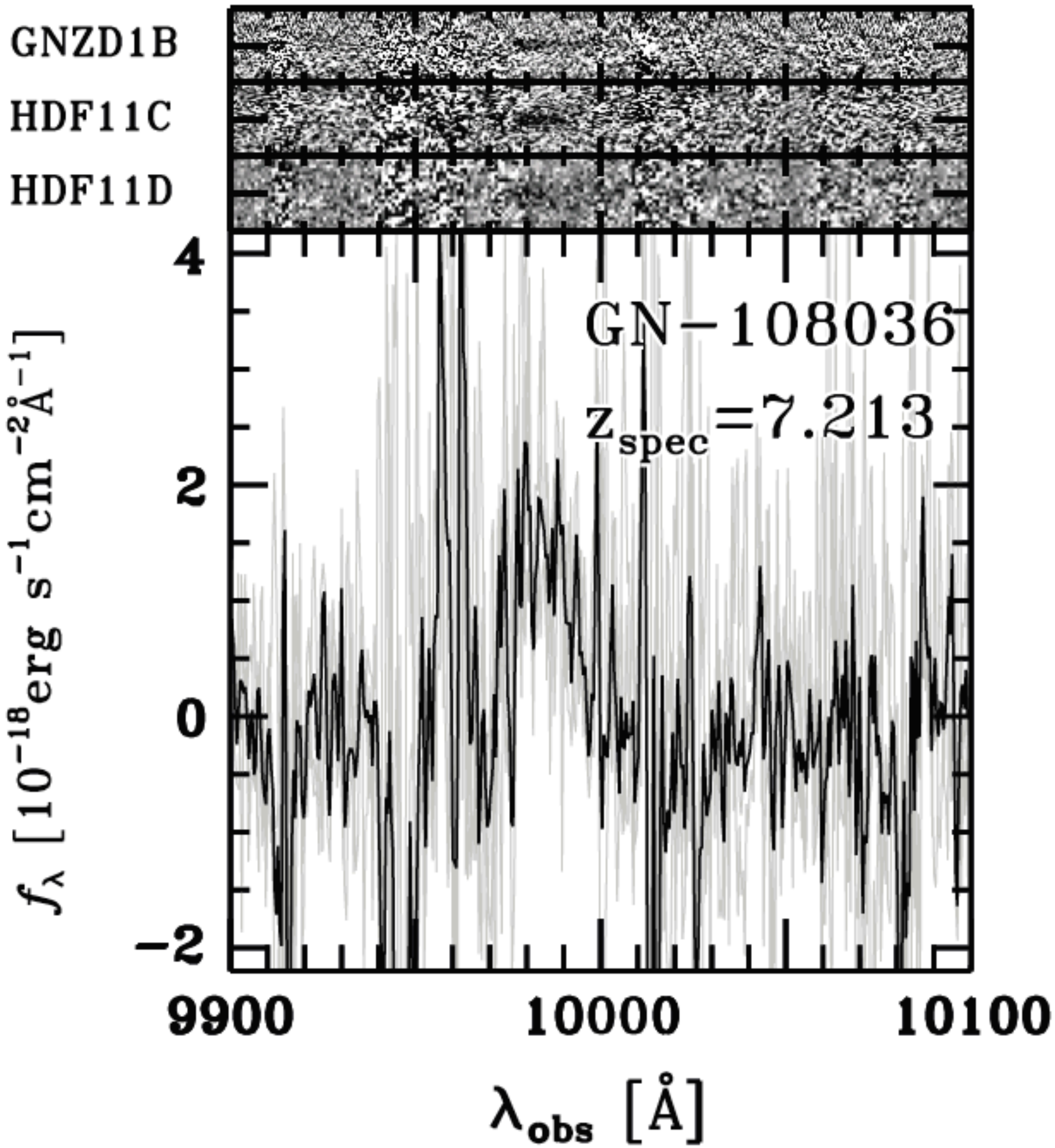

Ono et al, 2012

Lyman-α emitters

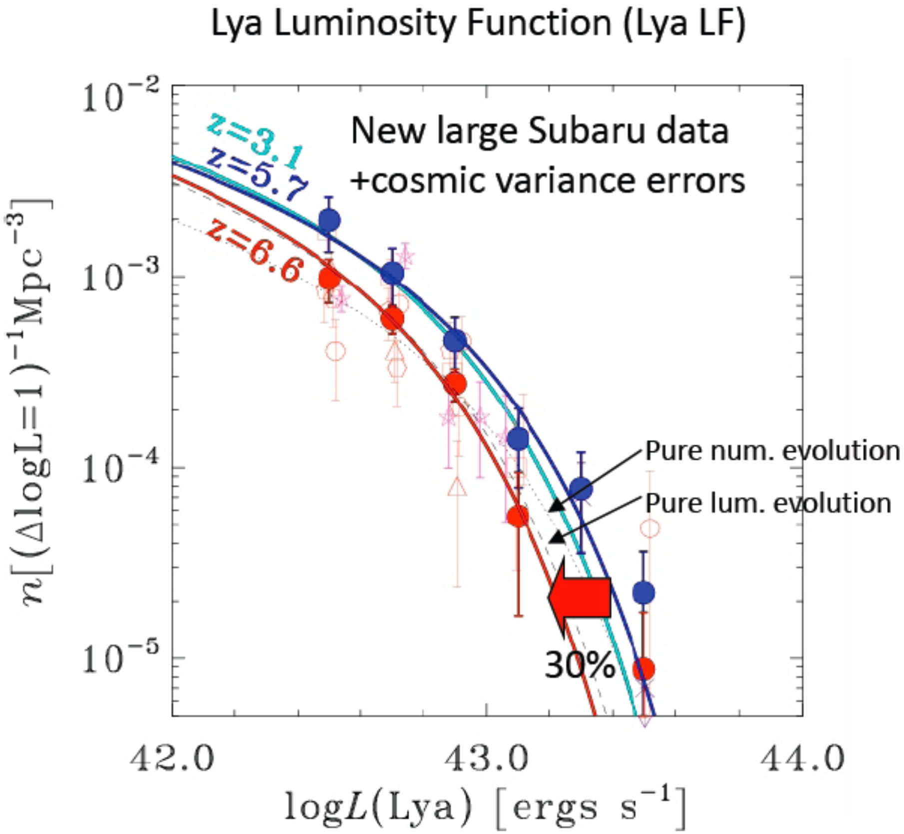

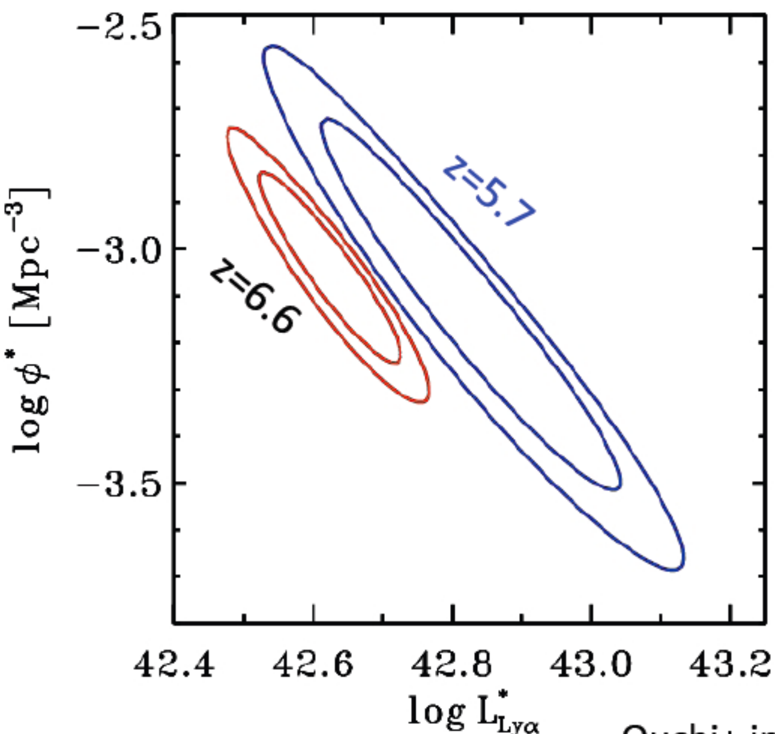

Ouchi+ in prep

Drop in the Ly-α emitters fraction at z=6-7

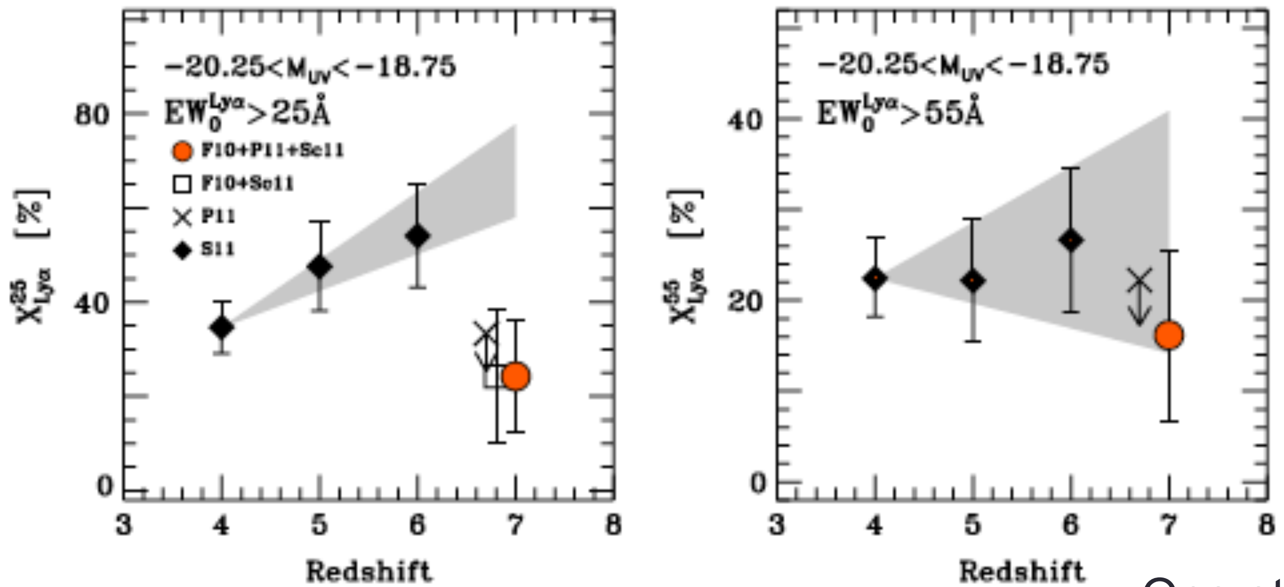

Ono et al, 2012

1. Evolution in the Neutral HI fraction
2. Evolution in the Galaxy properties
3. Evolution on the ionizing background
4. other

The IGM Temperature Evolution

Most of the absorption is caused by quasilinear densities that follow a simple equation of state:

$$T = T_0 \left(\frac{\rho}{\bar{\rho}}\right)^{\gamma-1}$$

Since cooling time is long these absorption lines retain information about the thermal history of the IGM

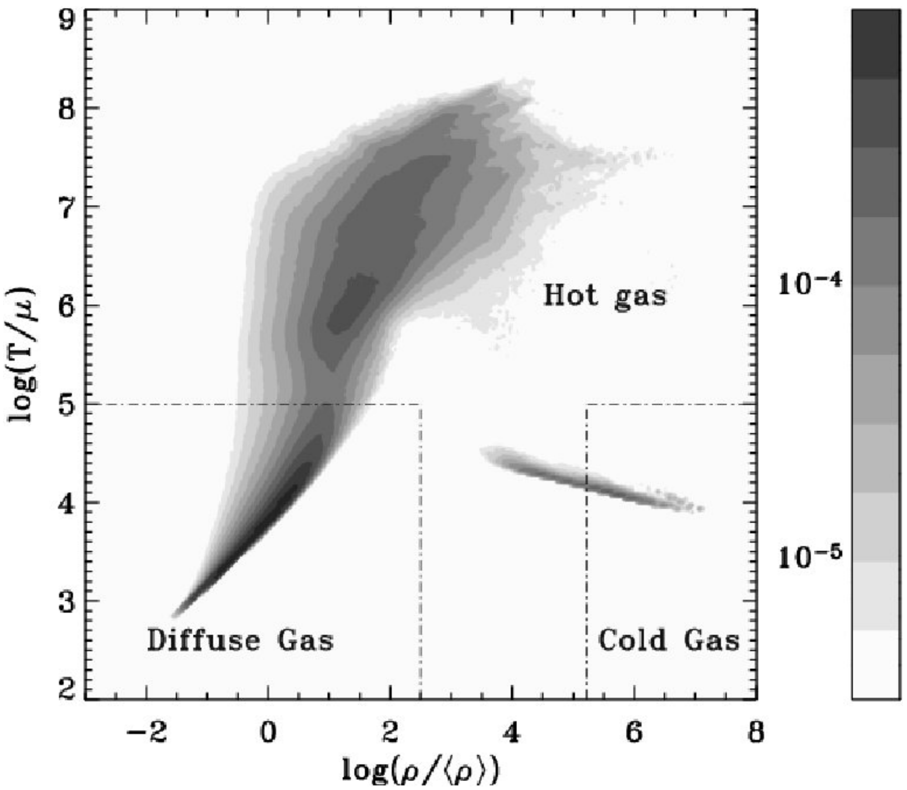

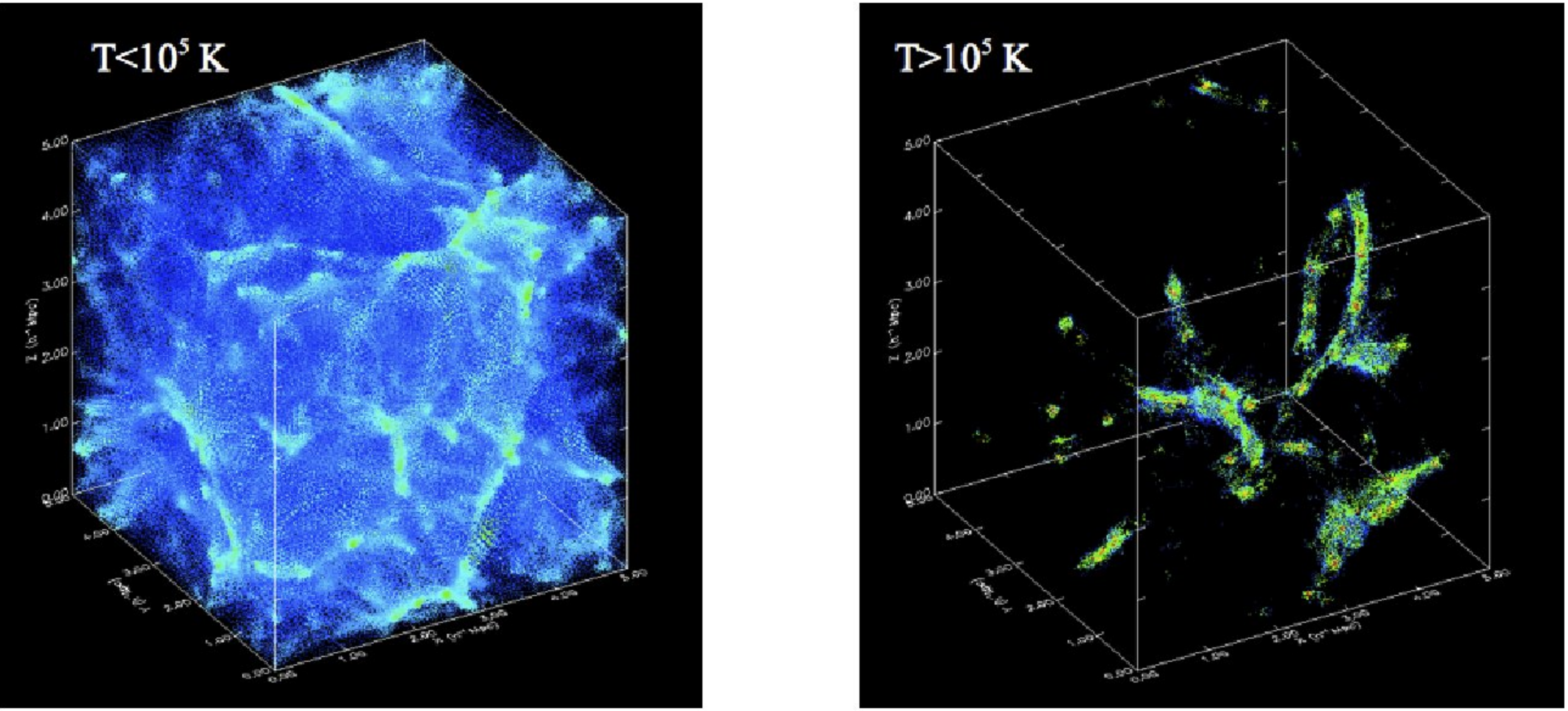

Efstathiou et al 1999

Measurement of IGM Temperature: Wavelet estimate of width of lines

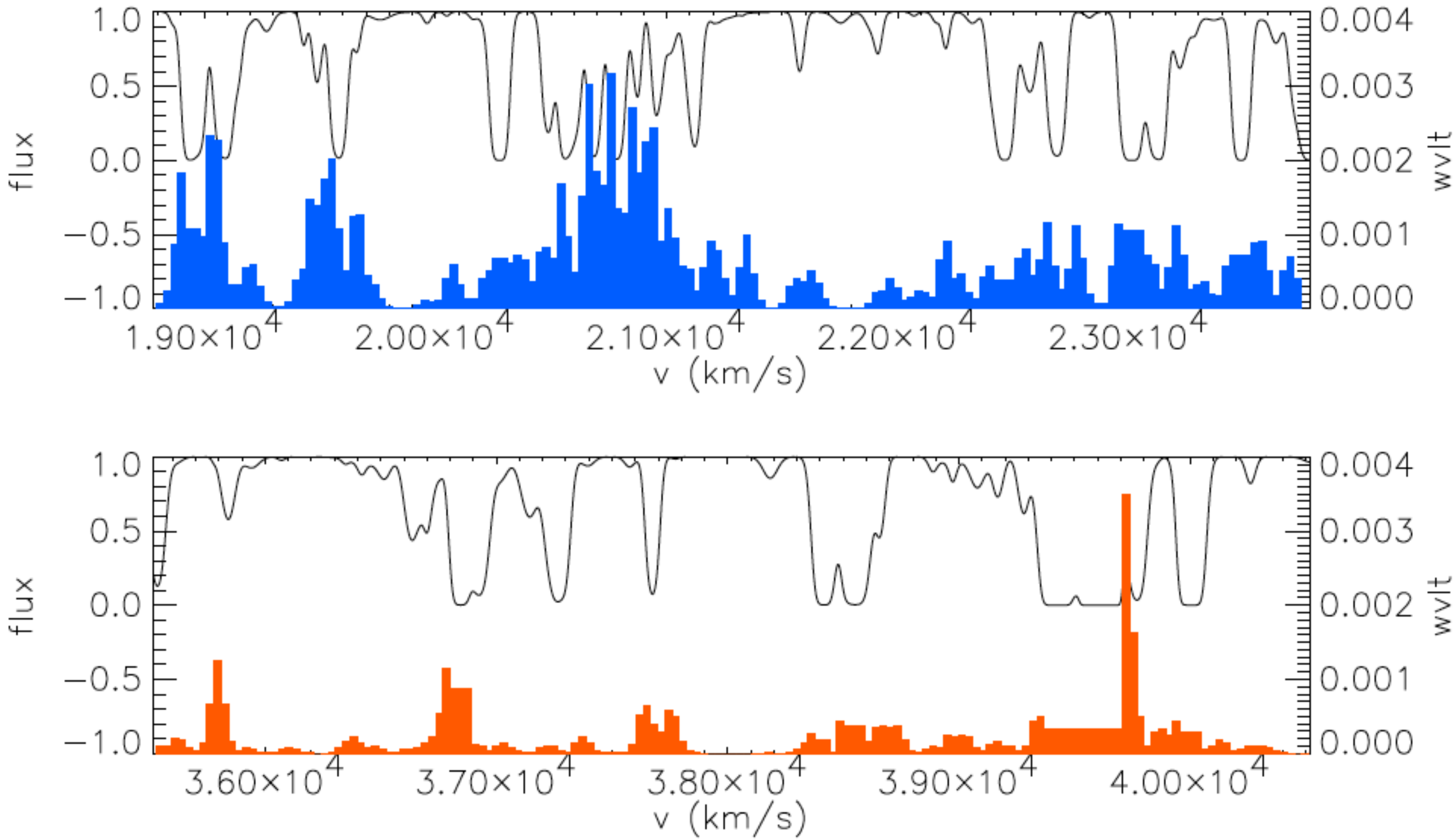

Theuns & Zaroubi 2001

The IGM temperature at low z

$$\frac{1}{T_0}\frac{dT_0}{dt} - \frac{1}{\mu}\frac{d\mu}{dt} = -2H_0 + \frac{\mu\Delta_\epsilon}{-\frac{3}{2}k_B T_0}$$

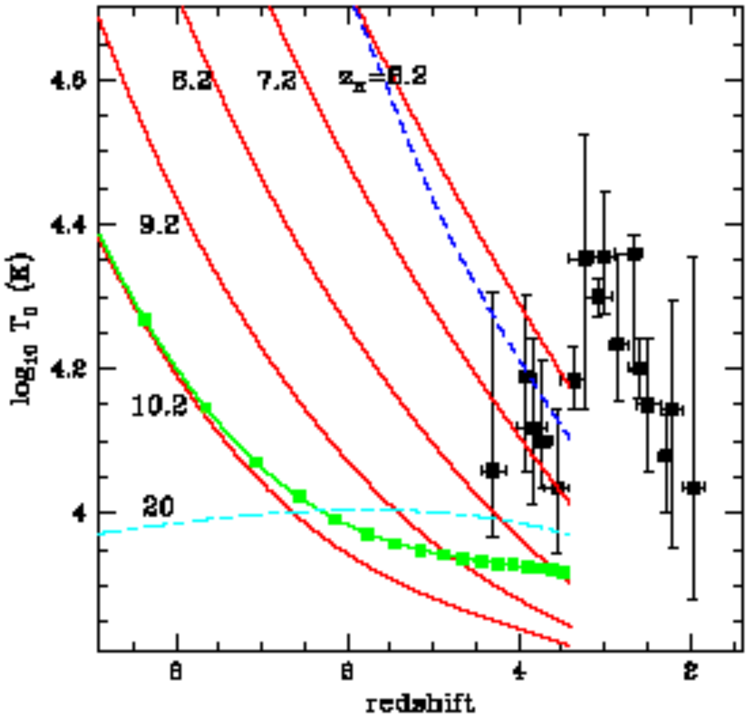

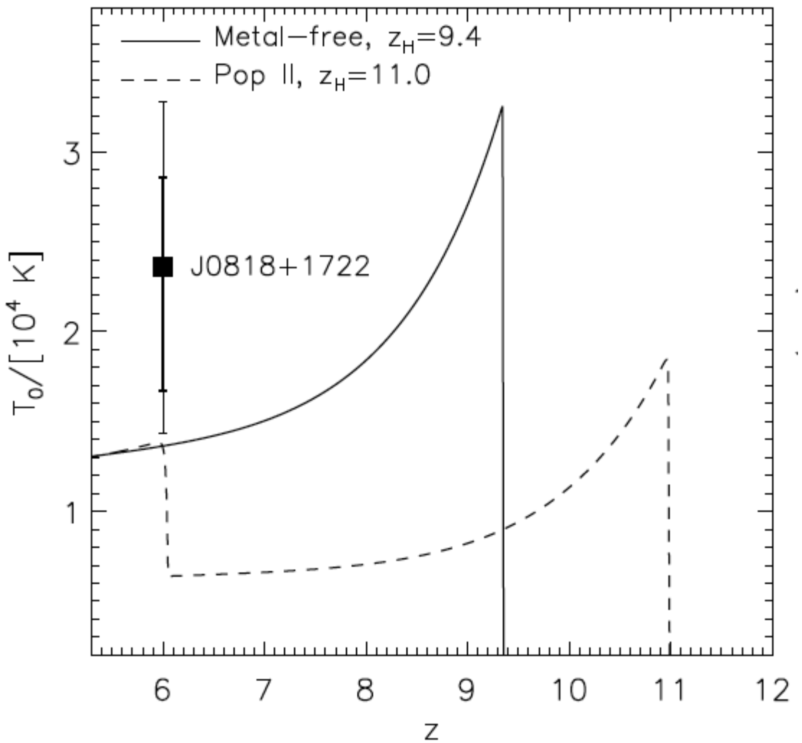

Theuns et al. 2002
Haiman & Hui 2003

Bolton et al. 2010

Measuring the ionizing emissivity

Galaxy surveys: $$\dot{N}_{\rm ion} \propto f_{912/1500} \, \dot{N}_{1500}$$

Lyman-α forest opacity: $$\dot{N}_{\rm ion} \propto \frac{\Gamma_{\rm ion}}{l_{\rm mfp}}$$

Galaxies at z~7-9 HST WPC3 data

WFC3/IR: 850 - 1170nm
2.1 × 2.3 arcmin field of view
0.13 arcsec $pixel^{-1}$
10 times survey power of NIC3

UDF 4.7 $arcmin^2$
60 orbits in YJH
Reaches m_{AB}~29 (5σ)

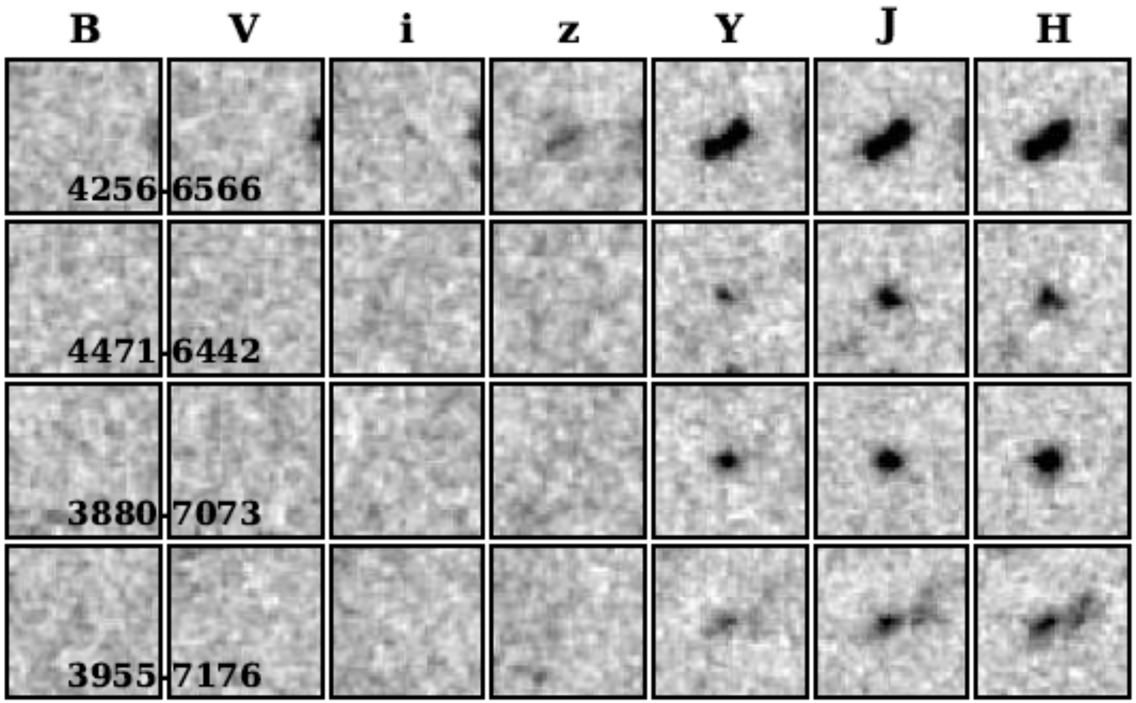

Oesch et al 2010
Bouwens et a. 2010

Galaxies

Galaxies appear to become bluer and show more Lyα with decreasing luminosity and increasing redshift.

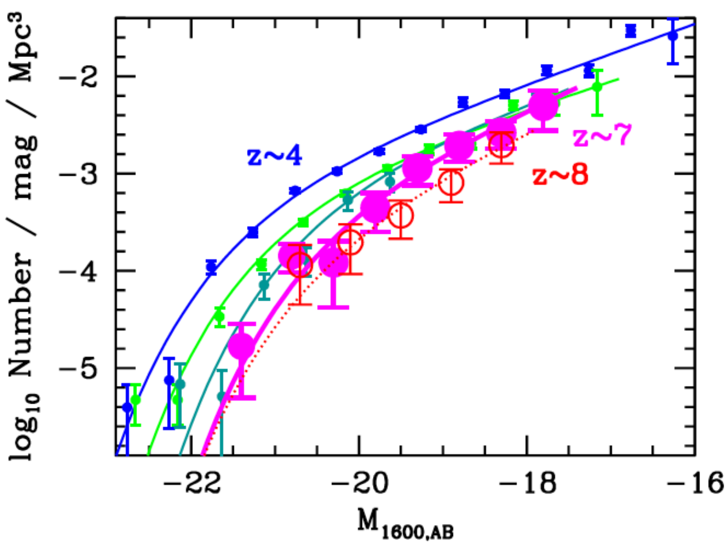

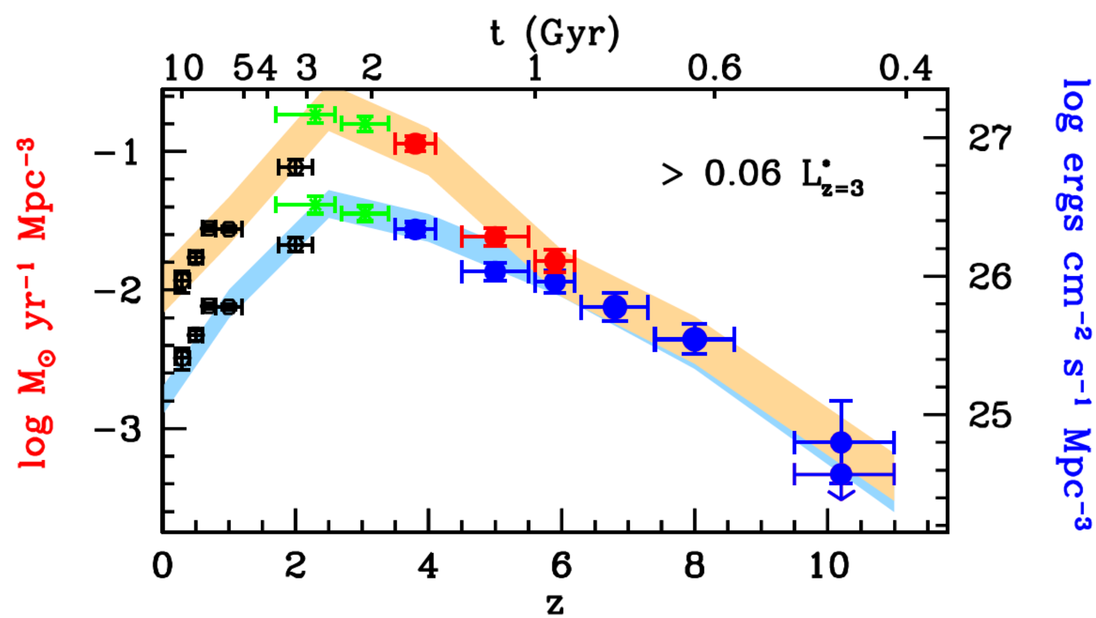

Bouwens et al. 2010

The current status: Star formation history.

f_{esc}=0.2, ξ_{ion} (β=-2), and LF down to M_{UV}=-13

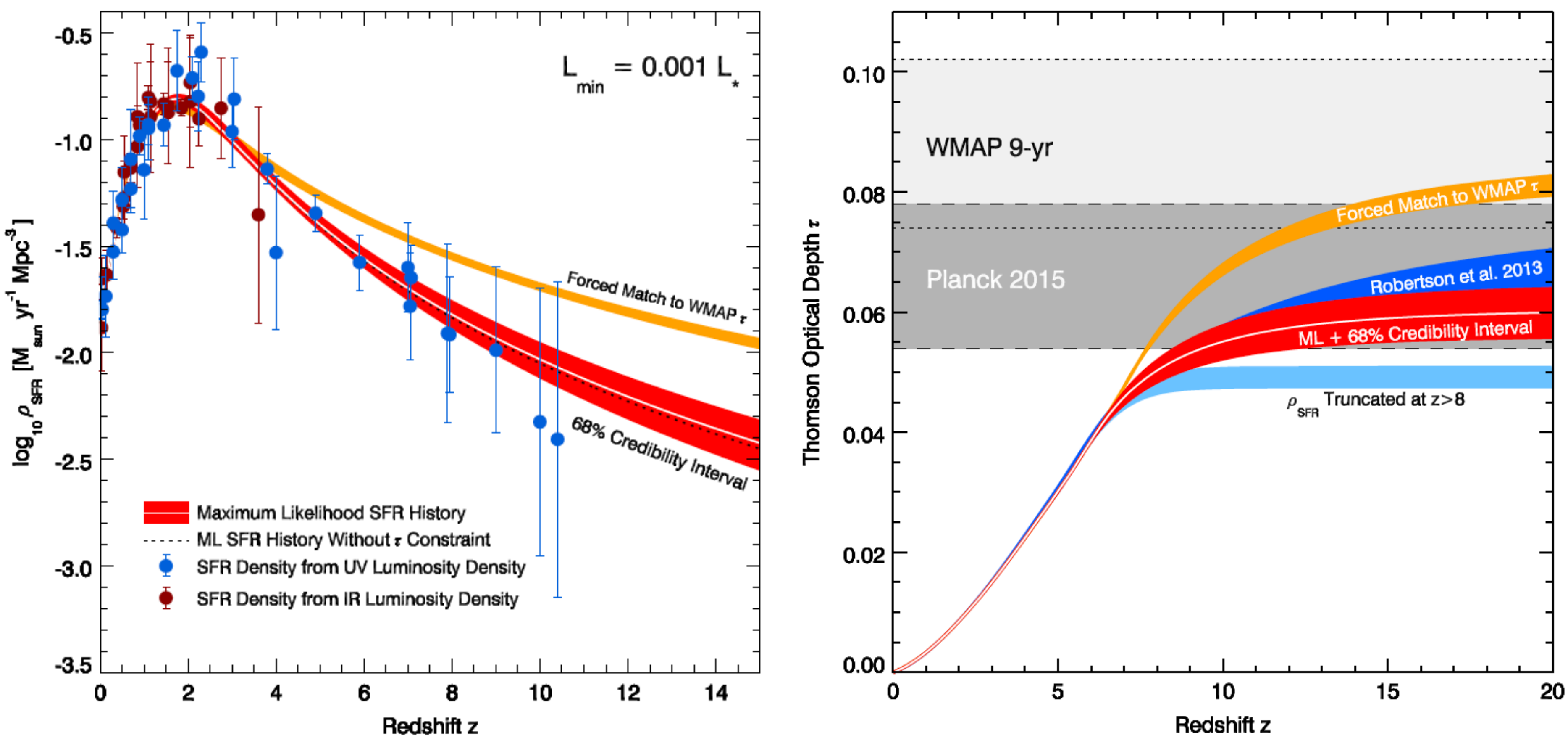

Implies rapid reionization

Robertson et al. 2015

Opacity of the IGM: Photon starved reionization

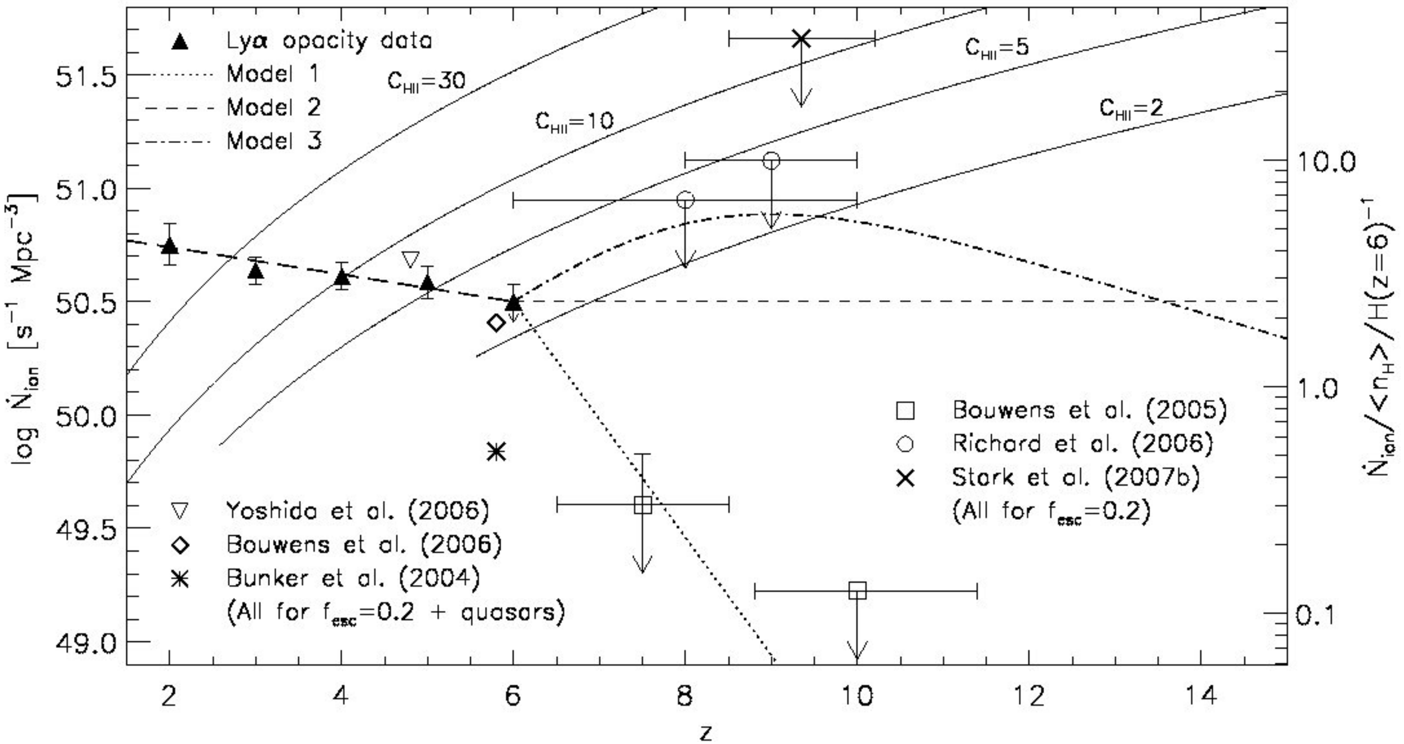

Implies slow reionization!!!!!!

Bolton & Haehnelt 2007

Are we missing photons?

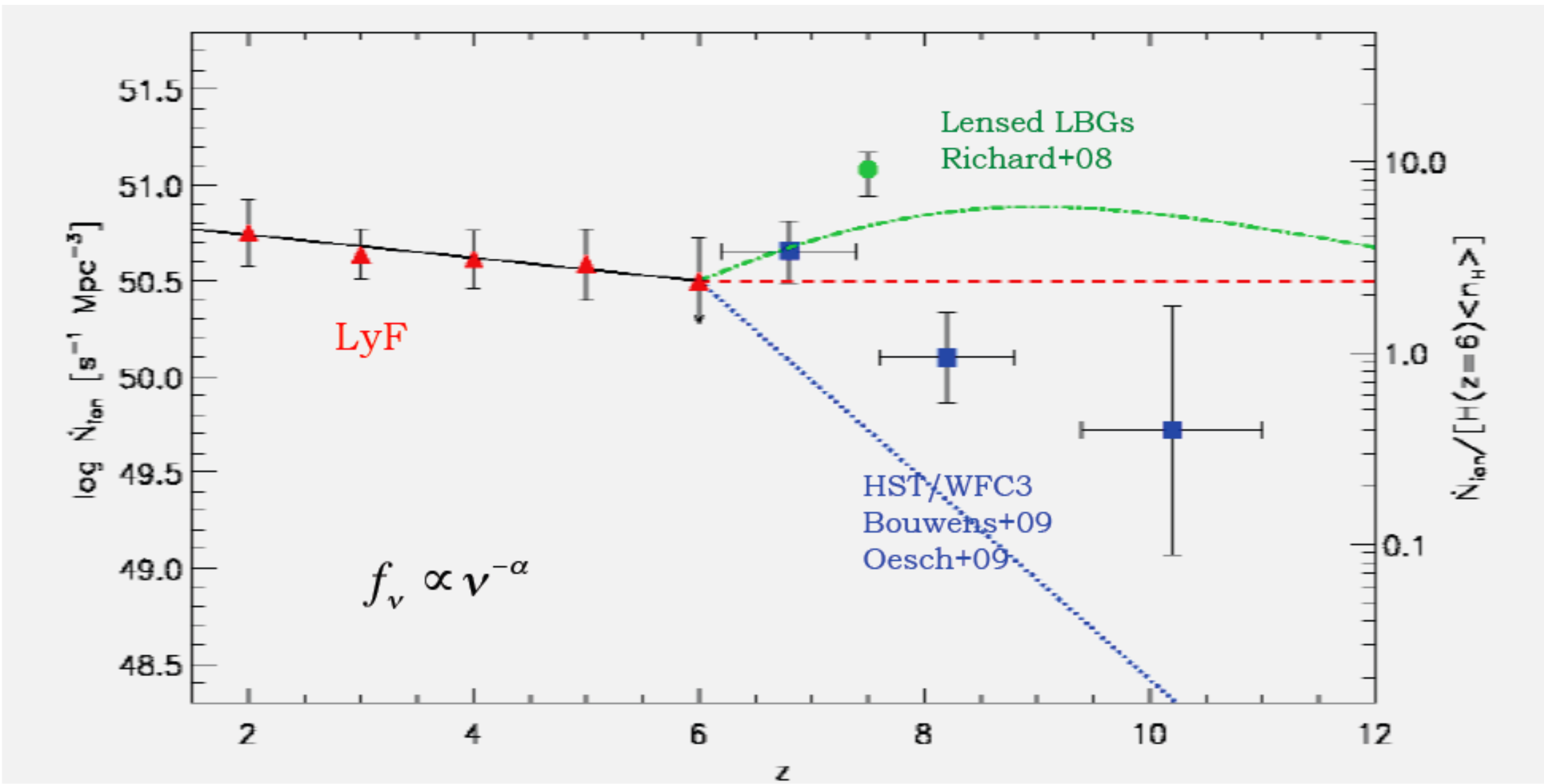

Courtesy of M. Haehnelt

The Current state of affairs

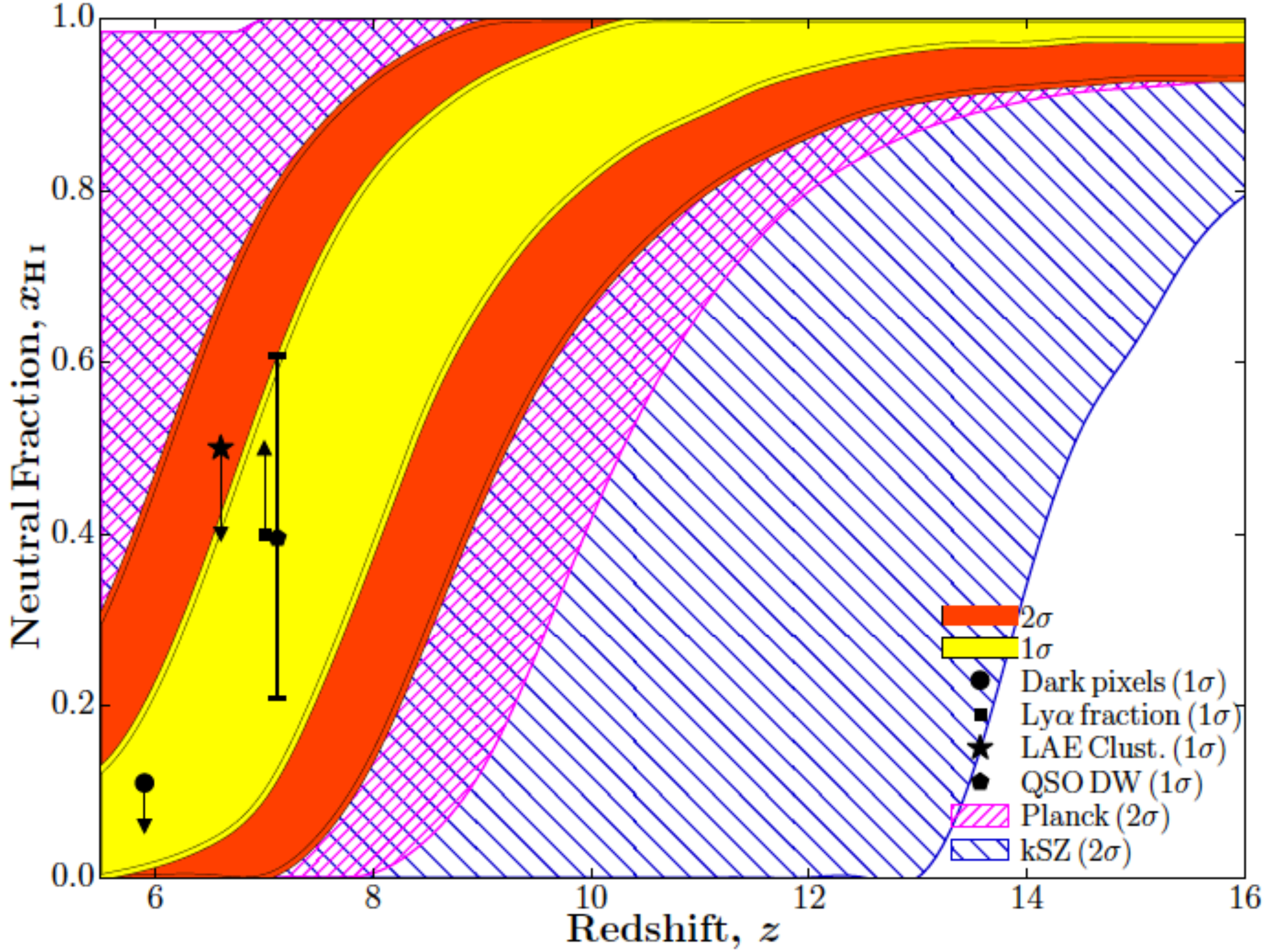

Greig & Mesinger 2016

The 21 cm probe

Historic overview

- H.C. van de Hulst (inspired by J. Oort) showed the potential of the 21 cm transition in astronomy - 1945
- The first astronomical observation of the 21 cm: H.I. Ewen & E.M. Purcell (1951, Nat. 168, 356)

C.A. Muller & J.H. Oort (1951, Nat. 168, 357-8)

- Excitation mechanism Wouthuysen (1952). Field (1958, 1959) gave the proper framework.
- Importance for cosmology was inspired by Zel'dovich's top down scenario.
- Scott & Rees (1992) pointed out that a signal could detected from high z 21 cm.
- Madau, Meiksin & Rees (1997) were the first to consider the interplay between the first sources and the 21 cm transition.
- Over the years many observational attempts failed. Shaver et al. 1999 argued that we can observe high redshift 21 cm radiation.

21-cm Physics

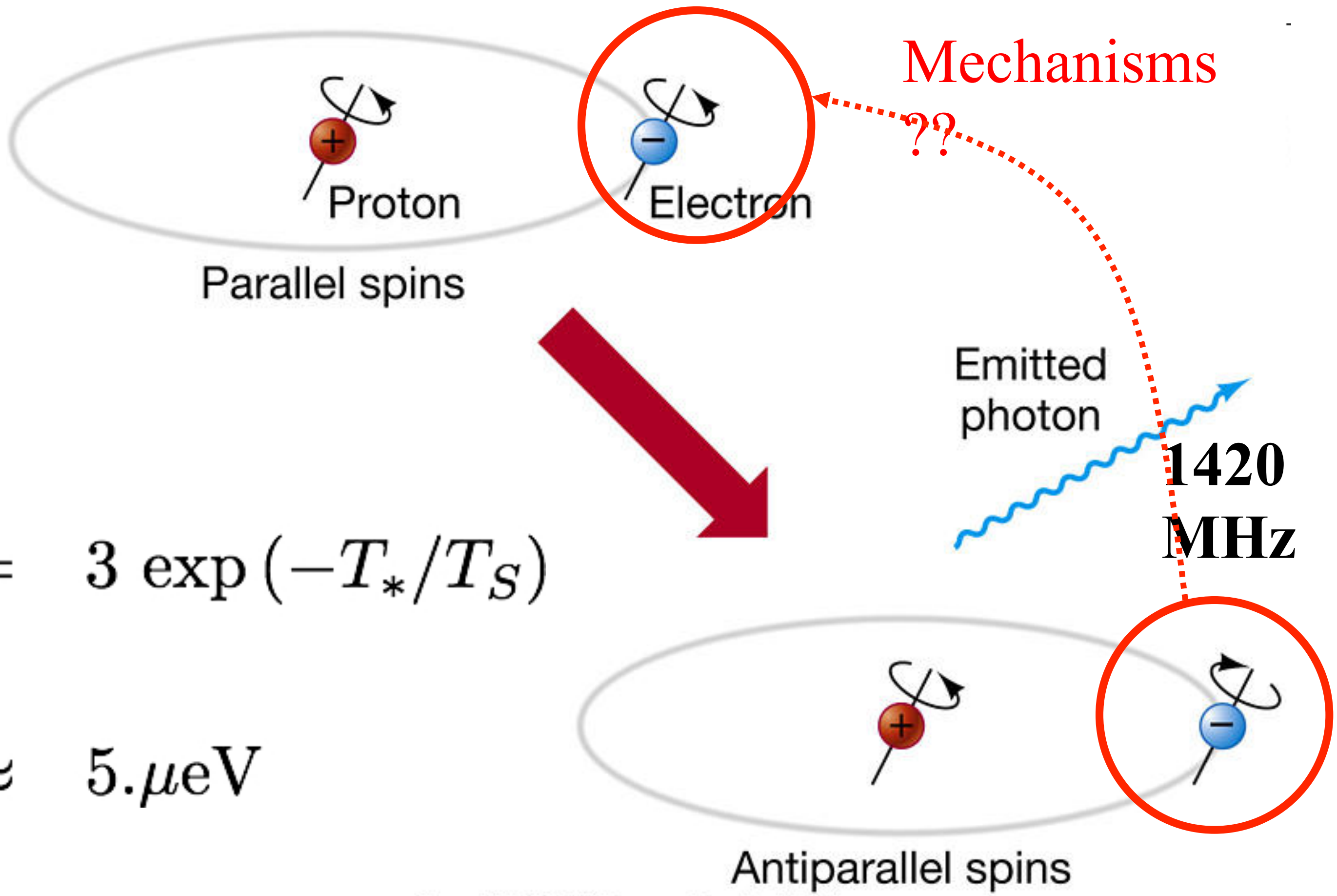

$$\frac{n_1}{n_0} = 3\exp\left(-T_*/T_S\right)$$

$$T_* \approx 5.\mu\text{eV}$$

Lifetime of ~10 Myrs

The 21 cm transition

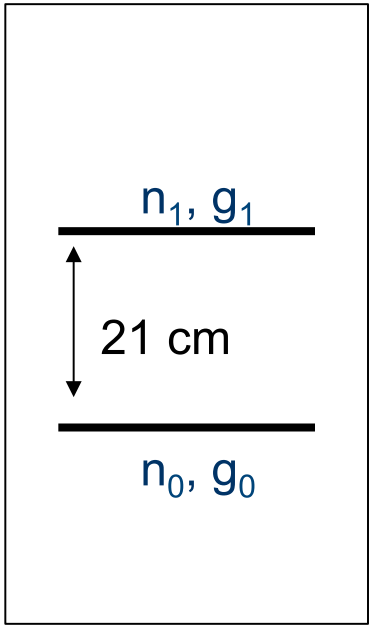

- The value of the T_s is given by:

$$T_s^{-1} = \frac{T_{CMB}^{-1} + x_c T_k^{-1} + x_\alpha T_k^{-1}}{1 + x_c + x_\alpha}$$

Field 1958
Madau et al 98
Ciardi&Madau 2003

Lyman-α Coupling

- The Wouthuysen-Field effect, also known as Lyman-alpha pumping.

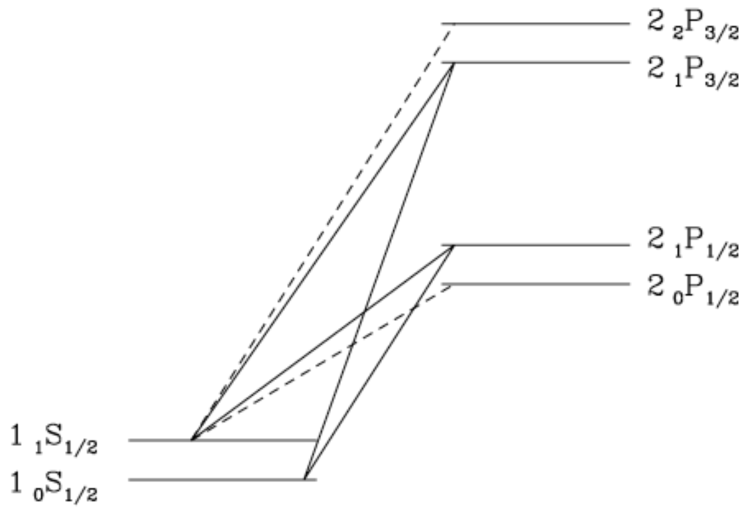

Dominant in both in the case of stars and Black-holes, due to photo and collisional excitations, respectively.

Wouthuysen 1952
Field 1958

of the larger component. Because of the slight depth of eclipse and the trouble with comparison stars, the above results by themselves cannot be considered as anything more than suggestive. However, E. F. Carpenter's observations taken in the blue, yellow, and ultra-violet on this night and the preceding one, show this effect very clearly and leave little doubt of its reality.

It should further be noted that if the present fragmentary results prove to be a fair sample, the system is free from those erratic light changes which add such complexities to the interpretation of other systems of this sort.

Flower and Cook Observatories,
University of Pennsylvania.

Woolard, Edgar W. A comparison of Brown's Lunar Tables with the theory from which they were constructed.

For 60 dates at half-day intervals, from 1948 April 24.0 to May 24.0 UT, the longitude and latitude of the moon to two decimals of a second of arc and the parallax to three decimals were taken from Brown's tables and compared with values that had been computed to 5 decimals directly from Brown's theoretical expressions by the Selective Sequence Electronic Computer of International Business Machines Corporation.

Significant differences between the SSEC and the tabular values were evident in the longitude and in the latitude. The discrepancy in the longitude is very small but is systematic, the principal part apparently having a period of about a month, with an amplitude of the order of 0″.1; the discrepancy in the latitude is strongly periodic, with an amplitude about 0″.15 and a period about a month.

An analysis of these differences to determine their source appeared advisable. The SSEC computations were therefore compared in detail with the tabular computations for the longitude on 14 selected dates, and for the latitude on 12 of these dates. The differences are for the most part satisfactorily accounted for by approximations and expedients adopted by Brown and Hedrick in the construction of the tables to facilitate their practical use, and are within the standards of accuracy that were set for the tables. The large discrepancy in the latitude, however, is principally due to an oversight in the tables; in constructing the tables, the effect of the long period variations of the lunar inclination upon several of the large terms in the latitude was inadvertently included twice.

The resulting error in the tabular latitude is large enough to be detected in observations; it has been found in a comparison of the tabular latitude with the observed latitude obtained with the 6-inch transit circle at the U. S. Naval Observatory during 1929–1949.

U. S. Naval Observatory,
Washington, D. C.

Wouthuysen, S. A. On the excitation mechanism of the 21-cm (radio-frequency) interstellar hydrogen emission line.

The mechanism proposed here is a radiative one: as a consequence of absorption and re-emission of Lyman-α resonance radiation, a redistribution over the two hyperfine-structure components of the ground level will take place. Under the assumption—here certainly permitted—that induced emissions can be negelcted, it can easily be shown that the relative distribution of the two levels in question, under stationary conditions, will depend solely on the shape of the radiation spectrum in the Lα region, and not on the absolute intensity.

The shape of the spectrum of resonance radiation, quasi-imprisoned in a large gas cloud, could only be determined by a careful study of the "scattering" process (absorption and re-emission) in a cloud of definite shape and dimensions. The spectrum will turn out to depend upon the localization in the cloud.

Some features can be inferred from more general considerations. Take a gas in a large container, with perfectly reflecting walls. Let the gas be in equilibrium at temperature T, together with Planck radiation of that same temperature. The scattering processes will not affect the radiation spectrum. One can infer from this fact that the photons, after an infinite number of scattering processes on gas atoms with kinetic temperature T, will obtain a statistical distribution over the spectrum proportional to the Planck-radiation spectrum of temperature T. After a finite but large number of scattering processes the Planck shape will be produced in a region around the initial frequency.

Photons reaching a point far inside an interstellar gas cloud, with a frequency near the Lα resonance frequency, will have suffered on the average a tremendous number of collisions. Hence in that region, which is wider the larger the optical depth of the cloud is for the Lyman radiation, the Planck spectrum corresponding to the gas-kinetic temperature will be established

as far as the shape is concerned. Because, however, the relative occupation of the two hyperfine-structure components of the ground state depends only upon the shape of the spectrum near the Lα frequency, this occupation will be the one corresponding to equilibrium at the gas temperature.

The conclusion is that the resonance radiation provides a long-range interaction between gas atoms, which forces the internal (spin-)degree of freedom into thermal equilibrium with the thermal motion of the atoms.

Institute for Theoretical
Physics of the City University,

Zechiel, Leon N. and Geoffrey Keller. A survey of eclipsing binary systems showing apsidal motion.

Thirty eclipsing binary systems of known or suspected apsidal motion were analyzed to determine whether a correlation could be made between the mass distribution within the stars and the spectral type. A set of combined photometric and spectroscopic elements for each system was assembled. Some systems have not been observed spectroscopically, and the values of the eccentricity and the apsidal period had to be estimated from photometric data alone in these cases. The data has been tabulated for all systems which have been adequately observed. Fourteen cases in which apsidal motion has been indicated, but for which the data are insufficient to support detailed analysis, were rejected.

The final sets of elements for each system were analyzed by the method of Sterne, yielding the apsidal coefficients, k_2, which are a measure of the degree of central condensation of the mass of the stars. Values of the effective polytropic index of each star were obtained from the quantities k_2 in the usual manner. The absolute dimensions of the systems were derived from the elements by various methods suited to the data available in each case.

The final results were embodied in a table, and a plot of the effective polytropic index versus the spectral type was made. A similar plot was constructed from the analysis by Russell in 1939. A comparison shows considerable change in the plot due to the reclassification of the spectra of several of the stars and to the inclusion of new data. There appears to be a limitation of n_{eff} to values between 2.9 and 4.1, with the lower values tending to be associated with earlier spectral types. The ratio of central density to mean density is 54 for a polytrope of index 3.0 and 614 for a polytrope of index 4.0. While the stars in this survey were not assumed to be polytropes these two cases represent models having values of k_2 corresponding roughly to the observed range. The spectral types represented in the survey ranged from O8.5 to F2.

Perkins Observatory,
Delaware, Ohio.

TITLES OF ADDITIONAL PAPERS PRESENTED AT THE MEETING IN CLEVELAND, OHIO

Anderson, J. Pamelia. The position of the moon at the time of the 1948 eclipse.
Bidelman, W. P. and W. W. Morgan. A remarkable O-type star.
Binnendijk, L. The space distribution of interstellar material in the Milky Way.
Bok, Bart J. and Margaret Olmsted. Magnitude standards for the southern hemisphere.
Cook, Allan F. II. Radiative equilibrium in a hydrogen atmosphere.
Eckert, W. J., Rebecca B. Jones and H. K. Clark. A precise lunar ephemeris.
Genatt, Sol H. Note on a graphical method for the prediction of occultations.
Goldberg, Leo, R. R. McMath, O. C. Mohler and A. K. Pierce. Identification of *CO* in the solar atmosphere.
Harwood, Margaret. The nova-like variable CM Aquilae.
Henriksen, S. W. Note on the kinematics of the moon's motion.
Johnson, Harold L. Magnitude systems.
McKellar, Andrew, G. J. Odgers and L. H. Aller. The chromospheric K-line during the recent eclipse of 31 Cygni.
Mears, D. D. Field techniques for occultation observation.
Millis, John. The genesis of Saturn and its rings.
Neyman, J. and C. D. Shane. A model of spatial distribution of galaxies. Preliminary report.
O'Keefe, John A. and J. Pamelia Anderson. Calculation of the earth's radius from occultation data.
Osterbrock, Donald A. The time of relaxation for stars in a fluctuating density field.
Panay, T. N. and John A. O'keefe. Progress on the measurements of darkening at the sun's limb from the results of the 1948 eclipse.
Scott, Elizabeth R. Theoretical counterparts of certain observable distributions relating to galaxies.
Swope, Henrietta H. Photographic magnitudes and colors in the globular cluster NGC 6397.
Thomsen, Warren J. The path and orbit of the detonating meteor of August 29, 1951.
White, Marvin S. Note on the accuracy of Hayn's charts as measured by photoelectric observation.
Wrubel, Marshal H. On the decay of a primeval stellar magnetic field.
Wylie, C. C. The path and orbit of the detonating meteor of July 28, 1951.

Collisional Coupling

- H-H collisions that excite the 21 cm transition. This interaction proceeds through electron exchange.
- H-e collisions. Especially important around primordial X-ray sources (mini-quasars).
  - This effect might also excite Lyman-alpha transition which adds to the T_s- T_{CMB} decoupling efficiency.

δT_b, The Brightness Temperature

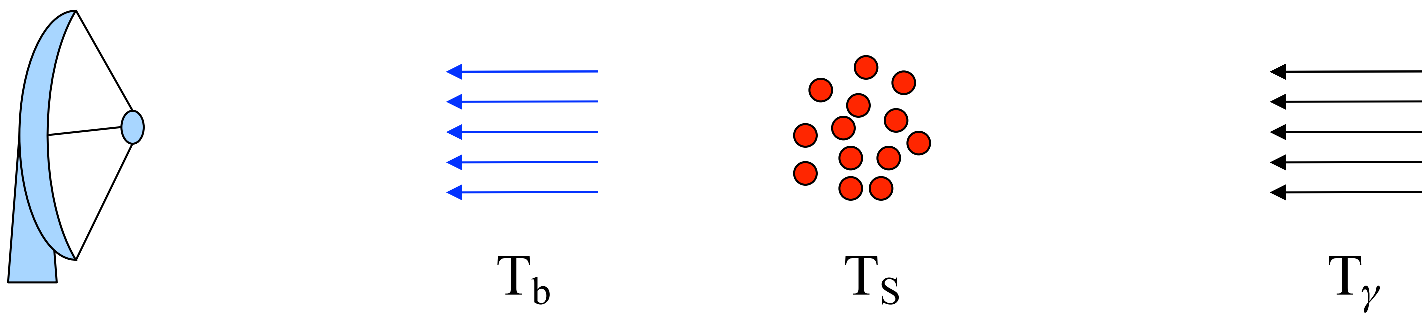

$$T_b(\nu) = T_S\left(1 - e^{-\tau_\nu}\right) + T_\gamma(\nu) e^{-\tau_\nu}$$

$$\delta T_b(\nu) \equiv T_b - T_\gamma = (T_S - T_\gamma)\left(1 - e^{-\tau_\nu}\right)$$

Where the optical depth is given by:

$$\tau_\nu = \int \mathrm{d}s\, \sigma_{01}\left(1 - e^{-E_{10}/k_B T_S}\right) \phi(\nu)\, n_0$$

$$\tau_\nu \approx \sigma_{01} \left(\frac{h\nu}{k_B T_s} \right) \left(\frac{N_{HI}}{4} \right) \phi(\nu)$$

$$\sigma_{01} \equiv \frac{3c^2 A_{10}}{8\pi\nu^2}$$

$A_{10} = 2.85\text{x}10^{-15}\ s^{-1}$ is the spontaneous emission coefficient.
N_{HI} is the column density of HI; 4 accounts for fraction in singlet state
$\phi(\nu)$ is the line profile.
An accurate calculation of the optical depth at a given redshift, which takes into account line profile broadening due to Hubble expansion and casts the relation in terms of number density, yields:

$$\begin{aligned} \tau_{\nu_0} &= \frac{3}{32\pi} \frac{hc^3 A_{10}}{k_B T_S \nu_0^2} \frac{\mathrm{x}_{HI} n_H}{(1+z)\left(\mathrm{d}v_\parallel/\mathrm{d}r_\parallel\right)} \\ &\approx 0.0092\,(1+\delta)\,(1+z)^{3/2}\,\frac{\mathrm{x}_{H\,I}}{T_S}\left[\frac{H(z)/(1+z)}{\mathrm{d}v_\parallel/\mathrm{d}r_\parallel}\right] \end{aligned}$$

δT_b: Brightness temperature

$$\delta T_b \approx 28\mathrm{mK}\,(1+\delta)\,x_{HI}\,\frac{T_s - T_{CMB}}{T_s}\,\frac{\Omega_b h^2}{0.02}\left[\frac{0.24}{\Omega_m}\left(\frac{1+z}{10}\right)\right]^{\frac{1}{2}}$$

Astrophysics

Cosmology

- The Interpretation might be very complicated
- Notice that the signal in absorption can be much smaller

The Global evolution of the Spin Temperature

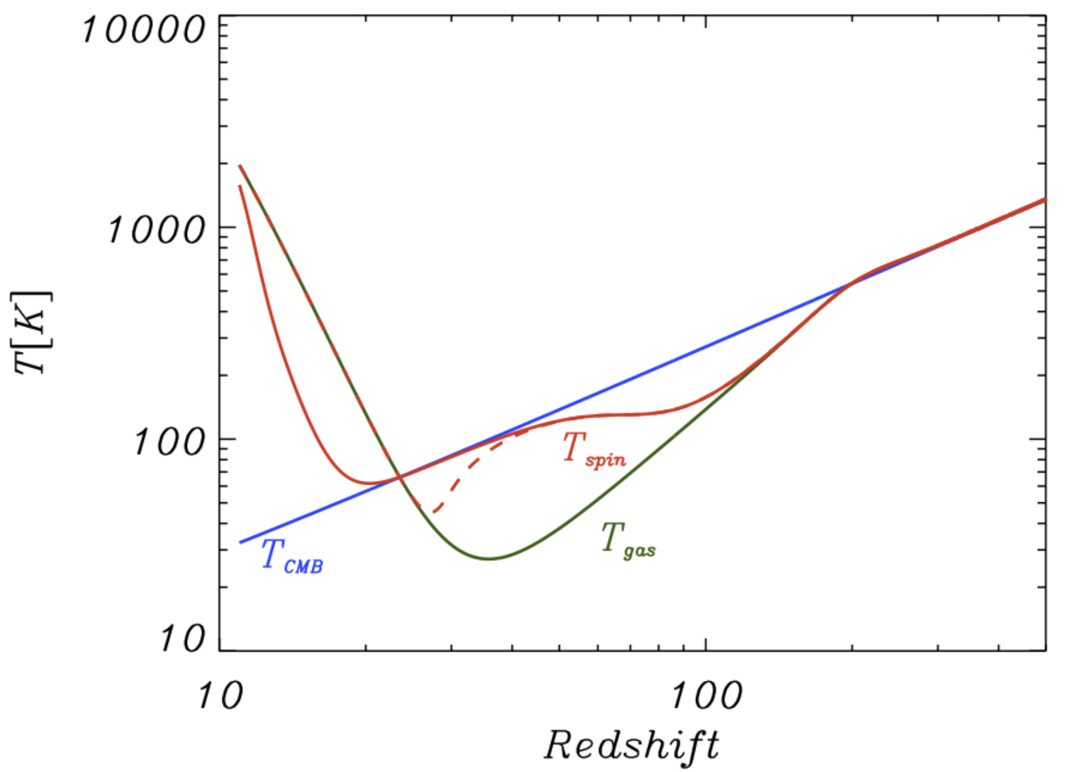

At z~20 T_s is tightly coupled to T_{CMB}. In order to observe the 21 cm radiation decoupling must occur.

Heating much above the CMB temp. and decoupling do not necessarily occur together.

Loeb & Zaldarriaga 2004,Pritchard & Loeb 2008, Baek et al. 2010, Thomas & Zaroubi 2010

The Global Evolution of δT_b

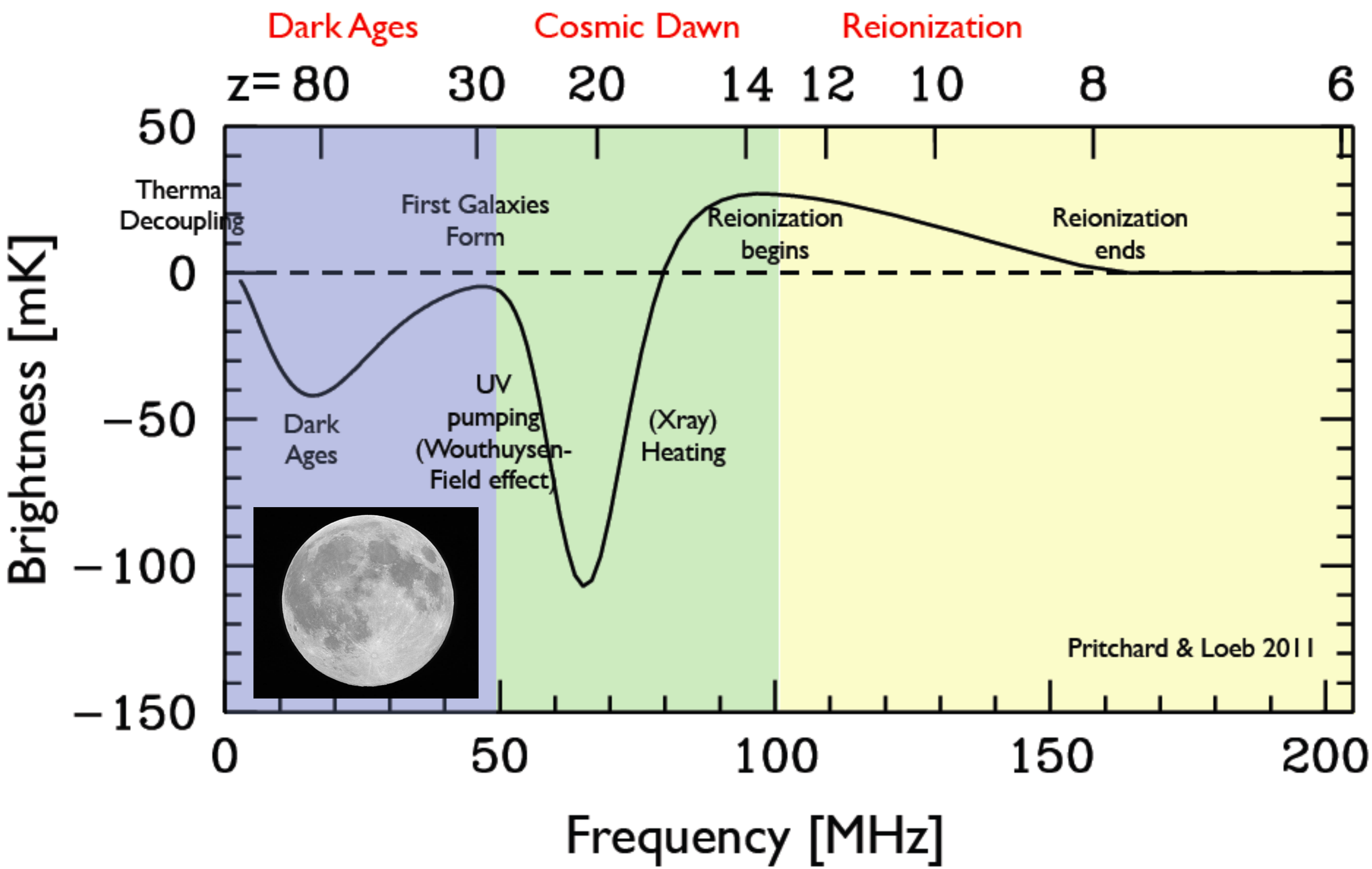

Ionization sources

Mean free path

$$\langle l_E \rangle \approx \frac{1}{n_H \sigma_H(E)}$$

Bound-free
Cross section

$$\sigma_H(E) = \sigma_0 \left(E_0/E\right)^3$$

$$n_H = 2.2 \text{ x } 10^{-7}\ \text{cm}^{-3}\ (1+z)^3$$
$$\sigma_0 = 6 \text{ x } 10^{-18}\ \text{cm}^2$$
$$E_0 = 13.6\ eV$$

At $z = 9$: For $E = E_0$ $\langle l_E \rangle \approx 2$ kpc comoving
For $E = 1$ keV $\langle l_E \rangle \approx 1$ Mpc comoving

UV photons

Large cross section but ejected electron has low energy

X-ray photons

Low cross section but ejected electron has high energy

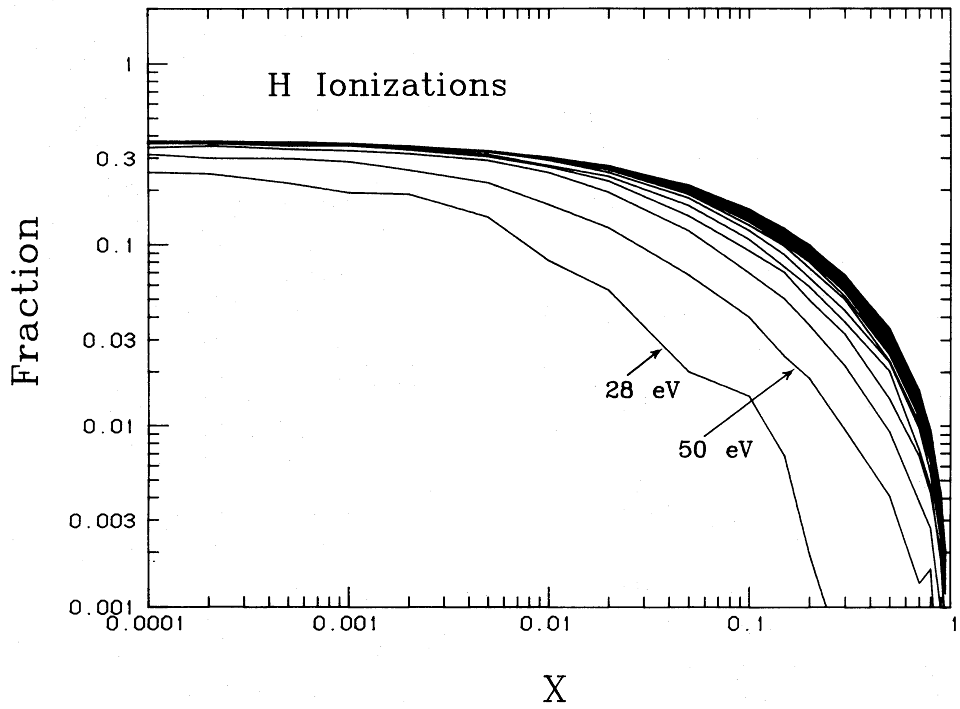

The fraction of photon energy that goes to reionization, heating and excitation is roughly 1:1:1 as calculated with Monte-Carlo radiative transfer code by Shull & van Steenberg (1986) and Valdes et al. 2009.

The signal: Stars vs. Miniqsos

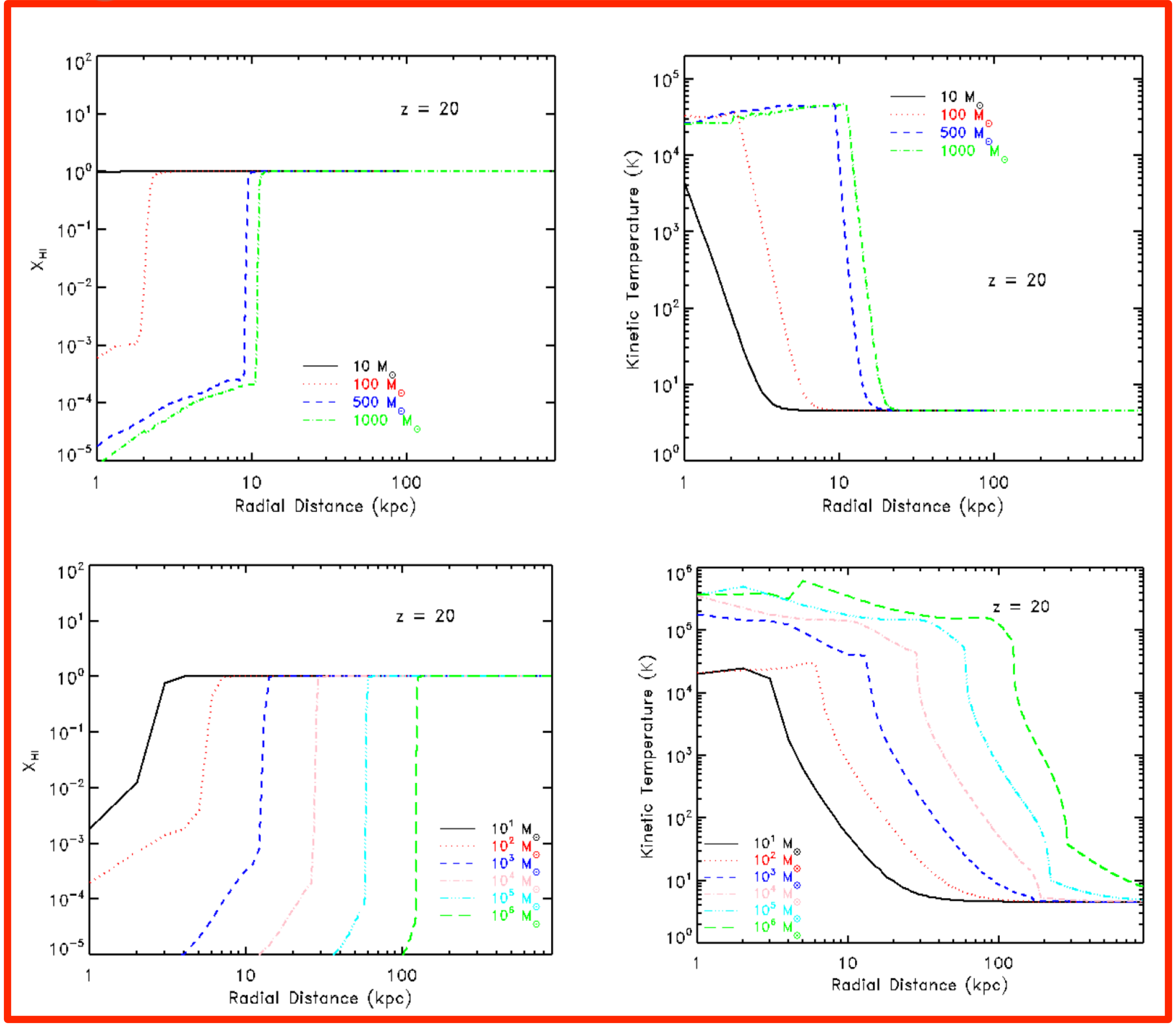

Thomas & Zaroubi 2008

What happens around a high Redshift x-ray source

Kinetic temperature is greatly heated just beyond the HII region, but further out it has been adiabatically cooled.

21cm absorption strongly dominates over the inner emission core

$M_{BH}=10^4\ M_{sun}$

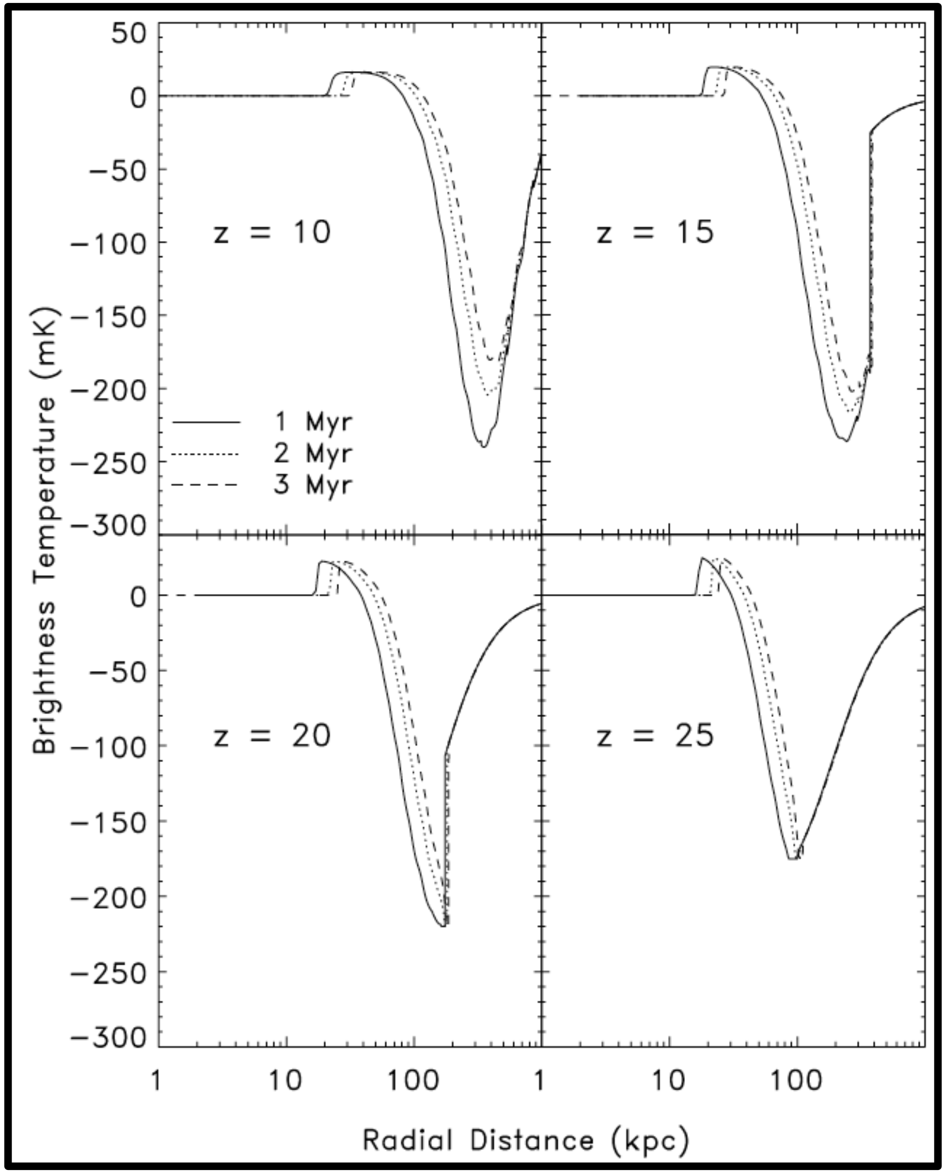

Thomas & Zaroubi 2008

Simulations of the EoR

- Cosmological Hydro simulations:
  1- High enough resolution to resolve halos in which ionization sources form. 2- Span Large Scales as well as small scales, especially since designed arrays have small 1' res. 3- In certain cases DM only simulations are sufficient.
- Out of equilibrium Radiative Transfer:
  1- Source and their flux. 2- Ionization of H and He (not always done). 3- Heating due to the radiative processes. 4- Spin temp decoupling (Lyα Radiative Trans.).
- It is very difficult to account for all the physical aspects of the problem and approximations are normally made. It also very difficult to dynamically couple the Hydro and Radiative transport parts.

Simulations of the EoR

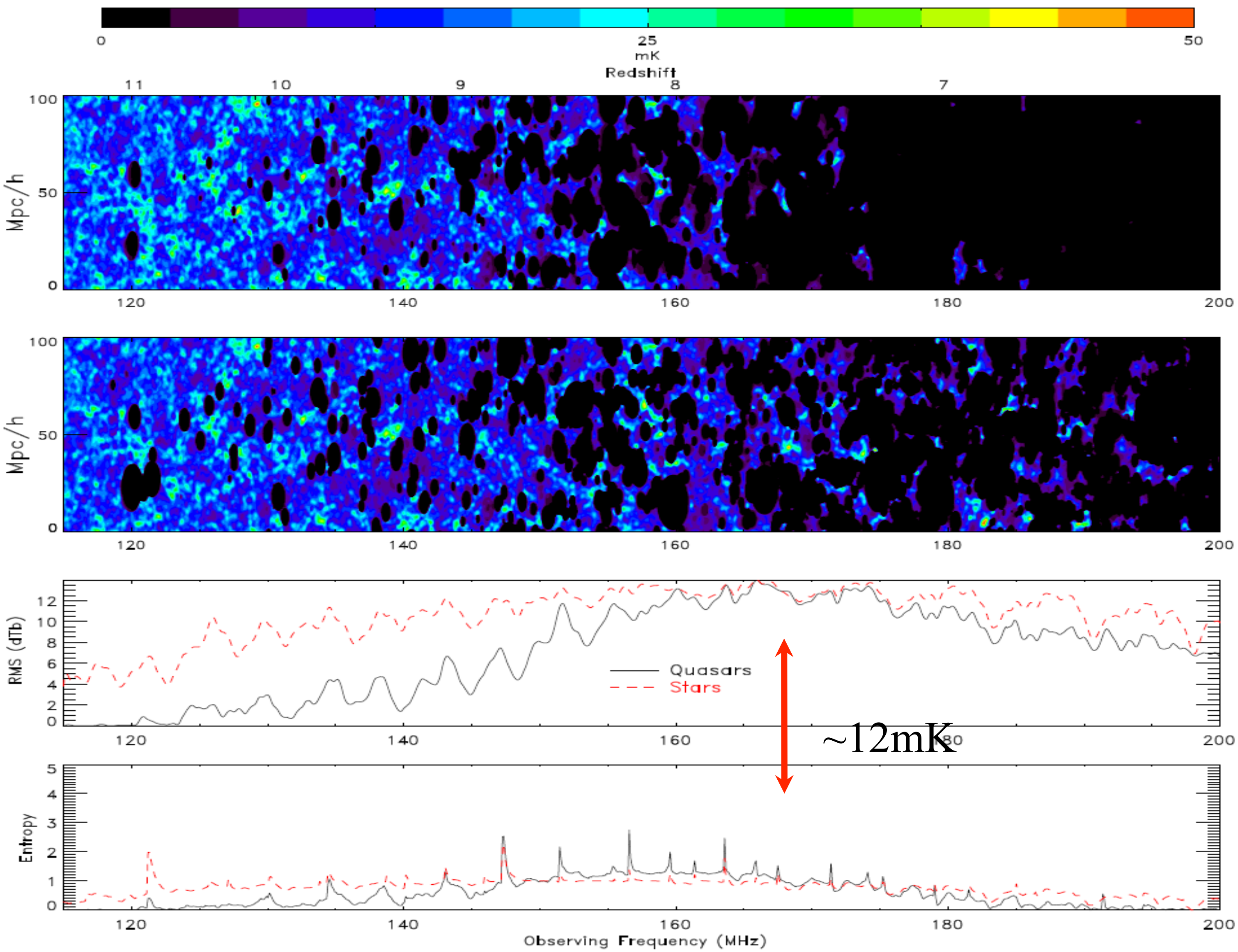

Thomas & zaroubi 2008

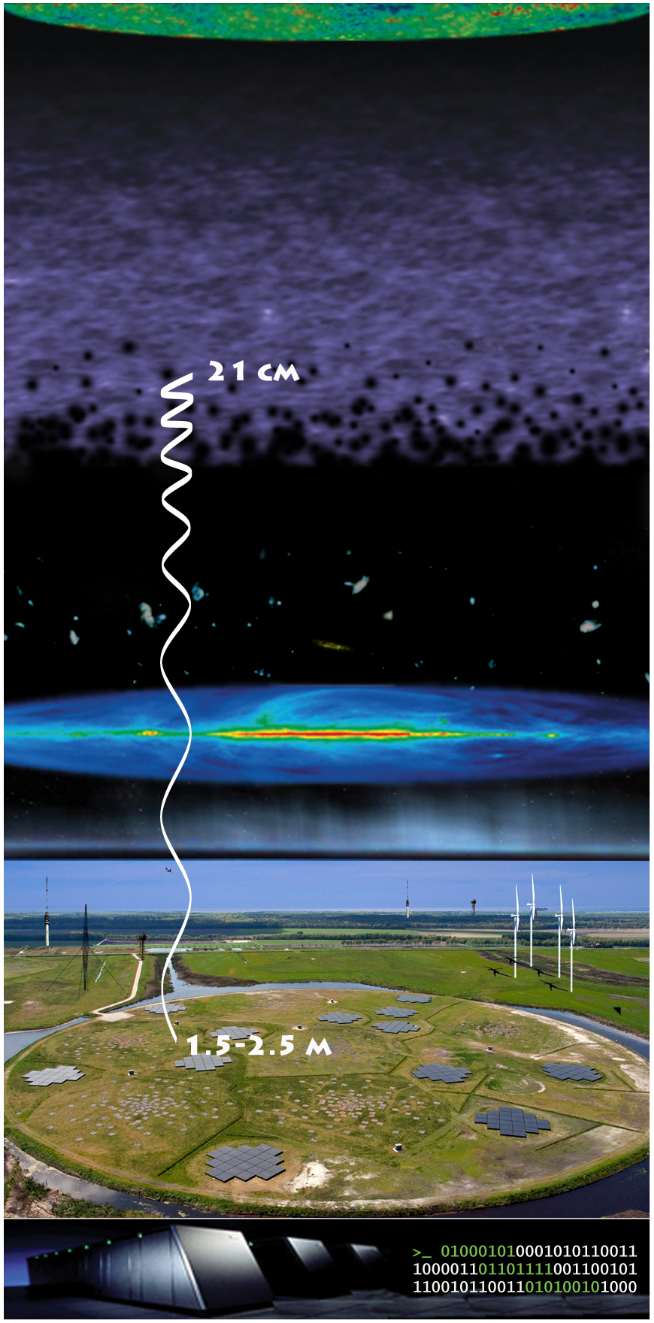

13.7 Gyr (z~1100)		Cosmic Microwave Background
		Dark Ages
13.2 Gyr (z~10)		Epoch of Reionization
11.5 Gyr (z~3)		Extragalactic foregrounds
1 kyr (z~0)		Galactic foregrounds
0.6 ms		Ionosphere
		Radio Frequency Interferences
0.2 ms		the LOFAR telescope core stations in the Netherlands
t = 0 s		Supercomputer BlueGene

LOFAR

MWA

PAPER

GMRT

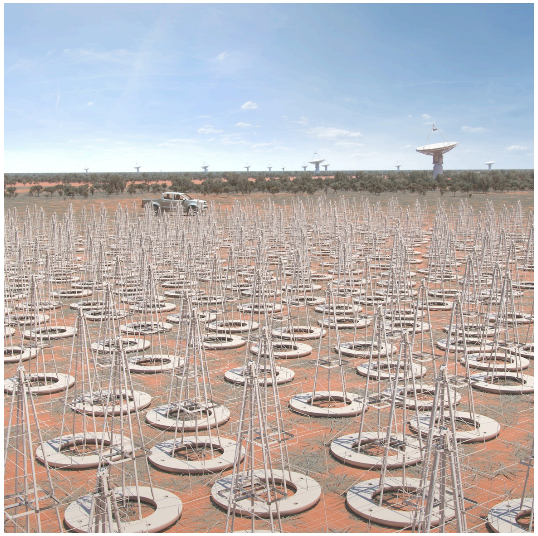

SKA

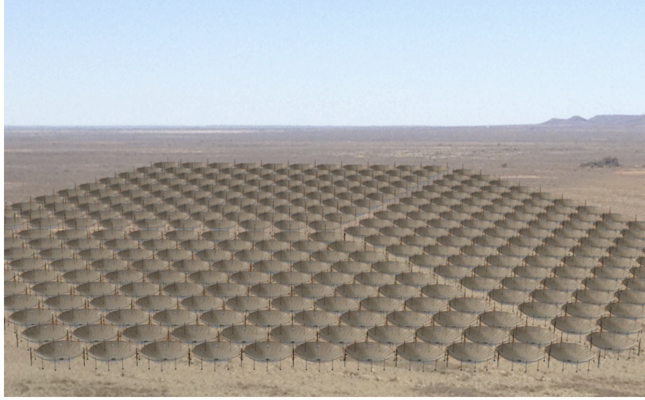

HERA

The calibration problem

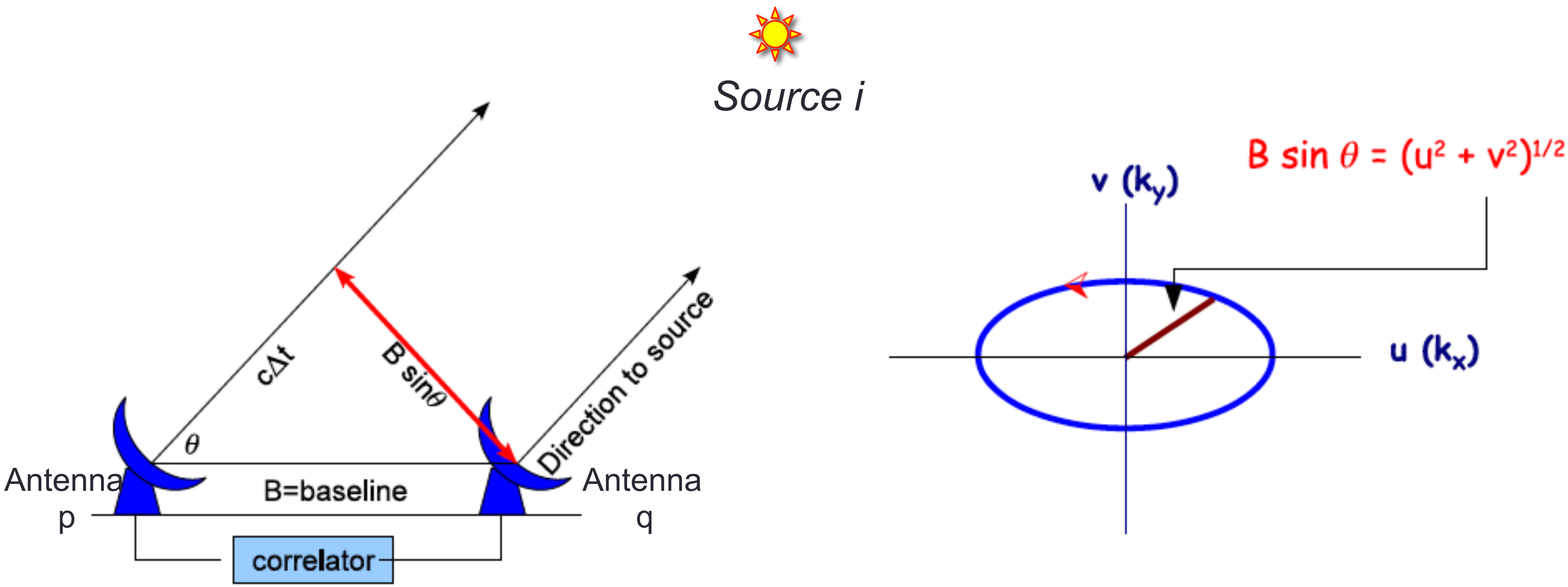

$$\mathbf{V}_{pq} = \sum_{i=1} \mathbf{J}_{pi}(\boldsymbol{\theta})\mathbf{C}_i\mathbf{J}^H_{qi}(\boldsymbol{\theta}) + \mathbf{N}_{pq}, \quad p,q \in \{1,2,\ldots,N\}$$

Measuring Redshifted HI: Challenges

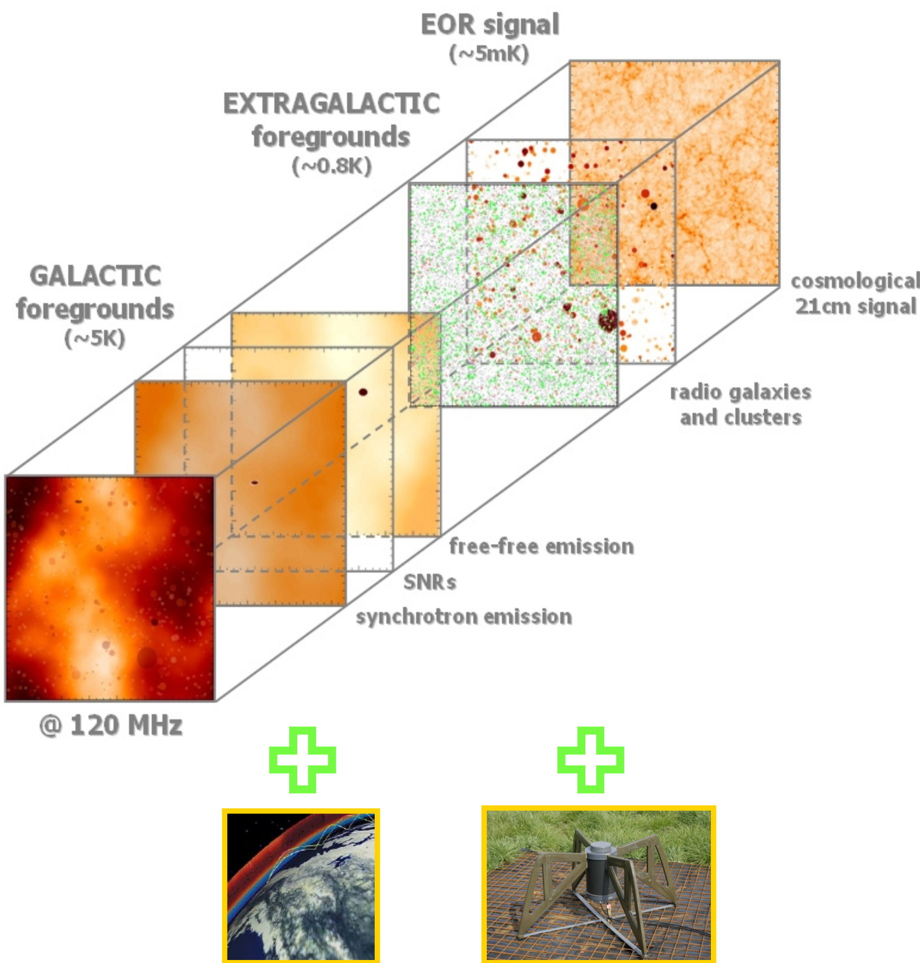

1. Astrophysical Challenges
   1. Foregrounds: total intensity
   2. Foregrounds: polarized
   3. Ionosphere
   4. Etc.
2. Instrumental challenges
   1. Beam stability
   2. Calibration
   3. Resolution
   4. uv coverage
   5. Etc.
3. Computational challenges
   1. Multi petabyte data set
   2. Calibration
   3. inversion

The Foregrounds

- 70% of the foregrounds are galactic.
  - Synchrotron (the most dominant)
  - Diffuse Bremsstrahlung
  - Individual supernovae remnants
- 30% Extra-galactic
  - Radio galaxies (given LOFAR resolution most of these sources fall in the confusion limit).
  - Radio clusters

The foregrounds are very complex across the sky but very smooth along the frequency

Measurement of Diffuse Foregrounds

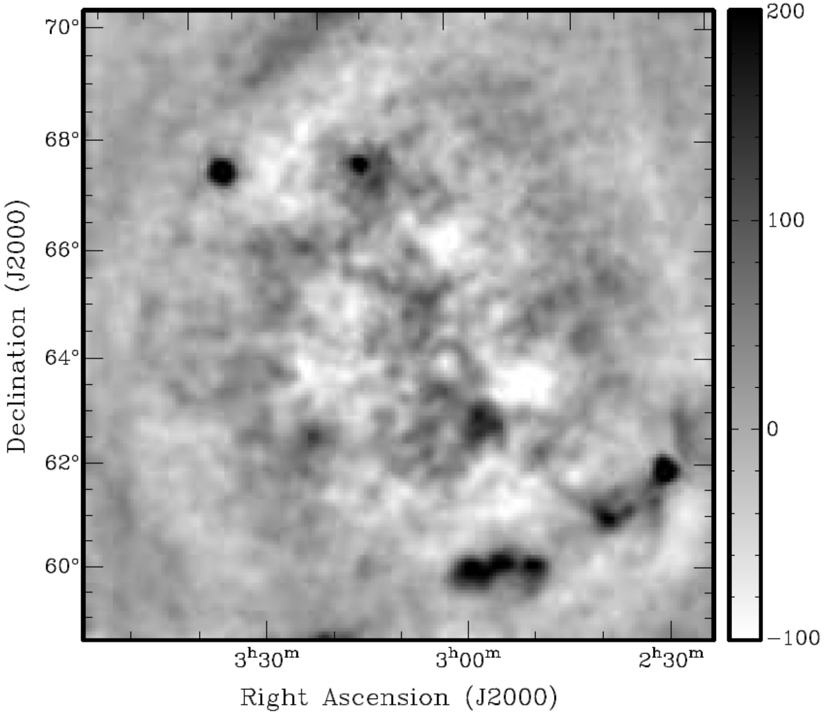

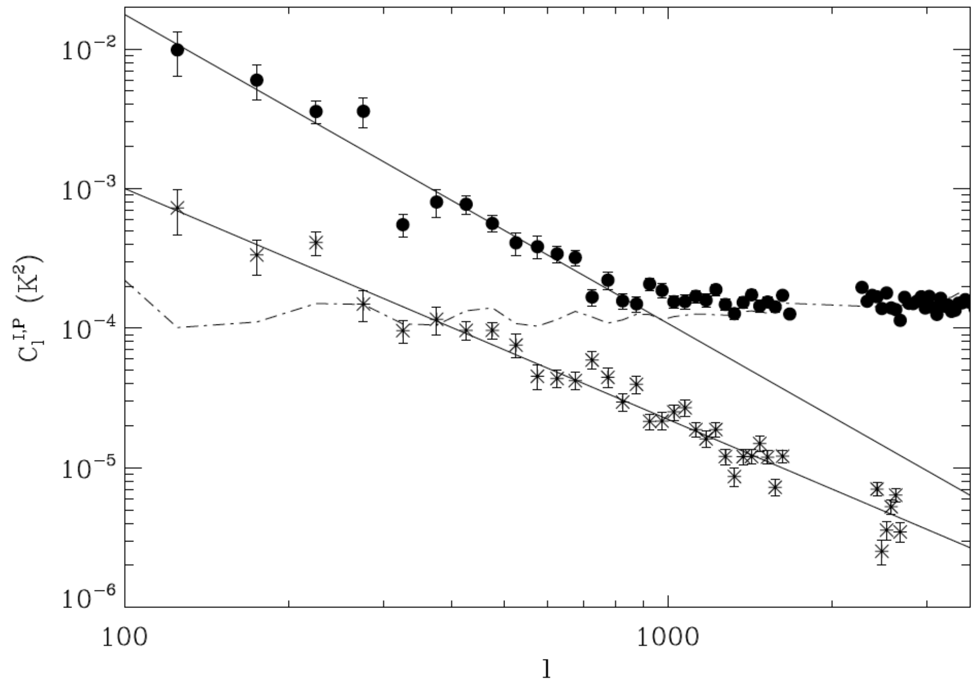

Bernardi et al. 2009, 2011

Bernardi et al. 2009, 2010

Extraction of the EoR signal

@150 MHz, 3arcmin

T_{EoR} ~ 5 mK
T_{FG} ~ 2 K
T_{noise} ~ 78 mK

Parametric fitting
(polynomial fitting)
Jelic et al. 2008

Non-parametric fitting
(Wp smoothing, ICA,..)
Harker et al. 2009
Chapman et al. 2012,2013

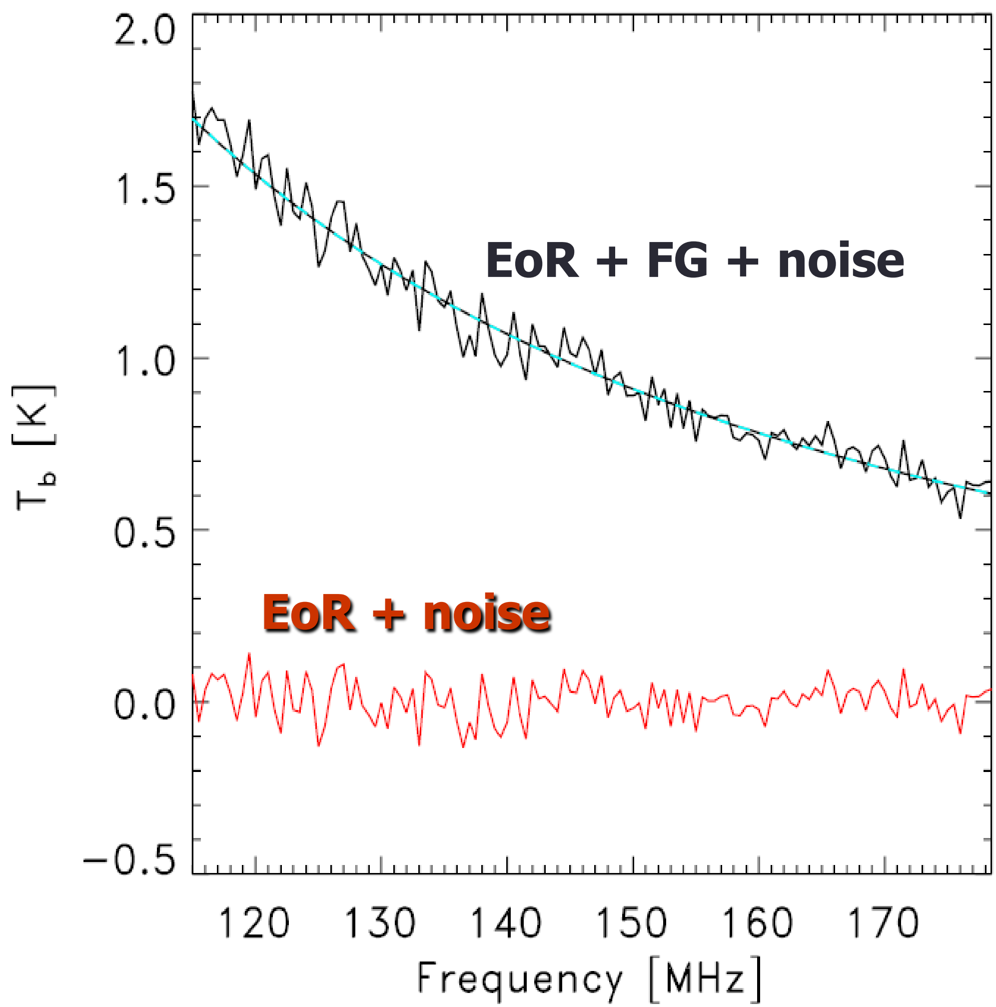

The LOFAR case

International LOFAR Telescope (ILT)

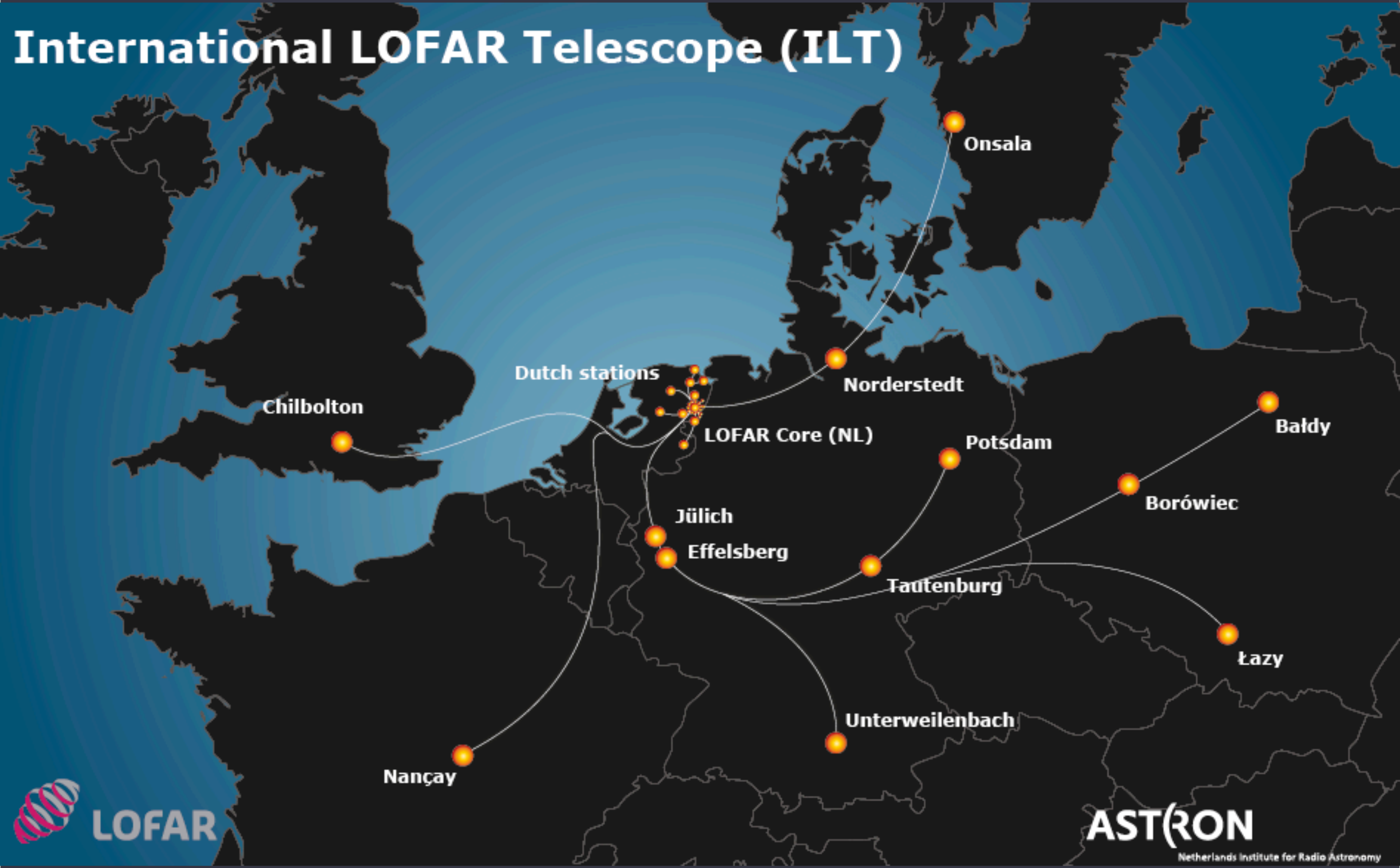

Autumn weather and muddy soil cause delays….

Nov 2008

field flattening activities

‘Field flattening’ for non-astronomers

LOFAR science

The specifications and capabilities of LOFAR were mainly driven by

6 Key Science Projects (KSP)

1) Surveys of the (northern) sky
2) Transients, Pulsars, (exo-)Planets
3) Epoch of Reionization
4) (UHE) Cosmic Rays + other near-field science
5) Cosmic Magnetism (polarimetry)
6) Sun and Solar system science

\+ other science applications still coming in…

All science done under 'umbrellas' of International Key Science Project teams, based at Leiden, Amsterdam, Groningen, Nijmegen (all NL) Bonn, Potsdam (Germany) Total more than 100 scientists involved. For their efforts they will be rewarded with guaranteed observing time (a fraction declining over a 5 year period)

The LOFAR EoR members

Main Science targets

1. ‘Global’ evolution of the EoR: Variance as a function of redshift.
2. Power spectrum at various redshifts
3. High order statistics
4. Imaging!!

5. Cross-correlation with other probes
6. The 21 cm forest

How to check reliability of results

Internal consistency checks

- Avoid problematic data, e.g., high RFI, very active ionosphere, etc.
- Observing multiple fields and obtain consistent results.
- Different times
- Frequencies
- Etc.

End to end pipeline

- Test observational strategy
- Performance of calibration methods
- Test various extraction techniques.
- Realistic estimates of errors of various statistics.
- What to expect from the results.
- Etc.

LOFAR EoR Windows

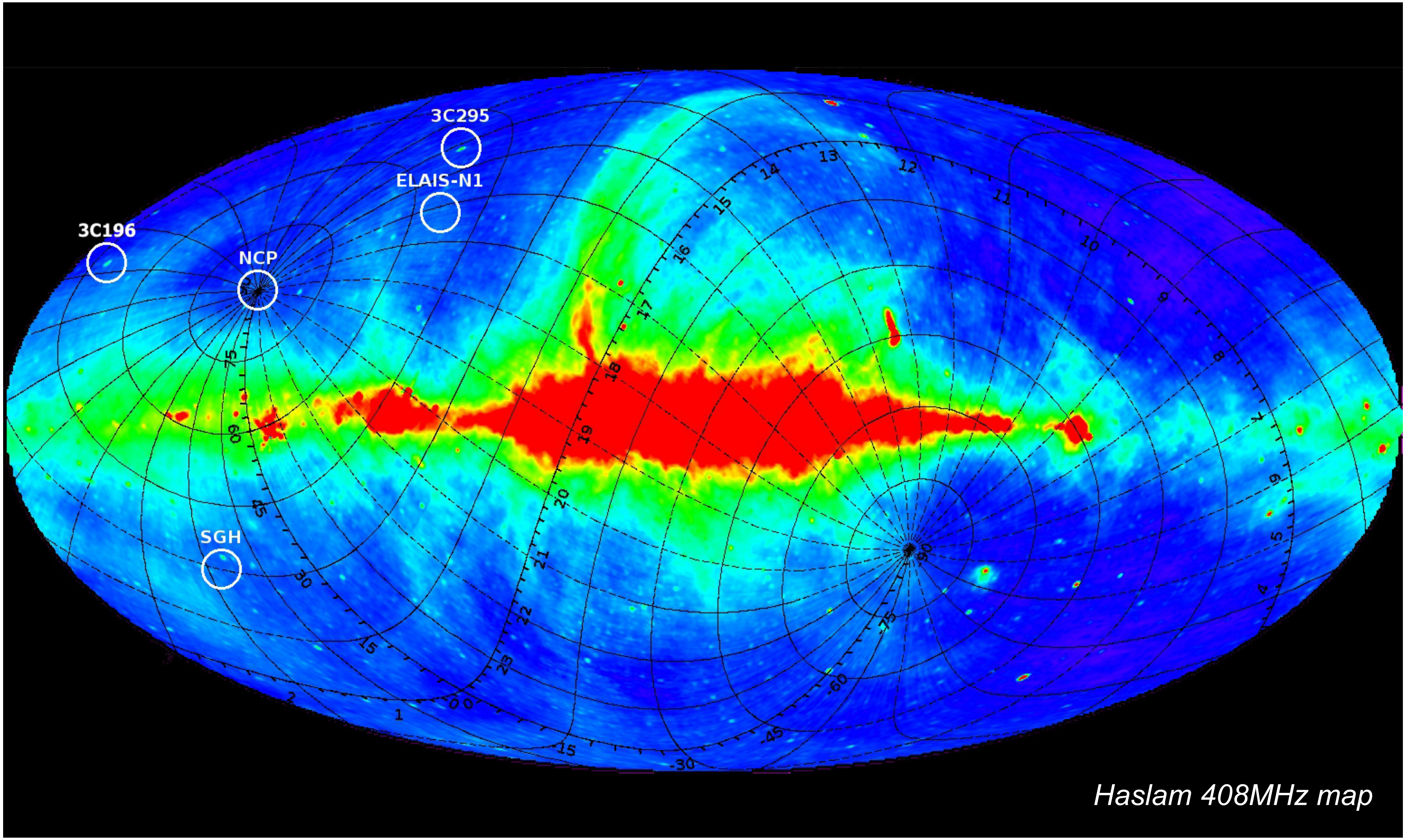

Haslam 408MHz map

Statistical measures of the EoR

Parameterization of the variance

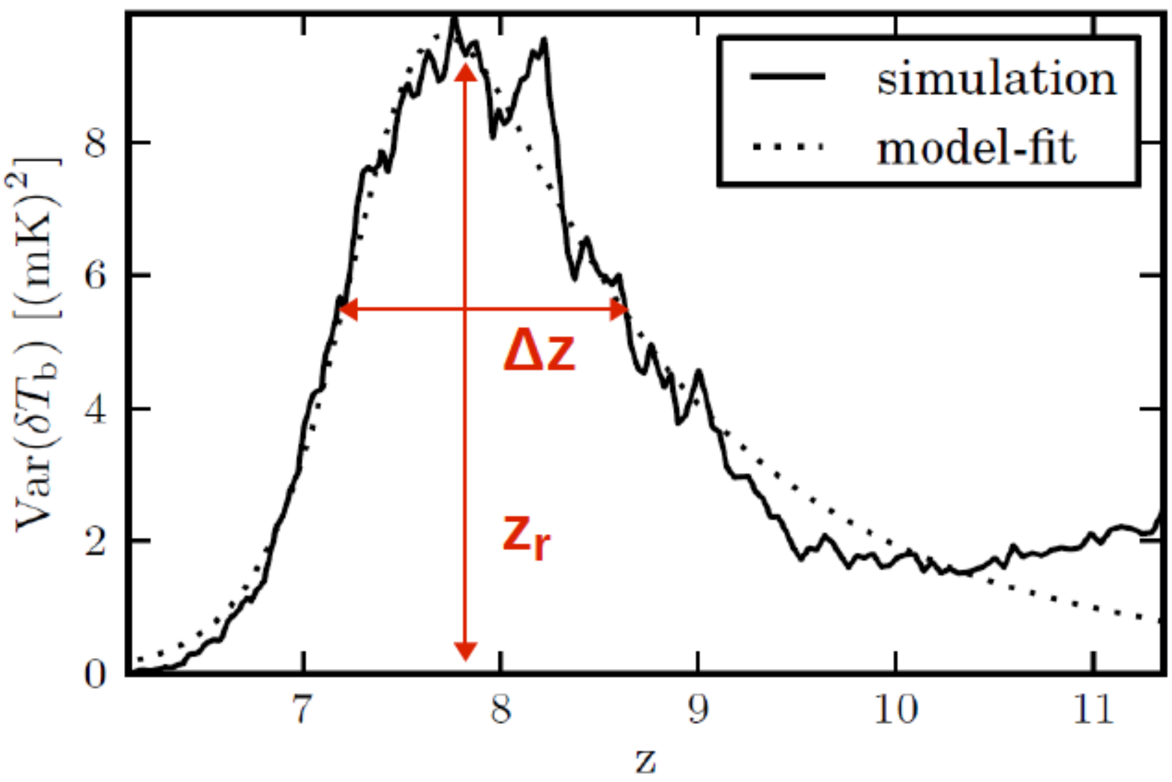

$$Var[\delta T_b(z)] = A\ f(z) \left(\frac{z}{z_0}\right)^{\beta}$$

$$f(z) = \frac{1}{2}\left[1 + \tanh\left(\frac{z - z_0}{\Delta z}\right)\right]$$

Patil et al. 2014, draft

The rms and Cross-rms statistic

$$RMS(\nu) = \sqrt{\left\langle \left(I_{i,j}(\nu) I_{i,j}(\nu) \right) - \left\langle I_{i,j}(\nu) \right\rangle \left\langle I_{i,j}(\nu) \right\rangle \right\rangle_{i,j}}$$

$$CRMS(\nu) = \sqrt{\left\langle \left(I_{i,j}(\nu) I_{i,j}(\nu') \right) - \left\langle I_{i,j}(\nu) \right\rangle \left\langle I_{i,j}(\nu') \right\rangle \right\rangle_{i,j}}$$

- Smooth the images with a Gaussian kernel
- Calculate the rms statistic and the Cross-rms: $\nu' = \nu + \Delta\nu$

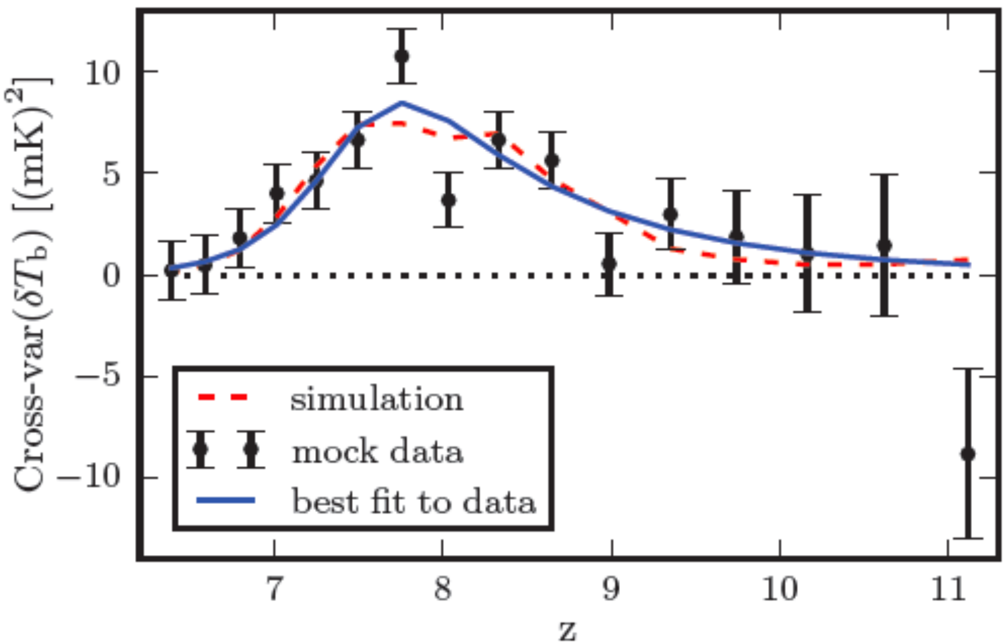

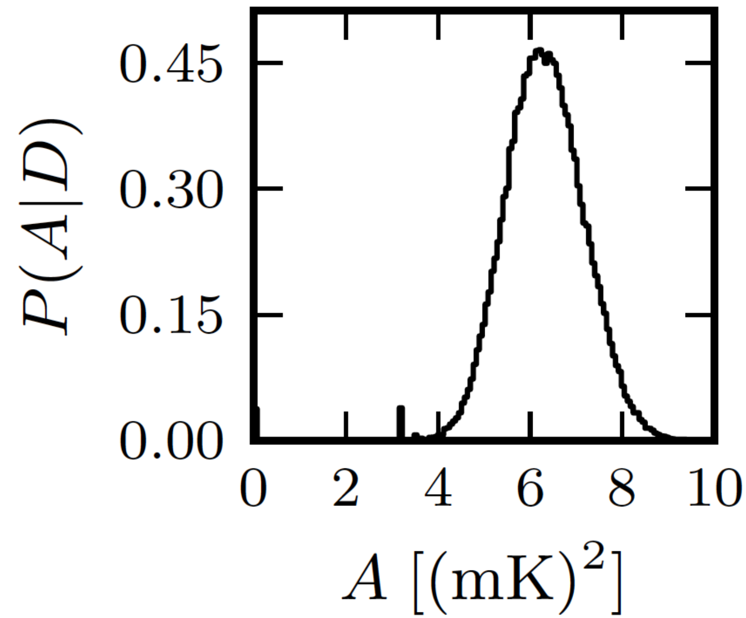

$$Var(\delta T_b) = A \left(\frac{z}{z_0} \right)^{\beta} \left(1 + \tanh\left(\frac{z - z_0}{\Delta z} \right) \right)$$

Patil et al. 2014

Power Spectrum Measurements

Harker et al 2010

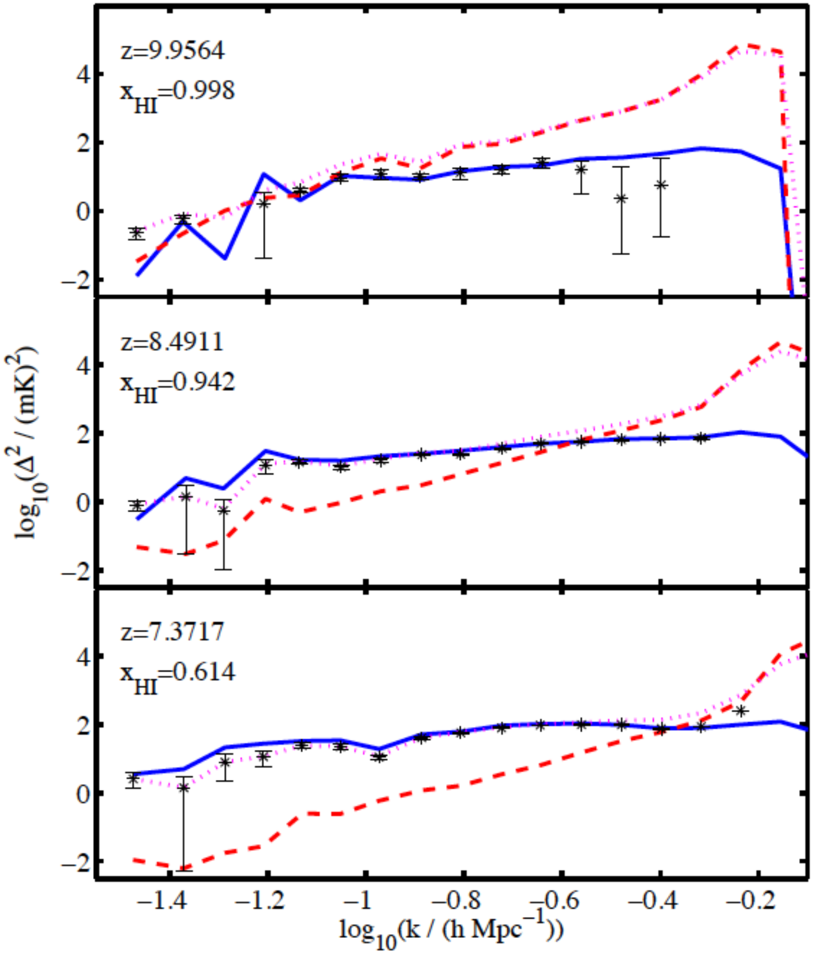

Chapman et al 2013

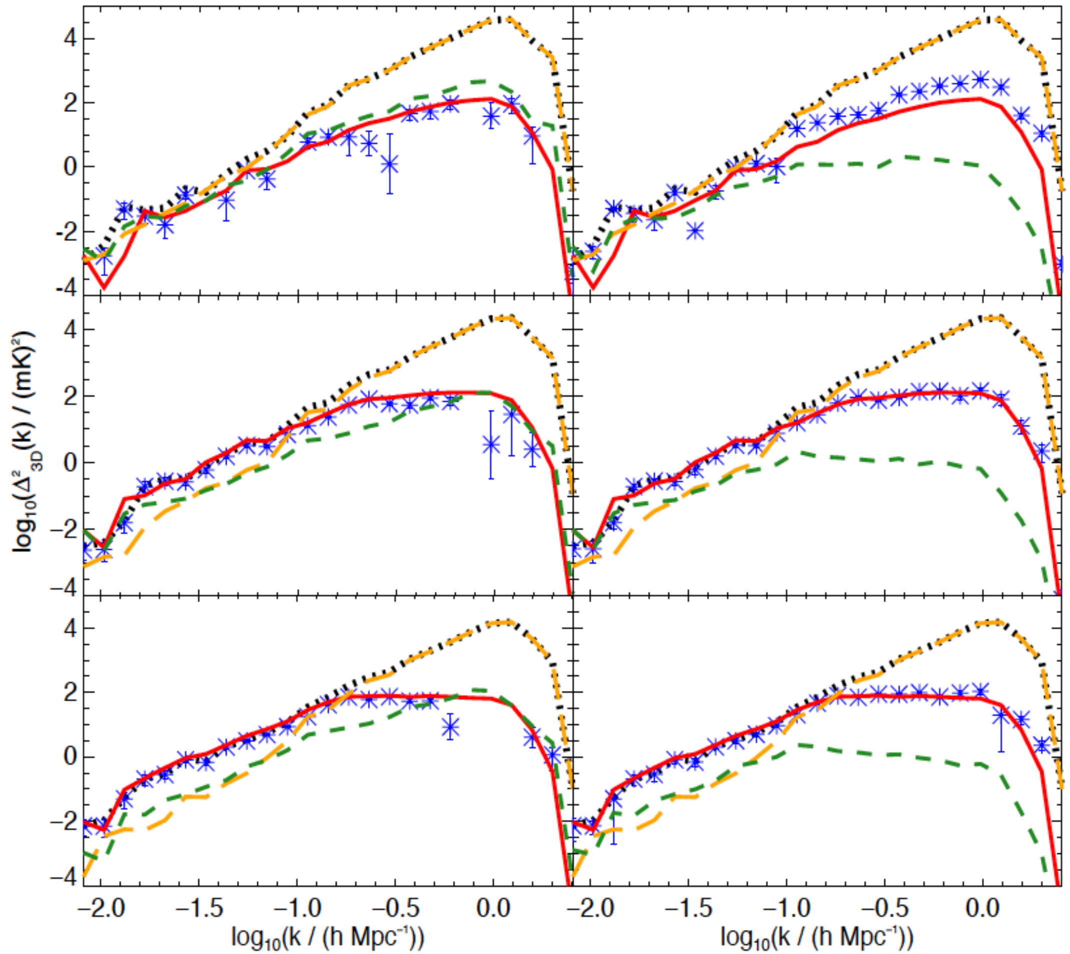

Extraction through skewness

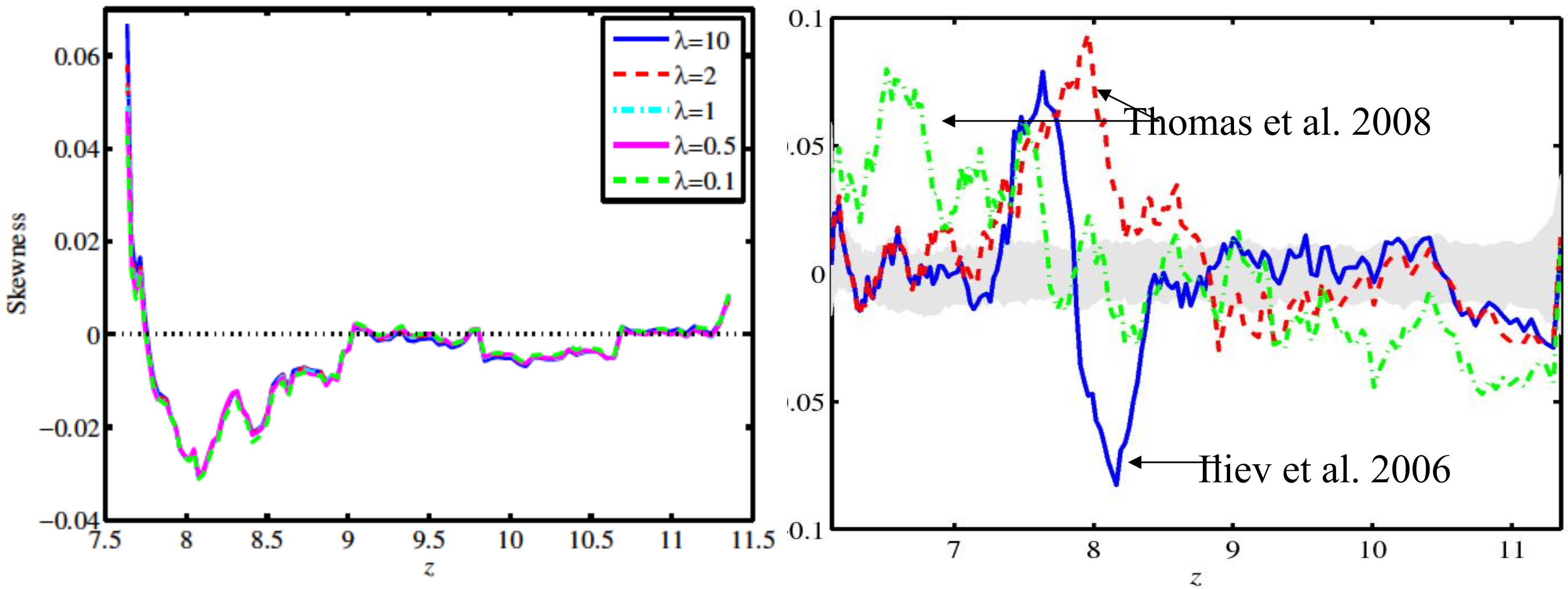

Harker et al. 2009

MWA current results

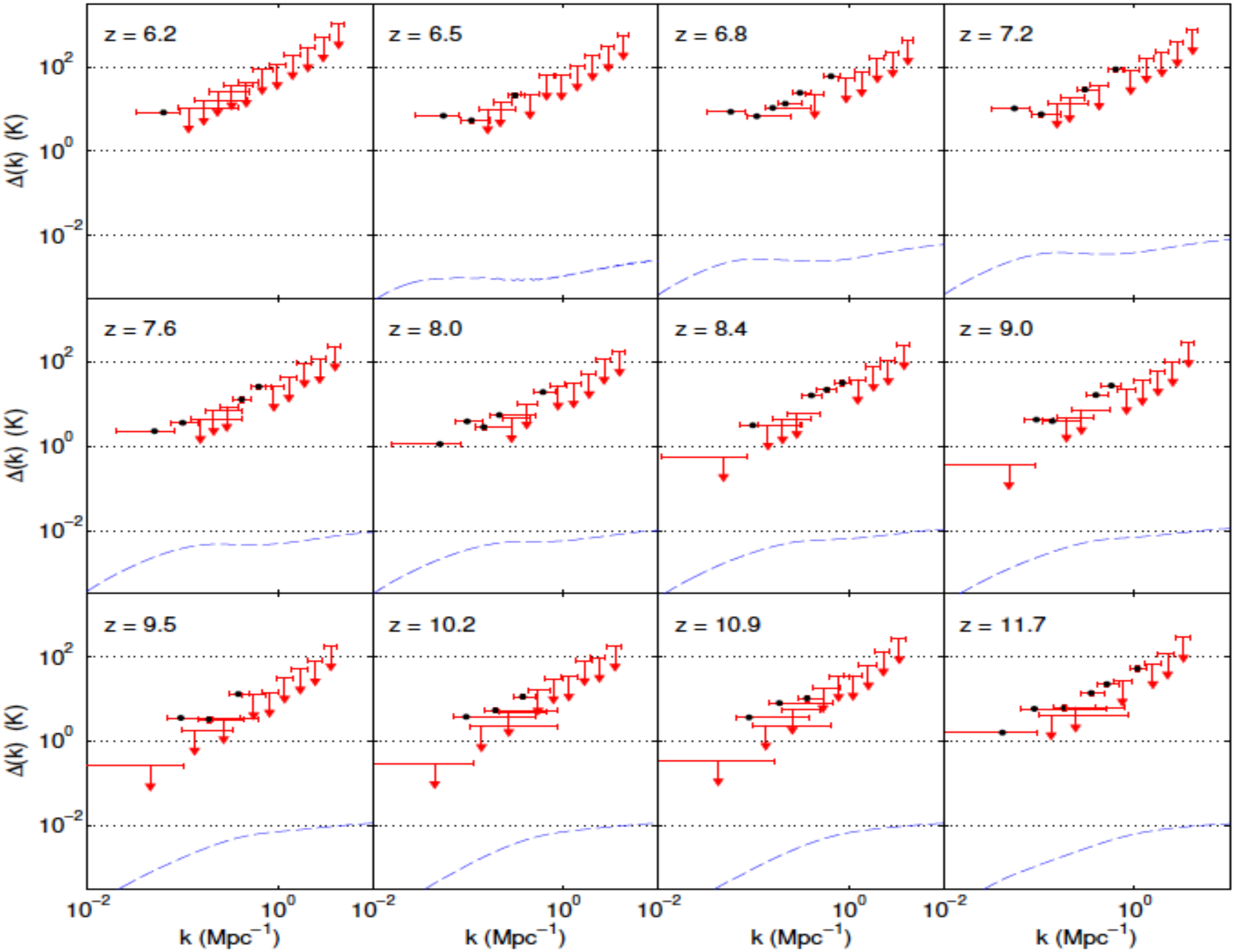

Dillon et al 2013

GMRT results

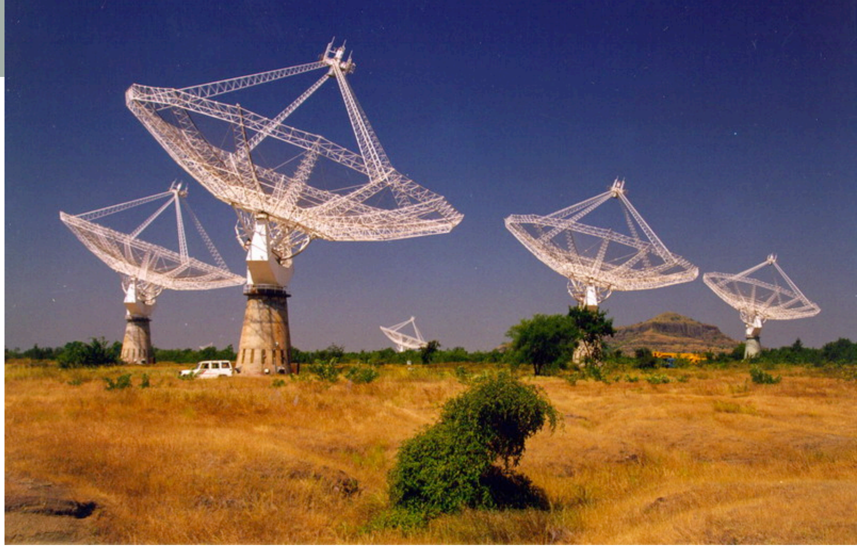

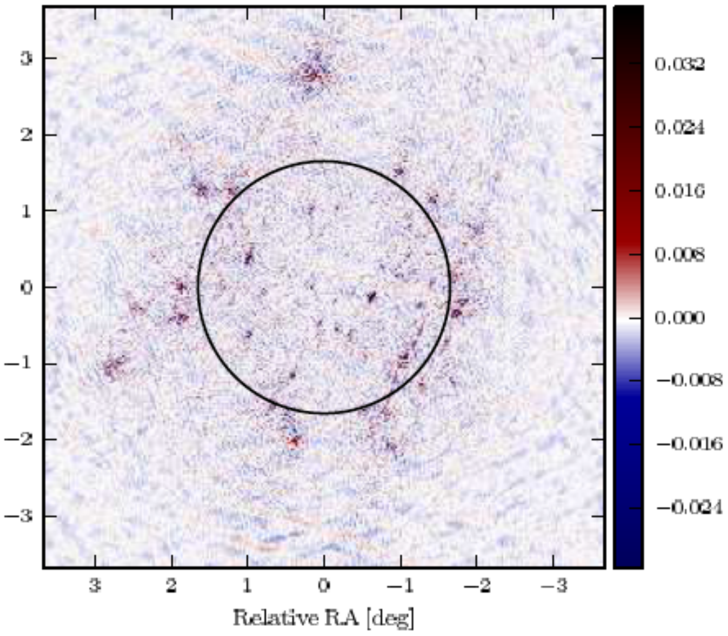

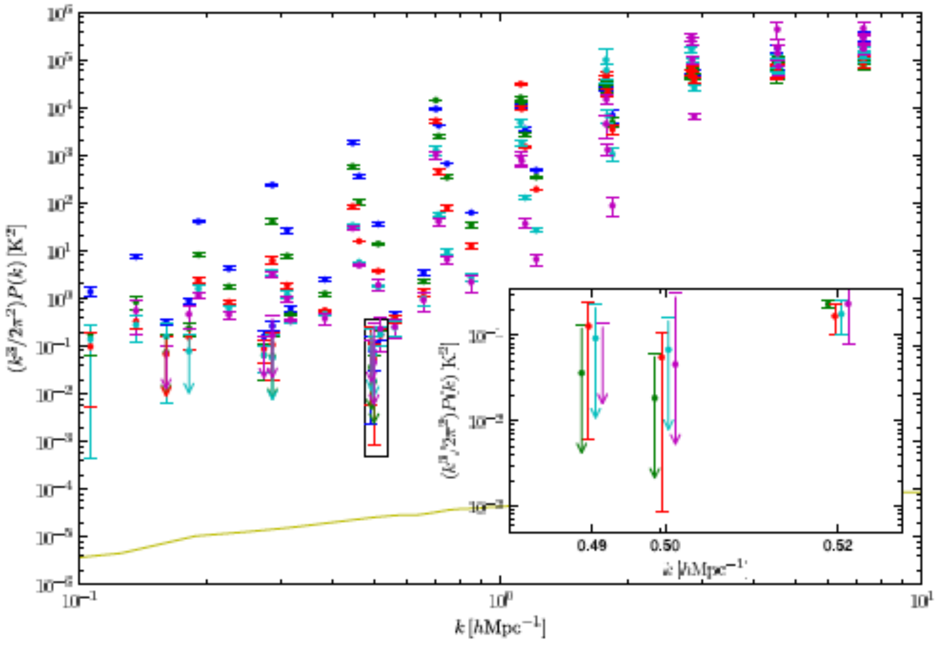

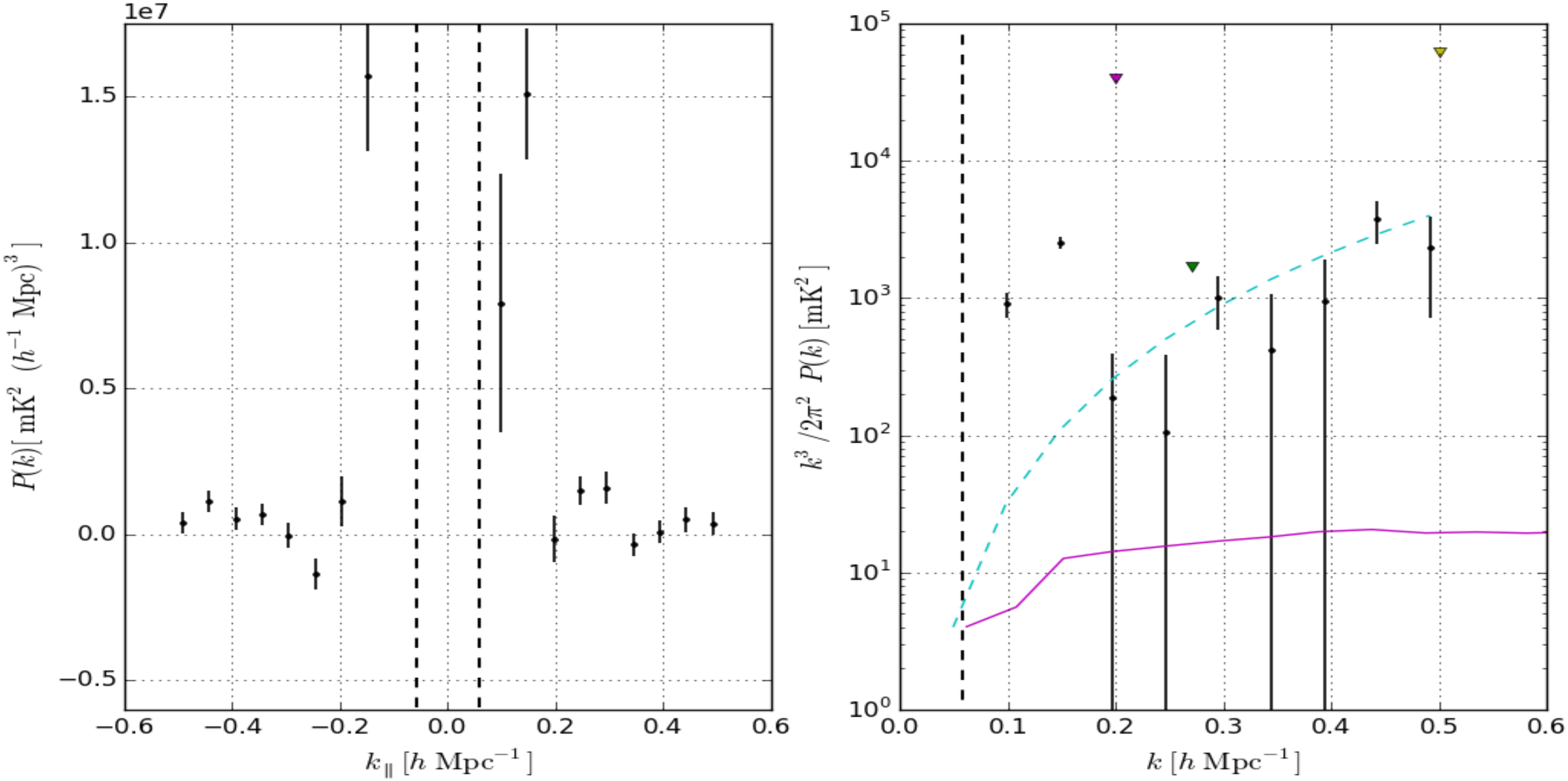

Ali et al 2015

Imaging the EoR with LOFAR

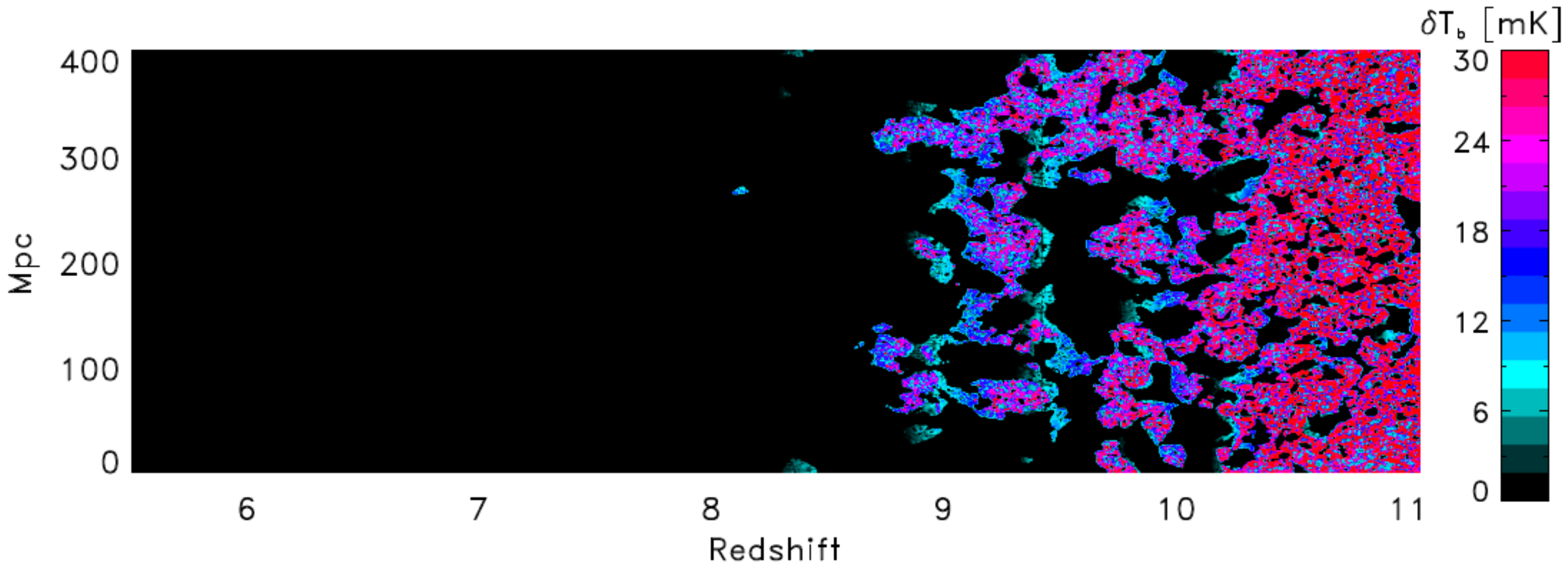

Imaging of the EoR with LOFAR

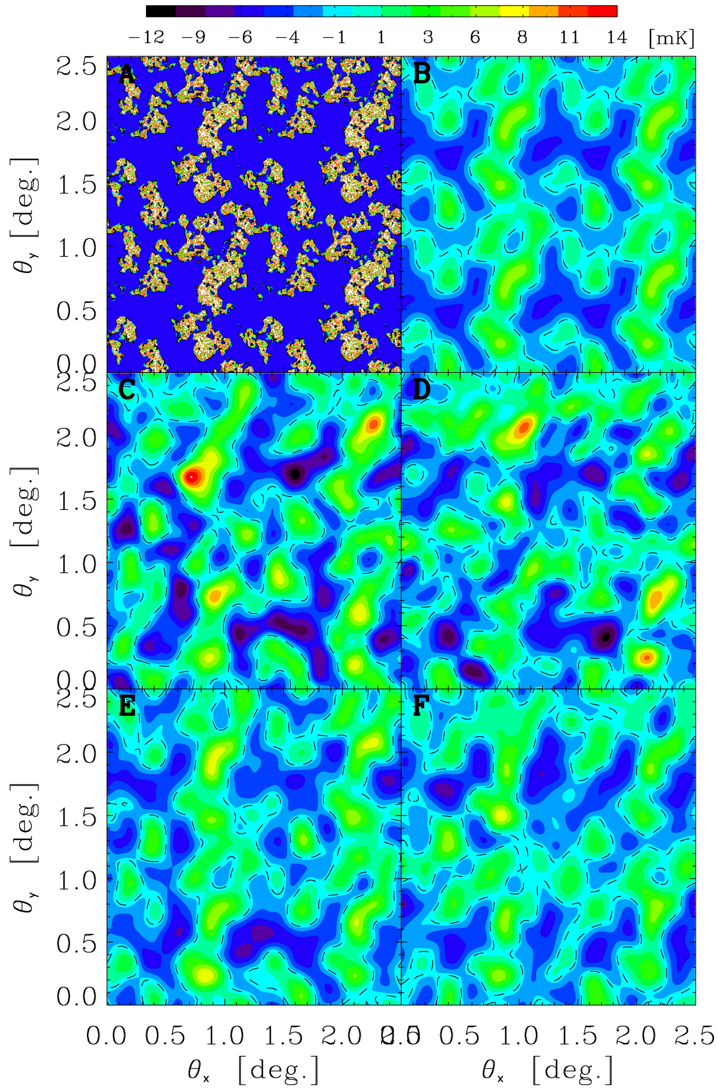

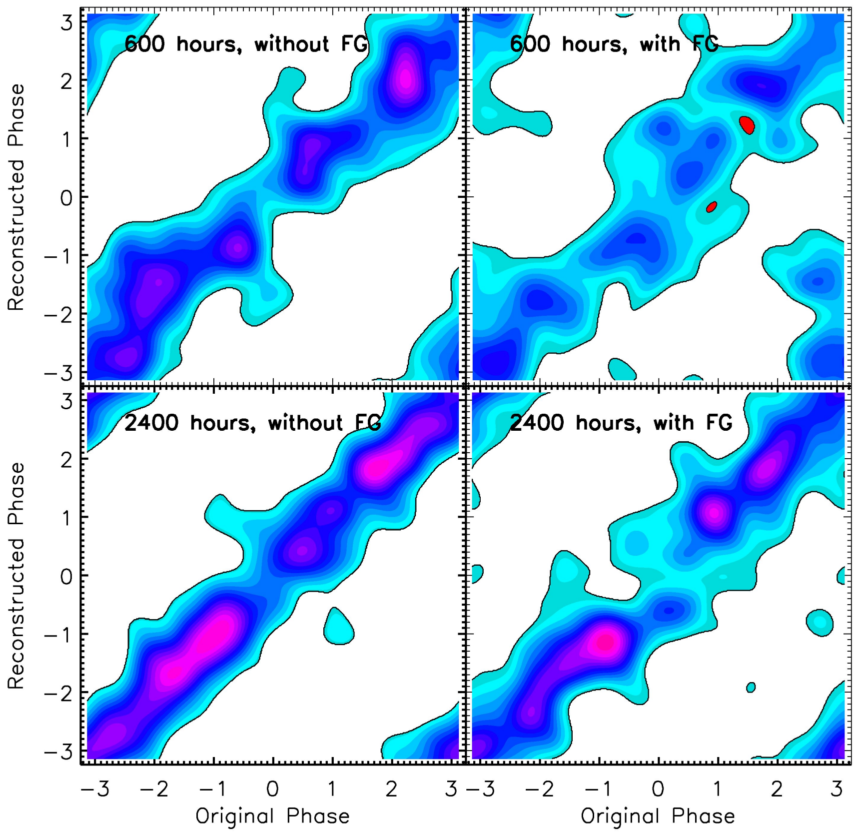

The foregrounds and the Signal Extraction!

The LOFAR-EoR Project: end-to-end pipeline

R. Thomas
PhD thesis

V. Jelić
PhD thesis

A. Offringa
PhD thesis

P. Labropulos
PhD thesis

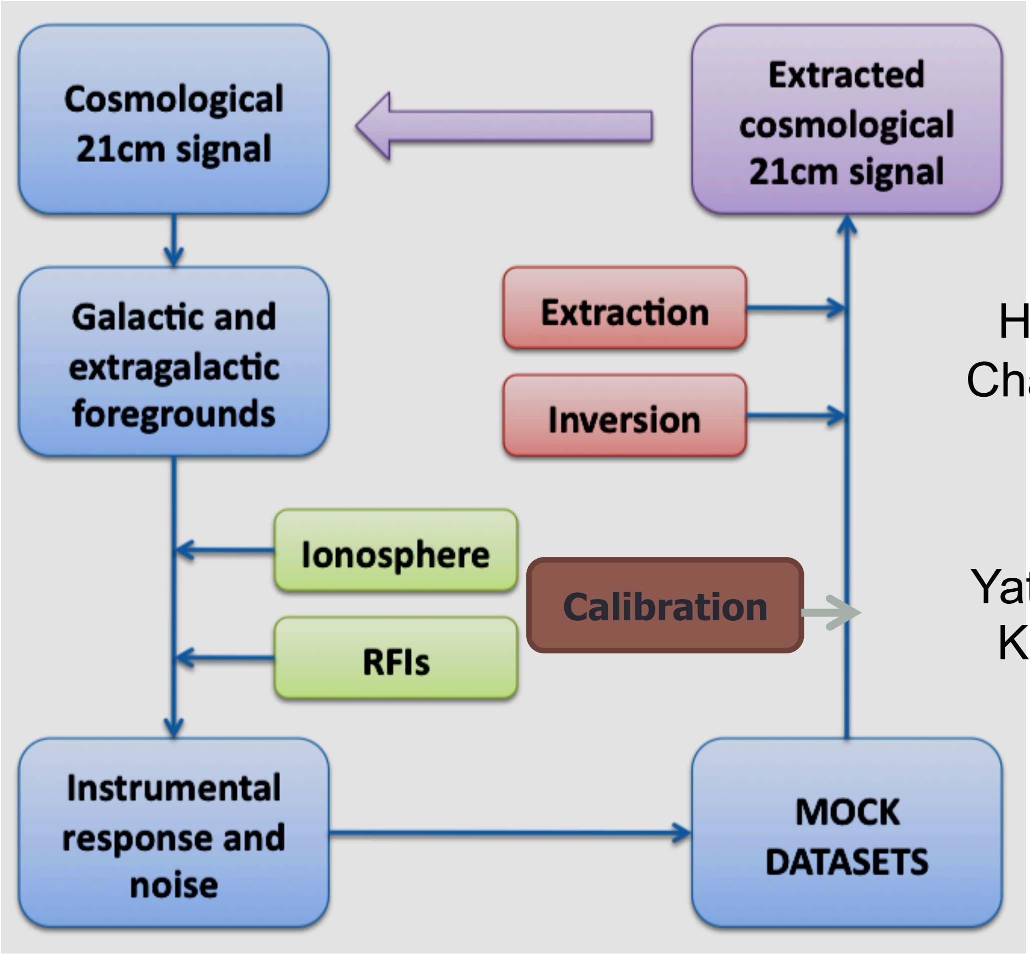

Jelic et al 2008
Harker at al 2009,2010
Chapman et al 2012,201

Yatawatta et al 2009,201
Kazemi at al 2011,2013

Example of extraction @ 150MHz 5' (σ) smoothed

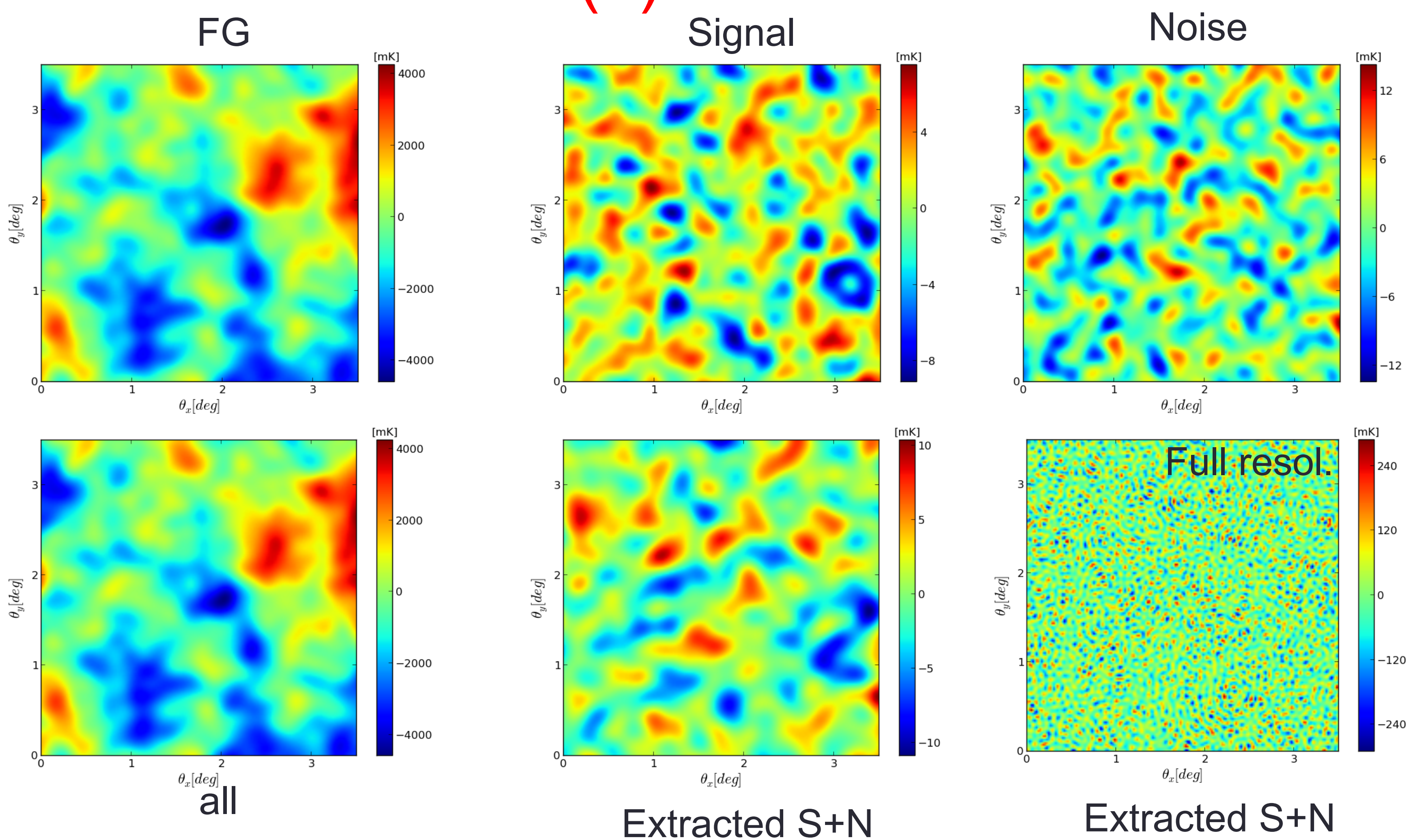

Problems with IM

- Calibration artifacts
- Foreground removal

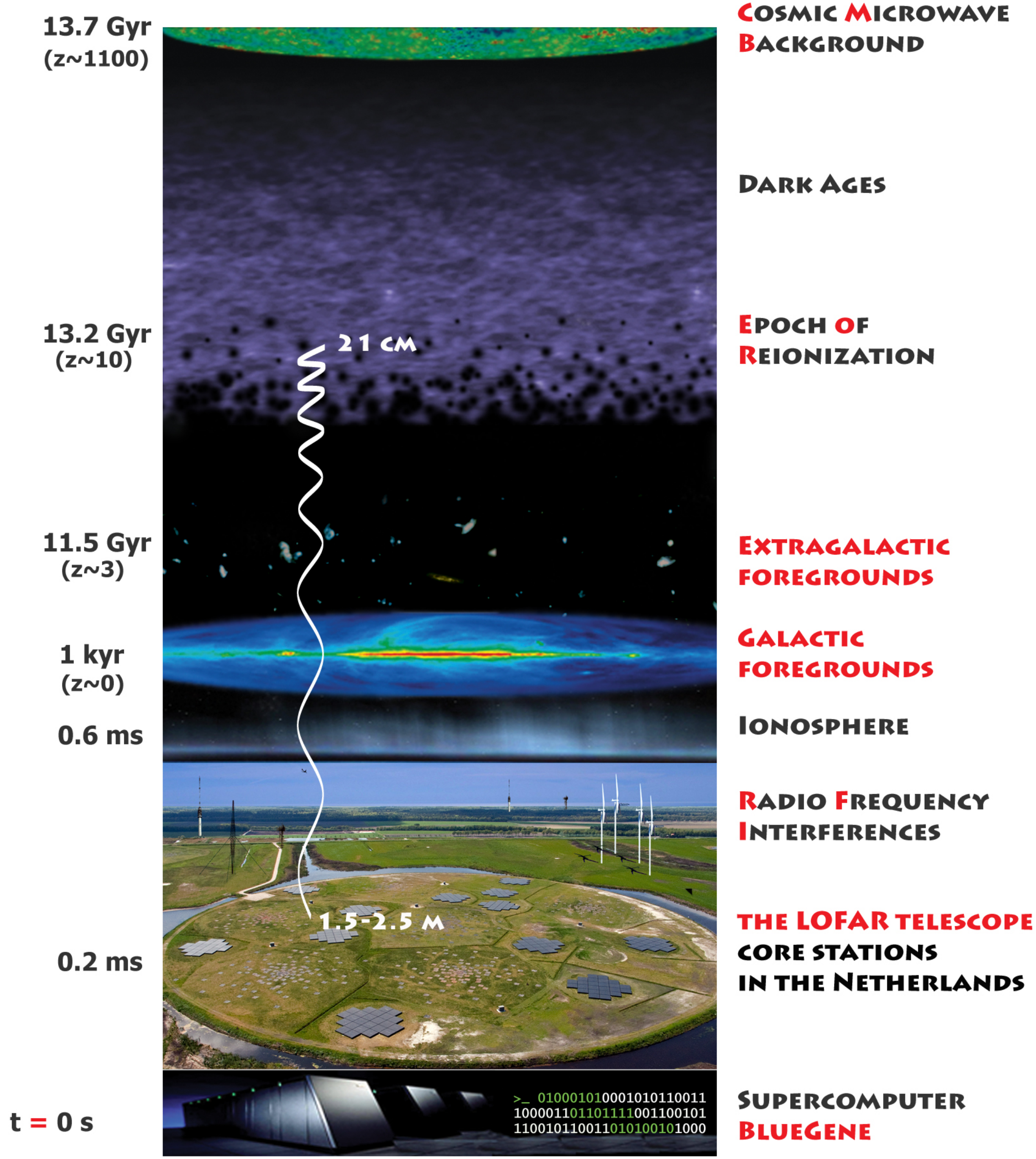

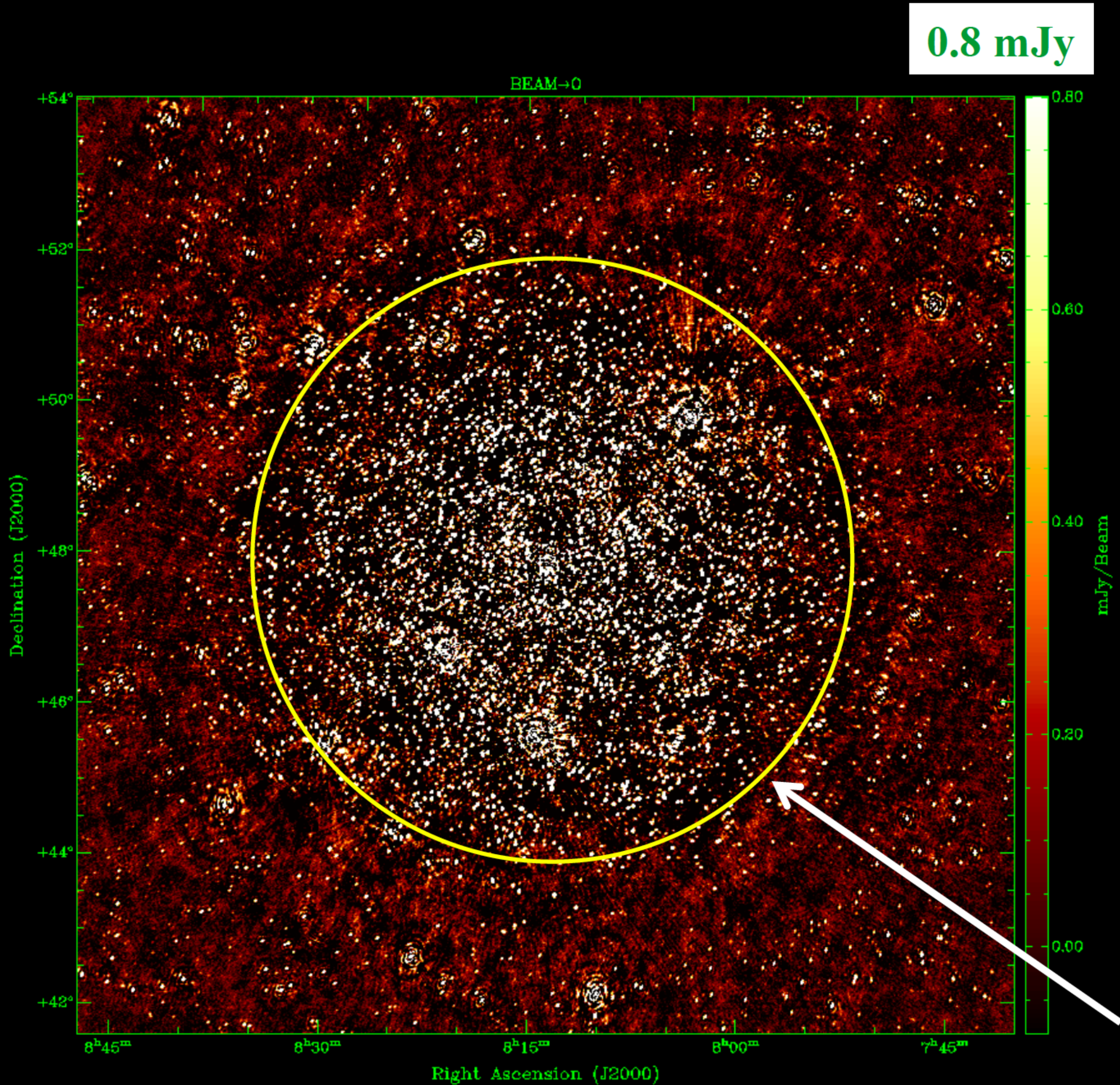

3C196 Field Image

- 145 MHz (~2m)
- 60MHz continuum
- 6 powers of 10

- 32 hours on 3C196 (8 hrs x 4 days)
- Dec 21,12-Feb08,13
- 30λ - 5000λ
- Resolution - 50”
- 12^0 x 12^0 Image

- ‘Noise’ < 75 μJy
- 3C196 - 79.97 Jy
- **DR: ~ 10^6:1**

Station beam (~8^0)

Courtesy of Banday

Polarization & Rotation Measure synthesis

Faraday Depth: $$\frac{\Phi}{[\mathrm{rad\ m^{-2}}]} = 0.81 \int_{source}^{observer} \frac{n_e}{[\mathrm{cm^{-3}}]} \frac{B_{\|}}{[\mu\mathrm{G}]} \frac{\mathrm{d}l}{[\mathrm{pc}]}$$

Complex linear Polarization: $$P(\lambda^2) = Q(\lambda^2) + iU(\lambda^2)$$

RM Synthesis: $$F(\Phi) = \frac{1}{W(\lambda^2)} \int_{-\infty}^{+\infty} P(\lambda^2) e^{-i2\Phi\lambda^2} \mathrm{d}\lambda^2$$

Brentjens & de Bruyn 2005

Simulations

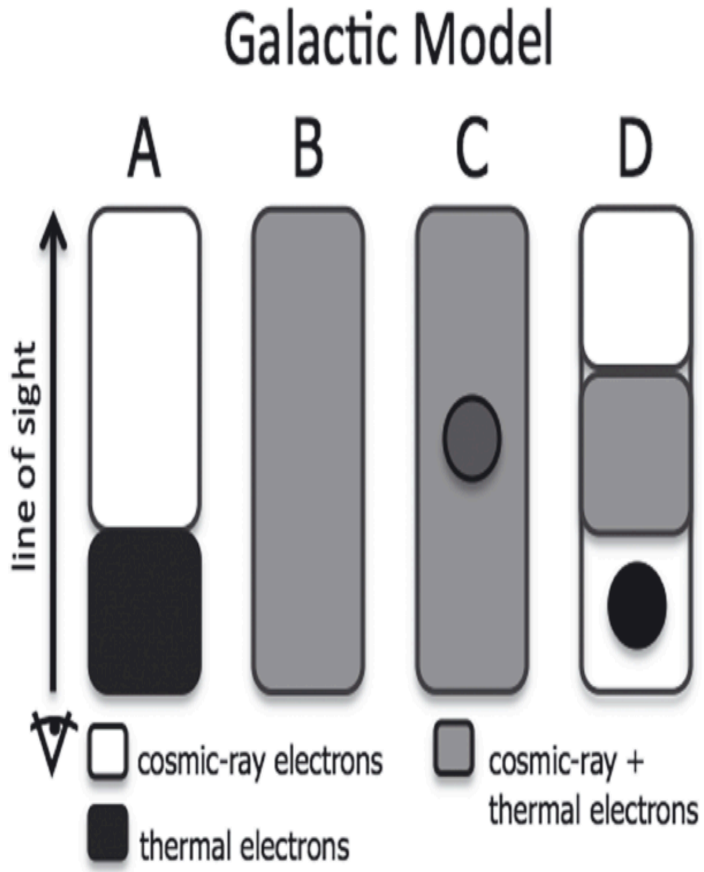

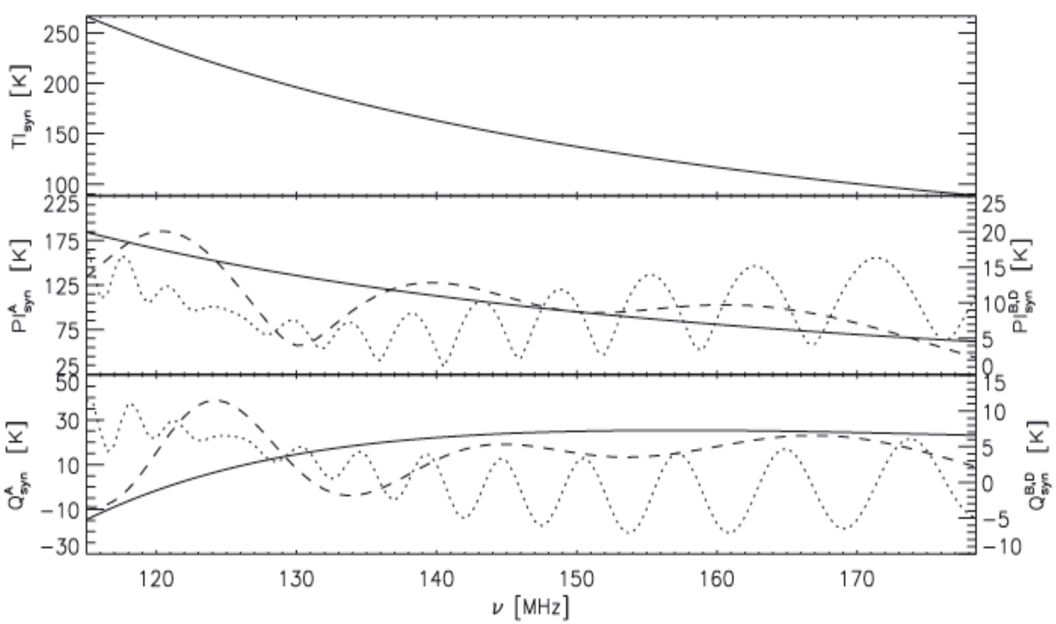

3C196 field

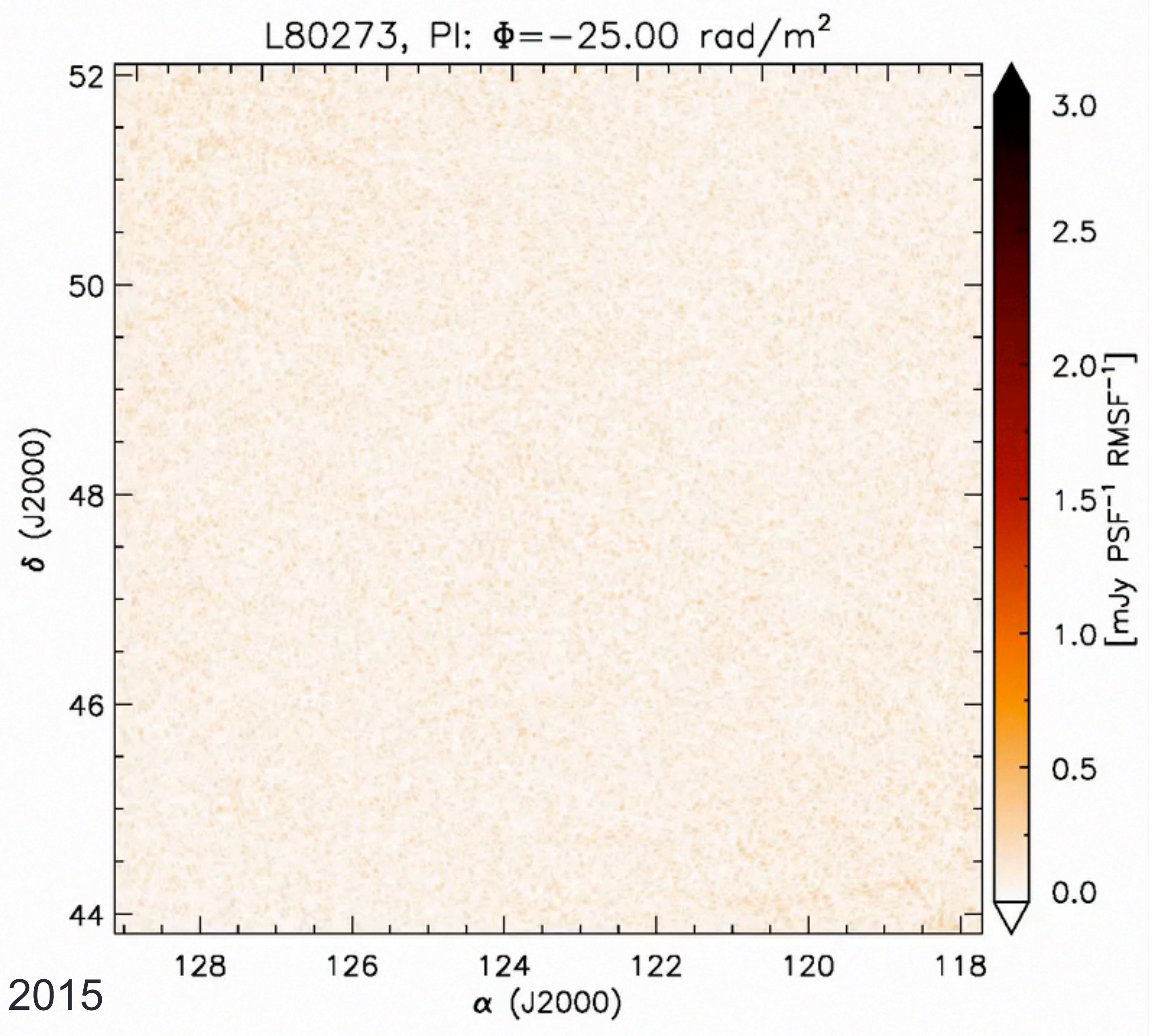

Jelic et al 2015

LOFAR-EoR observations

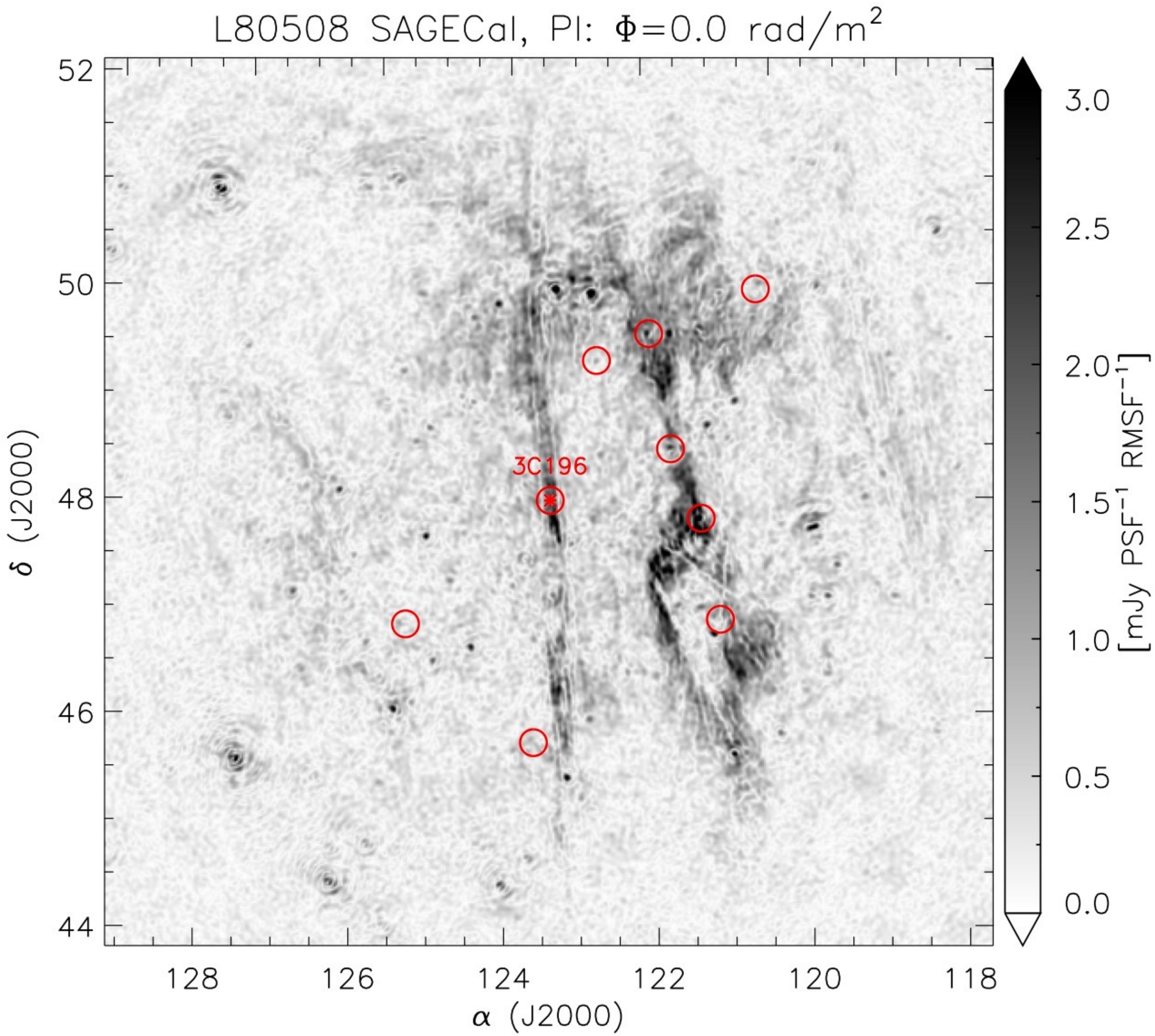

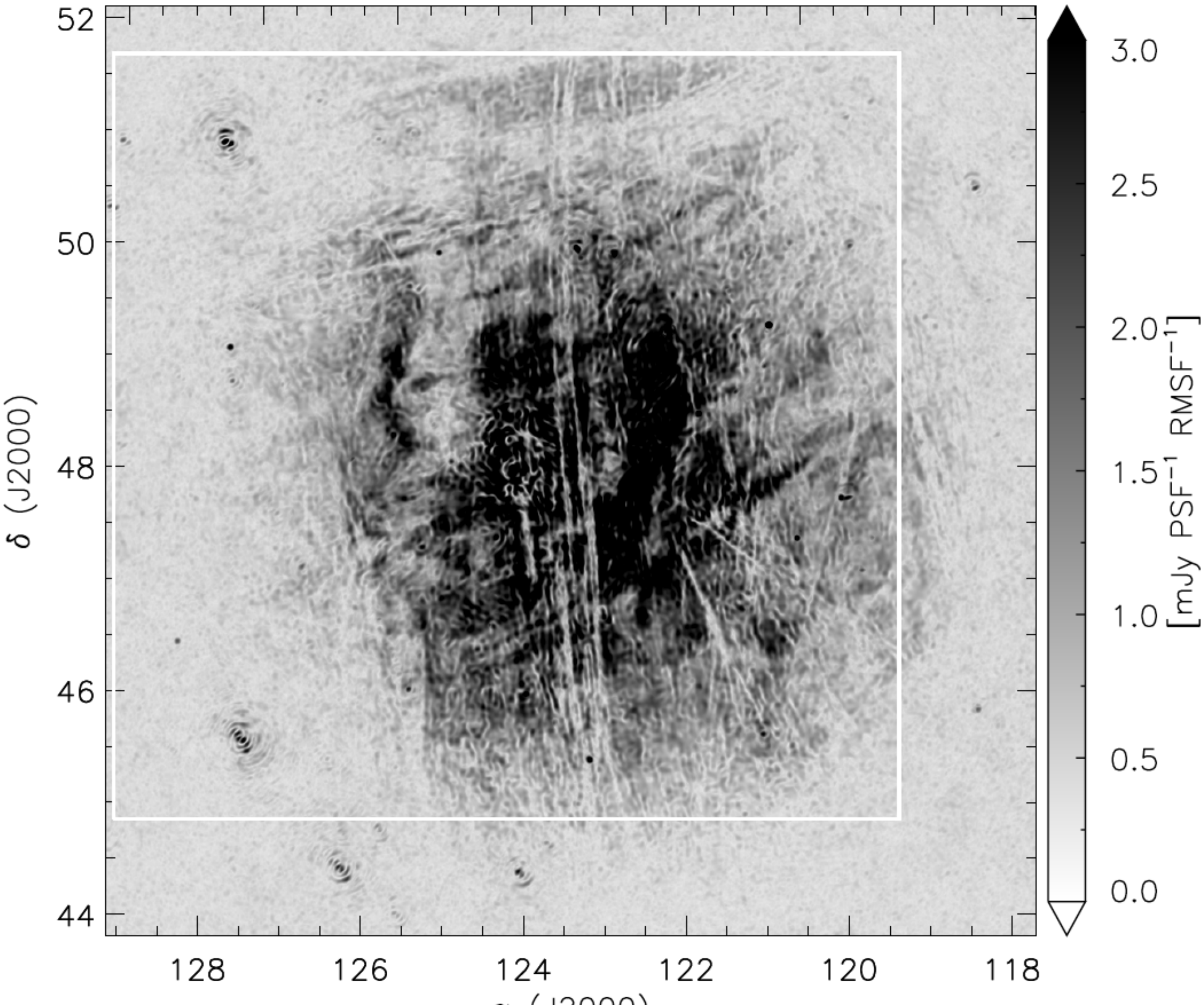

Jelic et al 2015

Image quality: NCP

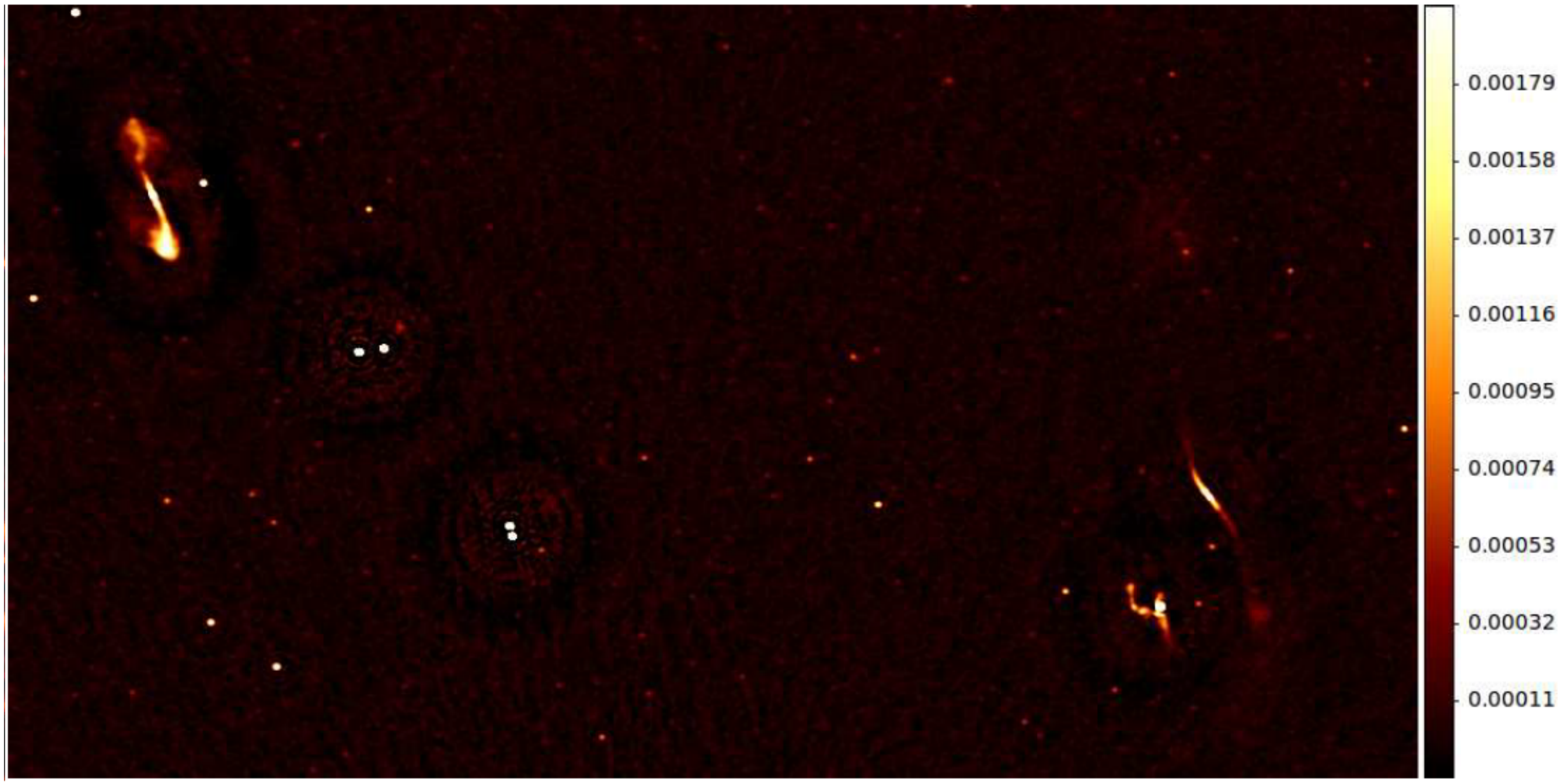

25-30 μJy, 6″ PSF, Dec 2012-Feb 2013, 80 km array, 0.5×0.25 degrees

NCP data: 114 hours

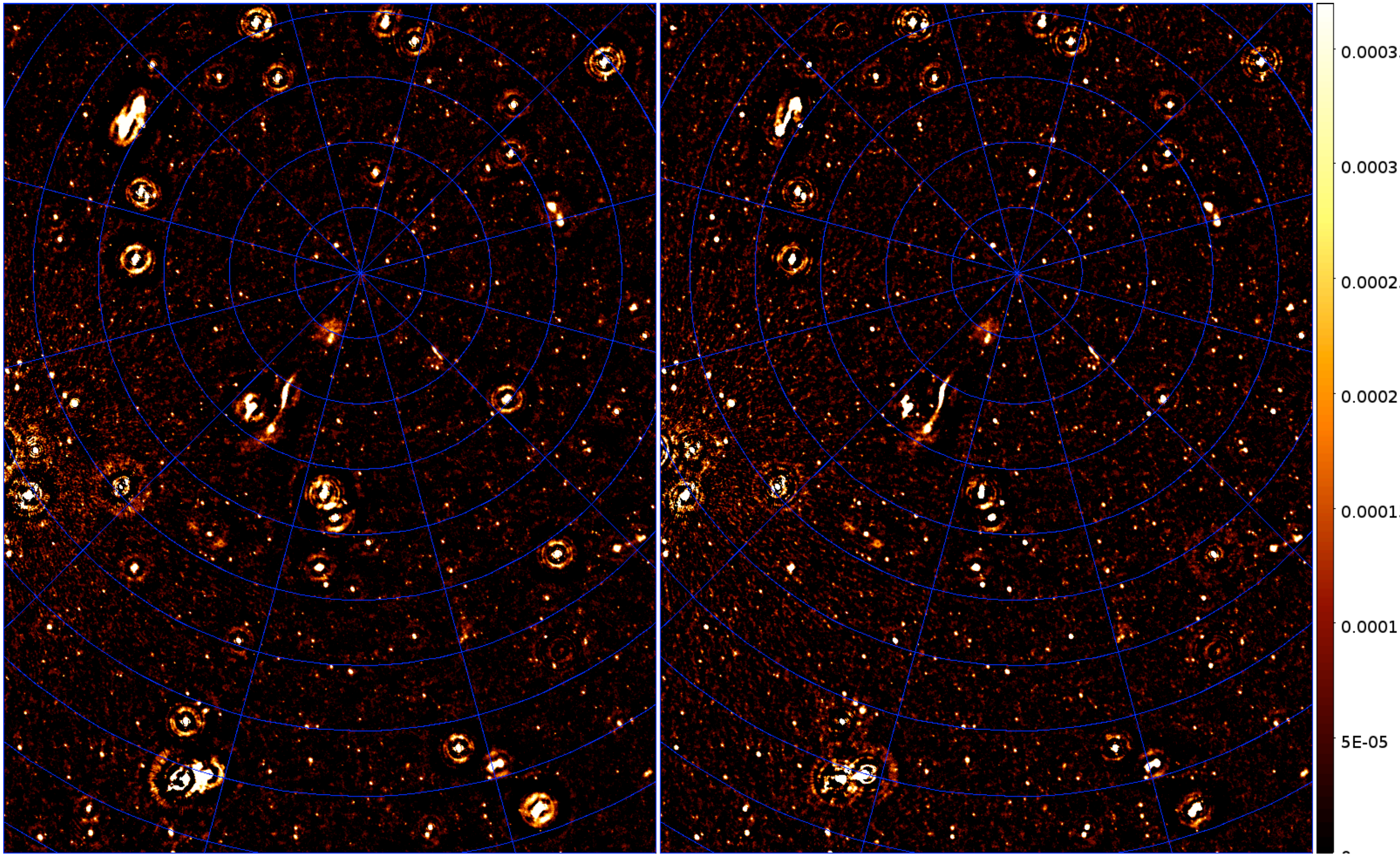

The future: SKA

SKA
SQUARE KILOMETRE ARRAY
www.skatelescope.org